Effects of space-relevant radiation on pre-osteoblasts

Dissertation

zur
Erlangung des Doktorgrades (Dr. rer. nat.)
der
Mathematisch-Naturwissenschaftlichen Fakultät
der
Rheinischen Friedrich-Wilhelms-Universität Bonn

vorgelegt von

Yueyuan Hu
aus
Xiangtan, Hunan, China

Bonn 2014

Angefertigt mit Genehmigung der Mathematisch-Naturwissenschaftlichen Fakultät der Rheinischen Friedrich-Wilhelms-Universität Bonn

1. Gutachter: Prof. Dr. Waldemar Kolanus

2. Gutachter: PD Dr. Ruth Hemmersbach

Tag der Promotion: February 12, 2014

Erscheinungsjahr: 2014

Table of Contents

List of figures

List of tables

1. Introduction

Space programs are now shifting towards long-term exploration missions, particularly to the Moon and Mars. However, space exploration is an adventure for humankind because of the extreme environment including microgravity and ionizing radiation. This environment causes a number of health problems. For example, the immune system response is weakened (Sonnenfeld, 2005), the muscular system experiences atrophy (Ruegg *et al.*, 2003), bone loss can be recognized during and after space travel (Nagaraja and Risin, 2013), and there is a substantial increase in the risk of carcinogenesis and of the development of degenerative diseases (Durante and Cucinotta, 2008). In space, heavy ions as a component of space radiation present substantial but poorly understood risks during and after space missions. Extended exposure to microgravity results in significant bone loss; coupled with space radiation exposure, this phenomenon may place astronauts at a greater risk for fracture due to a critical decrease in bone mineral density.

Until now, the biological effects of space relevant radiation on bone cells especially the bone forming osteoblasts are poorly understood. Therefore, it is crucial to understand the effects of ionizing radiation on osteoblasts and to develop effective countermeasures to reduce the bone fracture risk and to ensure the safety of space travelers during the mission and after return to Earth.

1.1 Space radiation

The radiation field in space is very complex and has a different quantity and quality compared to the conditions on Earth. The interplanetary radiation field contains primary galactic cosmic rays (GCR) and solar energetic particles (SEP). Charged particles traveling through materials such as shielding, spacecraft walls, space suits and human tissue produce secondary radiation via nuclear reactions (**Figure 1-1**).

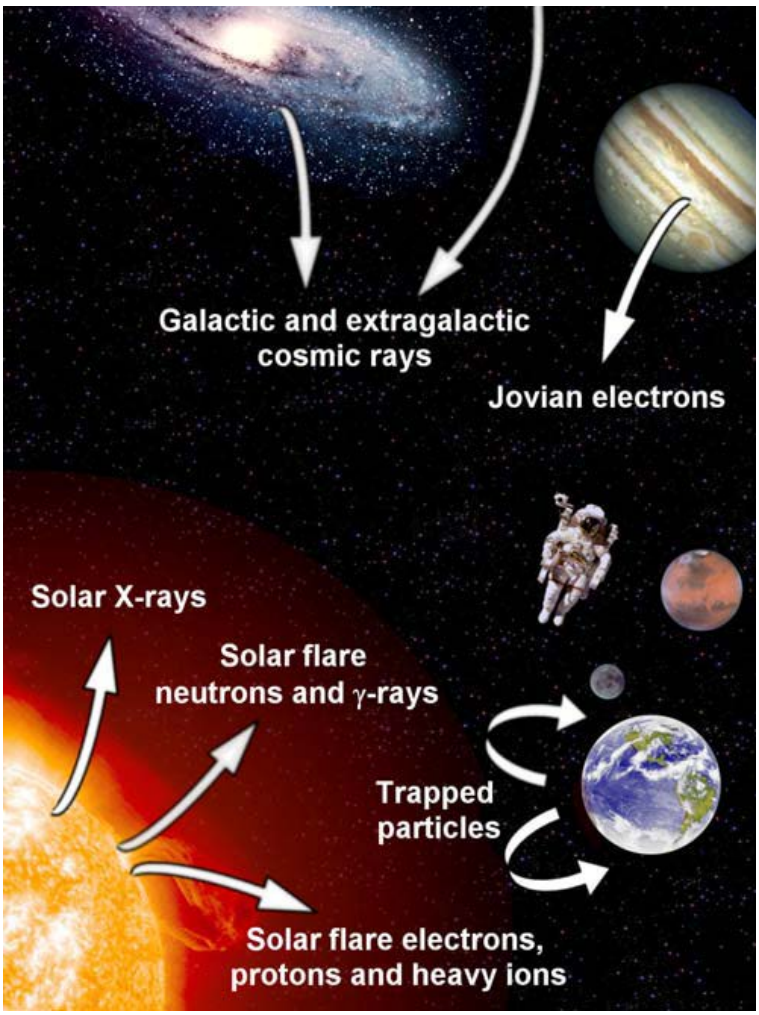

Figure 1-1 Space radiation environment in our solar system

Space radiation consists of galactic cosmic rays originating outside of our solar system (containing heavy charged particles), and solar energetic particles originating from solar flares or coronal mass ejections (mainly protons, electrons, ions, X-rays) (Figure from Hellweg and Baumstark-Khan 2007).

Solar particle events (SPEs) consist primarily of protons and helium ions and occur sporadically, depending on the solar activity which follows an 11-year cycle. During the solar minimum phase, few events occur, whereas during each solar maximum phase, large events may occur even several times and they may last for several days to weeks, with temporary increases of the radiation dose.

GCR originates from outside the solar system and consists mainly of charged particles (98% baryons and 2% electrons). These charged particles include about 1% heavy ions (HZE particles) which have high charge (Z) and energy (E) (Bucker and Facius, 1986;

Hellweg and Baumstark-Khan, 2007). The energy spectrum of GCR peaks near 1000 MeV per nucleon (MeV/n) (Wilson *et al.*, 1995). Recent measurements with the Radiation Assessment Detector on the Mars Science Laboratory (MSL) showed that, with current propulsion systems during the shortest exploratory round trip to Mars of 253 days, the accumulated equivalent dose [1] was found to be 0.66 ± 0.12 Sievert (Sv) inside MSL spacecraft (Zeitlin *et al.*, 2013).

During a trip to Mars, there is a good chance for at least one solar flare to occur which could drastically increase astronauts' exposure to 5 Sv if it happened in a phase of insufficient shielding such as an extravehicular activity (Thirsk *et al.*, 2009). Early warning systems for SPEs are necessary to prevent such exposures.

In low Earth orbit at an altitude of 350 - 420 km, the International Space Station (ISS) is still partly protected by the Earth's magnetosphere. The Van Allen radiation belts surround the Earth as tori with the thickest region at the equator plane. In these belts, particles from GCR and SPEs are trapped by the Earth's magnetic field. In the inner radiation belt at an altitude 2,000 - 10,000 km from Earth's surface, protons and electrons predominate which are formed by ionization of air components by cosmic radiation. In the outer radiation belt, 14,000 - 46,000 km from Earth's surface, ionized particles from the Earth's atmosphere and the solar wind are trapped.

On the ISS, an astronaut will receive a dose equivalent of about 0.3 Sv per year, compared to a person on Earth receiving an average dose of less than 0.005 Sv per year (Townsend and Fry, 2002).

Energy deposition is a measure for the qualitative differences of space radiation components. Energy deposition in matter by ionizing radiation[2] of different qualities is

[1] The equivalent dose is defined as the product of absorbed dose and the radiation quality factor Q. The biological effects of ionizing radiation are influenced amongst others by the absorbed dose, the dose rate and the quality of the radiation. For radiological protection purposes, the organ or tissue weighting factors are also taken into consideration.

[2] Ionizing radiation is defined as when the particles (including charged electrons or protons and uncharged photons or neutrons) can produce ionization in a medium or can initiate nuclear or elementary-particle transformations that then result in ionization or the production of radiation excitation.

described by the linear energy transfer (LET). The LET is the linear density of energy loss by transfer from the ionizing particles to the irradiated matter and can be described as energy loss per unit distance, *dE/dx (keV/µm)*. LET depends on the nature of the radiation as well as on the material traversed. Charged particles lose energy as they traverse matter, and as they approach the end of their range, there is an enhanced energy loss rate called Bragg peak, where the maximum LET occurs. For many biological endpoints, the relative biological effectiveness (RBE) [3] peaks at an LET of about 100 - 200 keV/µm and decreases sharply at very high LET (Cucinotta and Durante, 2006).

Shielding is necessary to protect humans on space explorations. Thick shielding is effective in absorbing protons of SPEs and can reduce the dose the astronauts are exposed to. It is much more difficult to shield GCR because of its high energy, strong penetrating ability and probability in inducing secondary radiation and increasing the absorbed dose. The absorbed dose or cancer induction rates resulting from annual GCR exposure is higher behind up to of 30 g/cm^2 of aluminum shielding (Wilson *et al.*, 1995) or 5 g/cm^2 of polyethylene compared to unshielded conditions (Wilson *et al.*, 1999). Present shielding approaches cannot sufficiently reduce the detrimental exposure to space radiation firstly because of high launch costs for thick shielding, and secondly because of the production of even more harmful secondary radiation during traversal of the shielding.

Furthermore, large uncertainties exist in the projection of health risks of space radiation, especially for energetic heavy ions with very high biological effectiveness (George *et al.*, 2003; Hall *et al.*, 2006). In recent years, worldwide efforts are focusing on understanding of the detrimental effects of space relevant radiation on cellular, tissue and whole body level.

[3] The RBE is defined as the ratio of the doses required by two different radiation qualities to cause the same level of effect and depends on dose, dose rate, fractionation, radiation quality, the irradiated tissue and the biological endpoint under consideration. The degree of biological effectiveness of different radiation types is mainly influenced by the way of energy transfer to the tissue (different LETs) (Barendsen 1994; Nikjoo *et al*. 1999).

1.2 Effects of ionizing radiation on humans

Depending on dose and dose rate, the whole body radiation exposure during space missions can result in acute, chronic or late effects.

High radiation doses and dose rates might be reached during SPE. The acute exposure to high doses can induce early health effects such as nausea, vomiting, coma or may be lethal depending on the dose, which will degrade crew survival and performance and thus can severely interfere with mission success.

Low dose rate but long-term radiation exposure to total radiation doses of 2-4 Sv/year which exceeds the permissible occupational dose would result in the chronic radiation syndrome (Reeves and Ainsworth, 1995). This syndrome may include sleep and/or appetite disturbances, generalized weakness and easy fatigability, headaches, bone pain and hot flashes, which is not negligible for human health and successful missions (Hellweg and Baumstark-Khan, 2007).

After astronauts return to Earth, an increased lifetime risk for late effects such as cataracts and cancer persists from exposure to GCR and SPE. Quantitative estimates of cancer risk from exposure to ionizing radiation are available from the studies of cancer incidence in the atomic bomb survivors from Nagasaki and Hiroshima in Japan. Within these studies, an increase in the risks of breast cancer in women, and of leukemia, non-melanoma skin cancer, and lung cancer in both genders was found (Land *et al.*, 1994; Little, 2009; Little and Charles, 1997; Schneider and Walsh, 2008). Some epidemiological studies with atomic bomb survivors also have shown that exposure to moderate to high doses of ionizing radiation increases the risk of cancer in most organs: breast, thyroid, esophagus, colon, bladder, ovary and lung (Bogart *et al.*, 2005; Laird, 1987; Preston *et al.*, 2012; Shay *et al.*, 2011).

Cancer radiotherapy relies on killing cancer cells by the physical energy transfer of ionizing radiation. When given at high doses, it can slow or stop tumor growth. Because of their exceptional properties, exhibiting a strong increase in dose at the end of the particle range called Bragg peak (**Figure 1-2**) when travelling through matter, charged particles are applied as therapeutic agents against cancer. Due to the larger mass

comparing to protons or even helium ions, heavy ions offer an improved dose conformation with better sparing of normal tissue structures close to the target. This advantage is lost for very heavy ions (above oxygen) because the RBE is already very high in the entrance region and does not increase much in the Bragg peak. Accelerated particles applied for cancer therapy such as protons and carbon ions can concentrate the effect of radiation on the tumor being treated, while at the same time the effect on the surrounding healthy tissue is minimized (Trikalinos *et al.*, 2009).

As for radiotherapy with photons, a risk for secondary cancer exists also after proton and carbon ion therapy. A final assessment of this risk is not yet possible (Shioyama *et al.*, 2003).

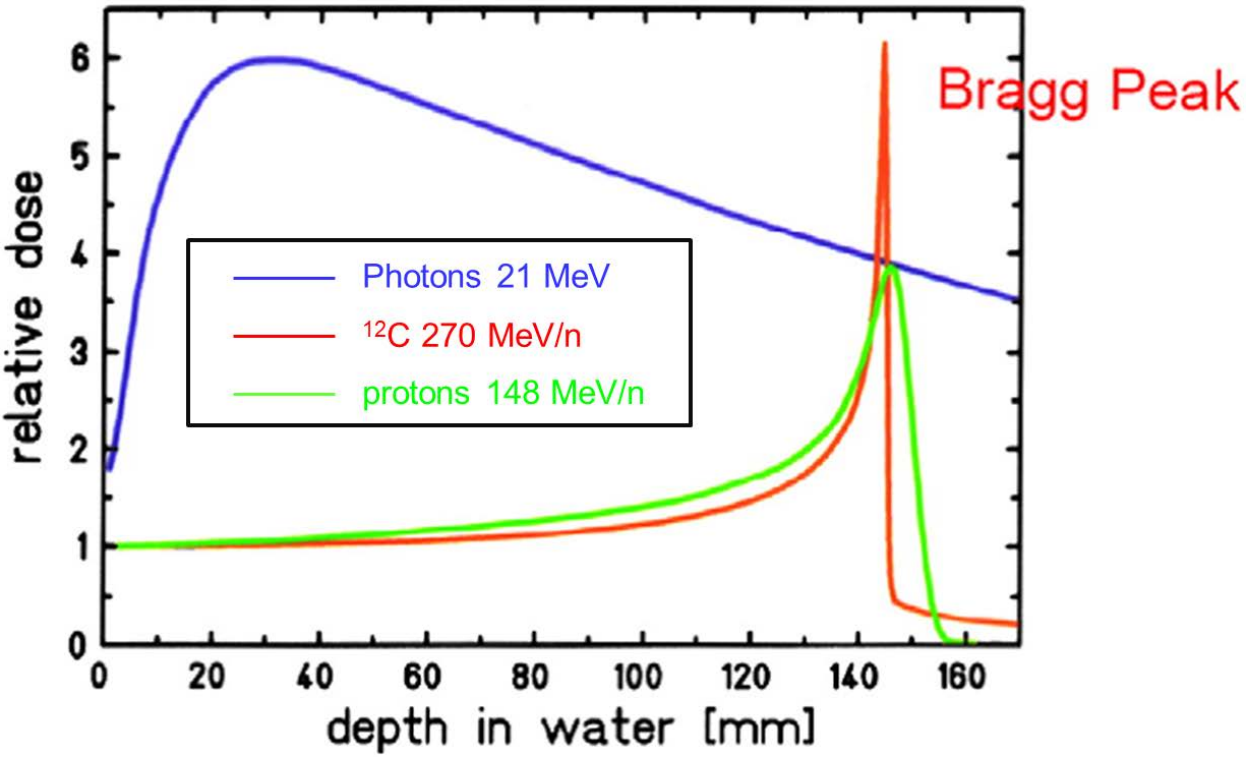

Figure 1-2 Depth distribution of radiation dose in water

Depth dose distribution with Bragg peak for carbon ions (270 MeV/n) and protons (148 MeV/n) in comparison to photons (Fokas *et al*., 2009).

The risk for space radiation induced tumorigenesis is believed to be very high because of the high biological effectiveness of HZE particles. For both astronauts traveling in space and radiotherapy patients, understanding of the tissue reactions and cellular stress responses to heavy ion exposure will be necessary for an accurate assessment of cancer risk and may provide targets for prevention.

1.3 Effects of ionizing radiation on cells

The biological effects of ionizing radiation on human beings are a consequence of physical and chemical reactions initiated by energy deposition in cells and tissues. DNA is a critical cellular target of ionizing radiation. The immediate response to DNA damages induced by ionizing radiation is the stimulation of the repair machinery and activation of cell cycle[4] checkpoints, followed by down-stream cellular responses such as apoptosis and other forms of cell death, differentiation or senescence.

Agents designed to protect irradiated cells from dysfunction of cellular differentiation and cell-cell communication, or those that can reverse the irradiated phenotype could provide a mean of impeding its downstream carcinogenic potential (Park *et al.*, 2003). More basic studies on tissue, cellular and molecular level using ground based facilities are necessary to identify targets for such agents.

1.3.1 Radiation induces DNA damage

Charged particles, γ- and X-rays penetrating tissue or cells initiate ionization of water and biomolecules along the movement track and induce DNA damage (**Figure 1-3**). These damages include a variety of structural lesions in DNA: oxidative base damage, single-strand breaks (SSB) and double-strand breaks (DSB) (Lau, 2005) as well as local multiple damages sites through direct and indirect interactions (Eccles *et al.*, 2010; Hada and Georgakilas, 2008). The complexity of radiation induced DNA damages depends on the radiation quality described by the LET. Substantial evidence indicates

[4] The cell cycle also called cell-division cycle is a series events taking place in a cell leading to its division and duplication. It consists of distinct phases, interphase and mitosis. The interphase is composed of G1 (cells are active and growing), S (cells are actively replicating DNA) and G2 phase (during this phase, cells are actively preparing for mitosis).

that high LET radiation induces a greater number of DNA damages and more complex clustered DNA lesions than low LET photons (**Figure 1-4**) (Bishay *et al.*, 2001; Fournier *et al.*, 2012; Gaziev, 1999). Those high-LET induced damages are thought to be much more difficult for cells to repair accurately (Fakir *et al.*, 2006; Kozubek and Krasavin, 1984).

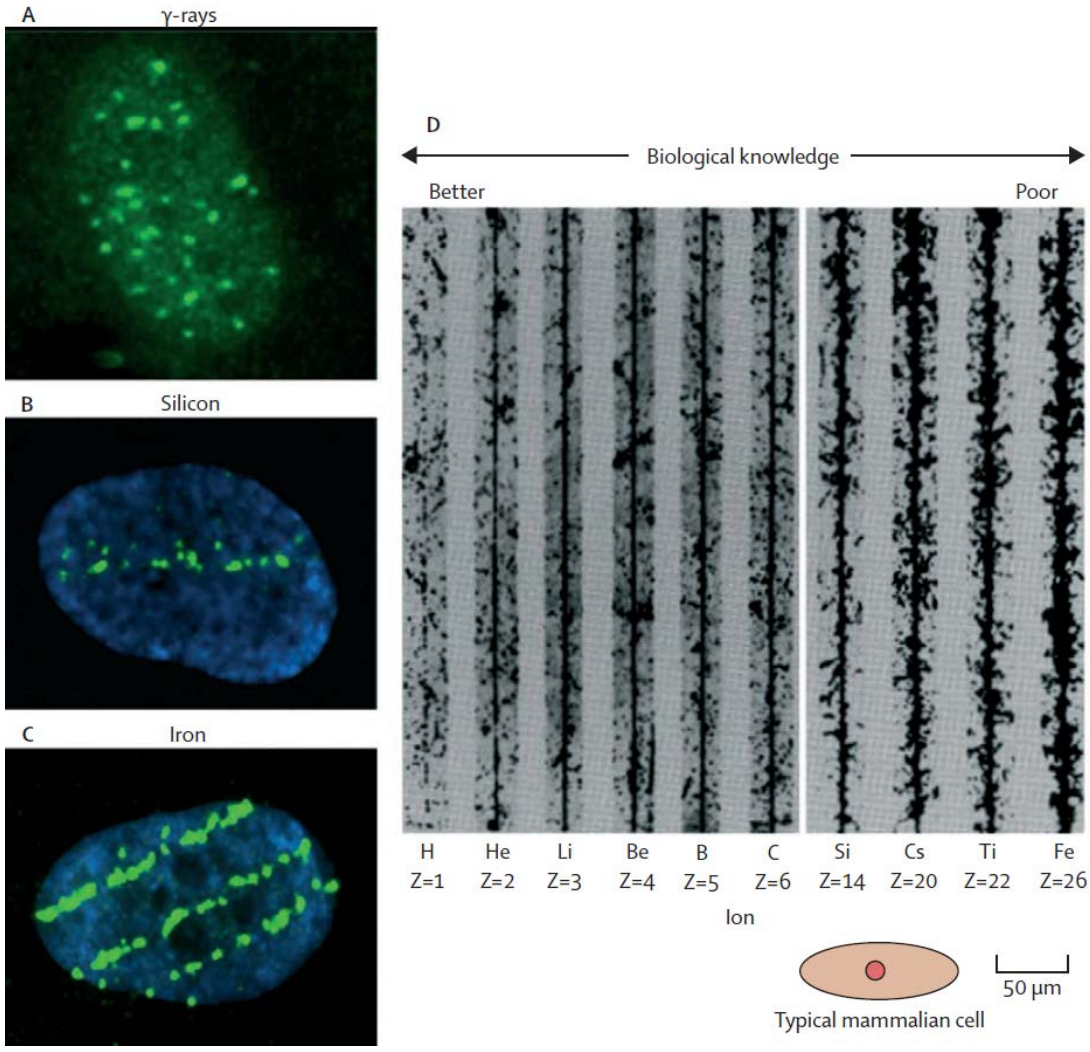

Figure 1-3 Comparison of particle tracks in human cells and nuclear emulsions

Immunostaining of γ-H2AX in human fibroblasts visualizing the cellular response to DNA double strand breaks after cells were exposed to sparsely ionizing radiation (γ-rays) (A) or to heavy charged particles such as silicon (B) and iron (C) ions. Tracks of different ions in nuclear emulsions show increasing ionization density as the ion's charge, Z, increases (D). Figures from: (Cucinotta and Durante, 2006)

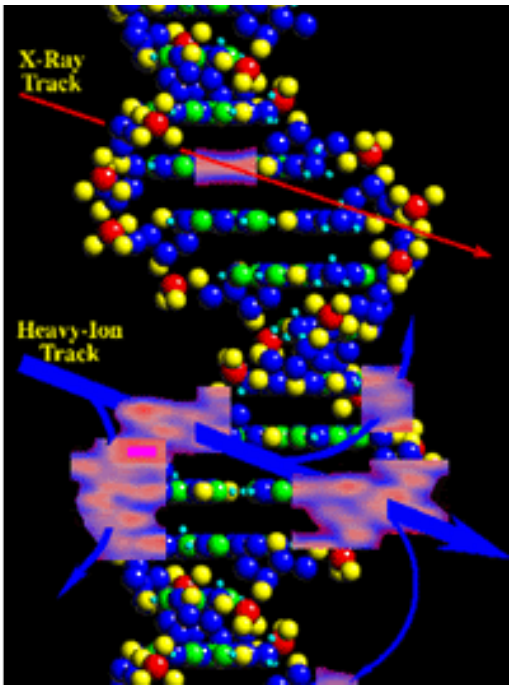

Figure 1-4 Radiation tracks produced by an X-ray photon and by a heavy charged particle in the DNA double helix

In this example, the heavy charged particle produces a highly complex DNA strand break, while the photon induces base damage. (Image credit by National Aeronautics and Space Administration (NASA))

Differences in damage-response pathways induced by low and high-LET radiation result in distinct gene expression and mutation profiles (Liu *et al.*, 2013). They might be associated with cancer initiation or progression including genomic instability (Baverstock, 2000; Eidemuller *et al.*, 2011; Eidemuller *et al.*, 2012), extra-cellular matrix remodeling, persistent inflammation (Multhoff and Radons, 2012), or with cataract formation (Muranov *et al.*, 2010), and damages to the central nervous system (Coderre *et al.*, 2006) and oxidative damage (Kvam and Tyrrell, 1997; Mishra, 2004).

1.3.2 Repair of DNA damage

Genotoxic stresses result in activation of a complex network of DNA damage checkpoints and repair pathways. To maintain integrity of DNA molecule after ionizing radiation induced DNA damage, three enzymes from the phosphatidylinositol-3-kinase-related (PIKK) family are activated by phosphorylation: ATM (ataxia telangiectasia

mutant), ATR (ataxia telangiectasia and Rad3-related protein) and DNA-PK (DNA-dependent protein kinase) (Cimprich and Cortez, 2008; Lovejoy and Cortez, 2009; Shrivastav *et al.*, 2008; Tichy *et al.*, 2010).

ATM is a serine/threonine protein kinase recruited and activated by DNA DSB. After its activation, it phosphorylates several key proteins including p53 and Chk2 which will initiate activation of the DNA damage checkpoint, leading to cell cycle arrest, DNA repair or apoptosis (Warmerdam and Kanaar, 2010). ATM is involved in the non-homologous end joining (NHEJ) repair pathway and is also crucial for homologous recombination (HR).

NHEJ is the only DSB repair process in mammalian cells in G1- and early S-phase.

DSB repair in late S- to G2-phase can be performed by HR. HR uses the homologue DNA sequence of the sister chromatid as an undamaged matrix and enables correct repair of DNA DSBs. In comparison to HR, NHEJ process is more error-prone but a fast and easy way to seal a two-ended break arising from the damages after treatment with ionizing radiation.

ATR, also known as FRAP-related protein 1 (FRP1), is a serine/threonine-specific protein kinase and is involved in sensing DNA damage (single-stranded DNA and stalled replication forks) and activating the DNA damage checkpoint, whereas ATM responds mainly to DNA double strand breaks. ATR and ATM respond to distinct stimuli and therefore have non-redundant functions. Thus, combined and complementary actions of ATM and ATR ensure the sensing of DNA damage and cell cycle checkpoint activation in response to damaging agents or stimuli.

DNA-PK is another protein kinase that is specifically required for NHEJ. During NHEJ, DNA-PK initially recognizes and binds to the damaged DNA and then targets the other repair activities to the site of DNA damage.

1.3.3 Radiation induces cell cycle arrest

After the initial sensing of DNA damage, the subsequent transmission is through ATM/ATR associated with activation of p53-dependent and -independent pathways to the cell-cycle machinery check-points.

Cyclin-dependent kinases (CDKs) are a family of protein kinases known as key regulators of cell cycle progression. Binding of cyclins to CDKs is required for cell cycle transition, and repression of the cyclin gene also contributes to blocking the entry into the next cycle phase (Wilson, 2004).

The activation of cell cycle checkpoints provides for cells a controlled temporary arrest in G1, S or G2/M phase (**Figure 1-5**). This allows cells to repair the ionizing radiation induced DNA damage resulting from e.g. radiotherapy or space flight and mediate cell fate, in order to survive and maintain the genomic integrity and stability. After radiation exposure, cells transiently accumulate in G1, S or G2 in dose- and radiation quality-dependent manner (Fernet *et al.*, 2010). Since many tumor cells are deficient in the G1/S checkpoint due to a non-functional p53 pathway, they lack effective G1 or S phase arrest induction. When cells are exposed to ionizing radiation in G2/M phase, two distinct checkpoints are activated: the early G2 checkpoint and the G2/M accumulation (Cucinotta *et al.*, 2001; Gogineni *et al.*, 2011; Metting and Little, 1995; Xu and Kastan, 2004; Xu *et al.*, 2002).

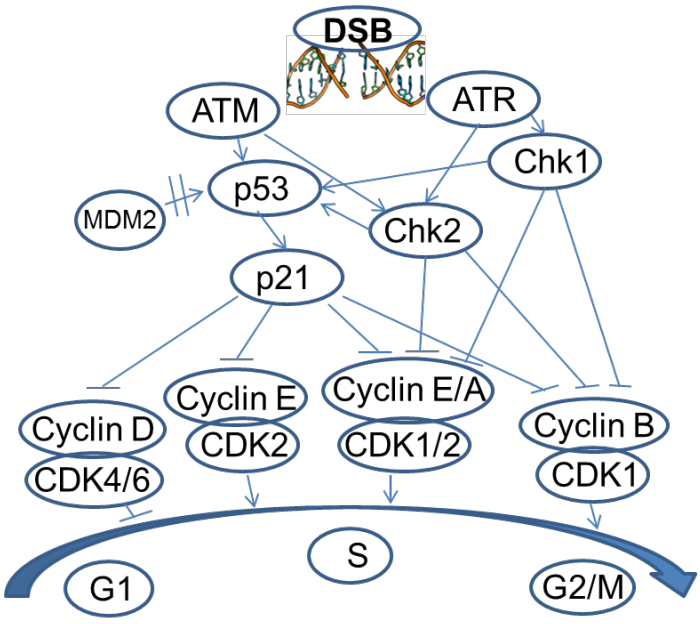

Figure 1-5 Molecular organization of cell cycle checkpoints that might result in cell cycle arrest in response to DNA DSBs

Multiple pathways lead to G1, S, G2/M arrest through p53/p21 dependent or independent pathways (Iliakis *et al.*, 2003; Pawlik and Keyomarsi, 2004).

1.3.4 p21 in cell cycle regulation

The tumor suppressor p53 is capable to induce cell cycle arrest and cell death in response to stress (Vousden, 2000). Many of its target genes, Cyclin-dependent kinase inhibitor 1 (CDKN1A) for example, are modulated to control the biological outcomes: cell cycle arrest, DNA repair, and reorganization of actin cytoskeleton and cell death (Avkin *et al.*, 2006; Li *et al.*, 1994; Quaas *et al.*, 2012; Suzuki *et al.*, 2012; Wani *et al.*, 2002; Yadav *et al.*, 2012; Yi *et al.*, 2012). The protein product of CDKN1A, p21, was originally identified as an inhibitor of CDKs. $p21^{CDKN1A}$ is also considered as a positive regulator of the cell cycle. A certain level of p21 expression is required for normal cell cycle progression, as p21 stabilizes and promotes active cyclin-CDKs complex formation (Pan *et al.*, 2002). Under non-stressed conditions, p21 is expressed at low levels and promotes cell cycle progression; when cells are under various outer or/and inner stresses, $p21^{CDKN1A}$ expression is increased through p53-dependent and independent pathways. $p21^{CDKN1A}$ implicates in cell cycle checkpoints in G1 and S phases by inhibiting activities of cyclin E-CDK2 complex (Harper *et al.*, 1993) and in the G2 and M phases by inhibiting cyclin B/A-CDK1 or CDK2 activities (Bates *et al.*, 1998; Niculescu, III *et al.*, 1998) (**Figure 1-6**).

Studies show that depletion of p21 expression by anti-sense RNA promotes cell cycle re-entry and DNA synthesis. The phosphorylation of retinoblastoma protein (pRb) is found to be essential for G1/S transition, and at the same time, p21 can inhibit pRb phosphorylation and induce cell cycle arrest in G1, or inactivate E2F1 which leads to cell cycle arrest and cellular senescence. Furthermore, p21 induced G2 arrest appears to be more prominent in pRb-null cells (Niculescu, III *et al*. 1998).

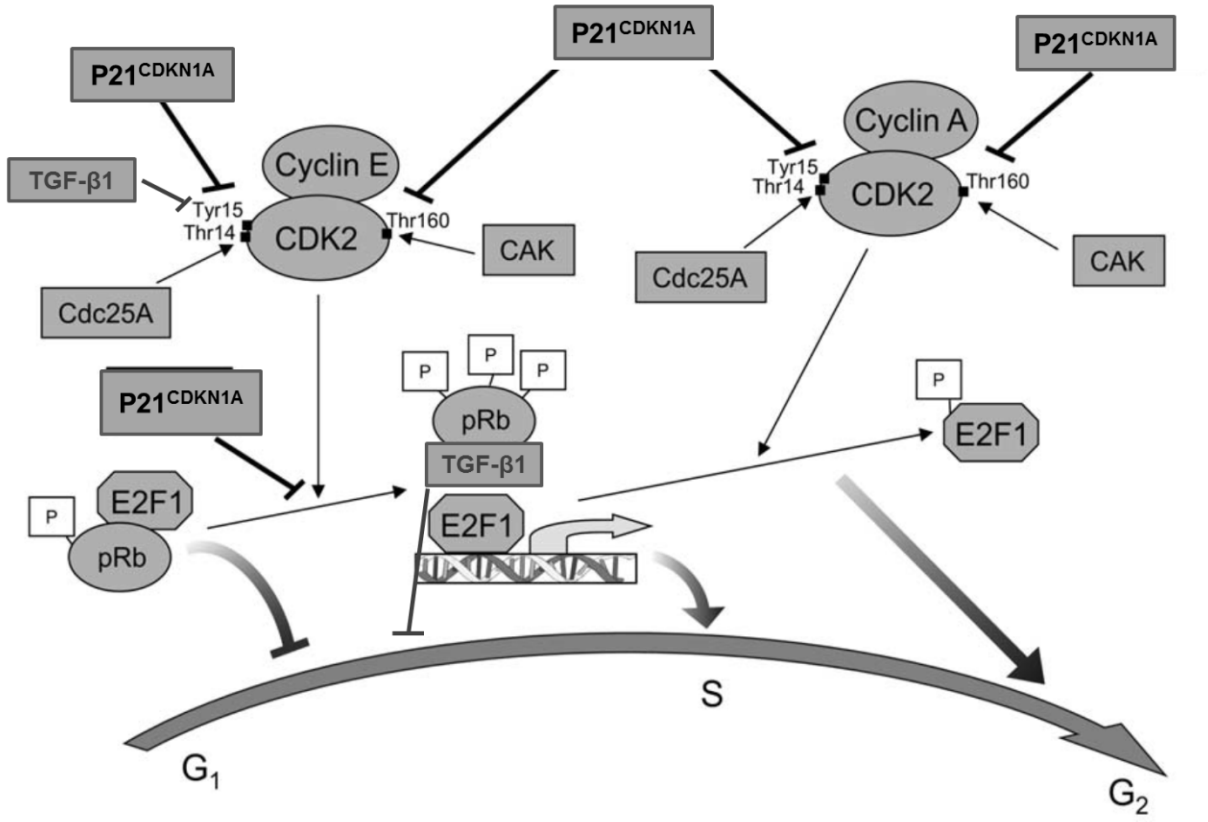

Figure 1-6 Negative regulation of G1, S and G2 transition by p21

Black squares indicate phosphorylation sites on tyrosine (Tyr) or threonine (Thr) residues of cyclin-dependent kinase 2 (CDK2). Graph created by (Romanov *et al.*, 2012)

1.3.5 p53 and Mdm2 regulation

Tumor suppressor proteins like p53 are present at a low concentration in normal cells. Mdm2 (Mouse double minute 2 homolog) is one of the p53 target genes and encodes an E3 ubiquitin ligase which negatively controls p53 and its downstream signaling pathways (Fry *et al.*, 2005; Fu *et al.*, 2009; Itahana *et al.*, 2007). Both p53 and Mdm2 have a short half-life and their nuclear concentrations are kept at very low levels as a result of proper functioning of the regulatory circuit described below (Deb, 2002; Freedman and Levine, 1999; Freedman *et al.*, 1999).

Under stress conditions such as hypoxia or DNA damage, p53 accumulates in the nucleus where it is activated and causes cell cycle arrest or apoptosis. Once the nuclear p53 levels increase, the transcription of the Mdm2 gene is activated, raising the level of

Mdm2 protein. In turn, Mdm2 binds to p53, which blocks its N-terminal transactivation domain and targets p53 for degradation via the ubiquitin-proteasome system following ubiquitinylation through its E3 ligase activity. Thereafter, the ability of Mdm2 to bind to p53 is blocked or altered in a fashion that prevents Mdm2-mediated degradation because of overexpression of Mdm2. Then p53 levels can rise again and increase Mdm2 protein expression. Oscillatory dynamics of p53 levels in the cell nucleus with one or more p53 peaks result from the p53-Mdm2 negative feedback loop (Manfredi, 2010; Marine and Lozano, 2010; Yu *et al.*, 2000).

1.3.6 Radiation induces cellular senescence

Senescence is a permanent cell cycle arrest controlled by two major pathways, the p16-pRb pathway and p53-p21 pathway. Cellular senescence can be induced by telomere dysfunction, DNA damage, and chromatin instability and oncogene activation. The stress induced proliferation suppression is tightly associated with cell cycle arrest.

The cell cycle arrest in G1 phase is commonly following ATM and p53 dependent temporary transcriptional activation of the CDKN1A gene encoding p21. Additionally, in a p53 independent manner, p21 has been recognized as an over-expressed marker in senescent cells and later found to be capable of inducing premature senescence in both normal and tumor cells (Noda *et al.*, 1994).

The other signaling pathway through the tumor suppressor protein p16 could also be activated through the p38 mitogen-activated protein kinase (MAPK) mediated p16 expression when p53 is inactivated. It maintains cells in senescent state due to radiation induced DNA damage.

1.4 Radiation effects on osteoblast differentiation

Bone loss is one of the serious obstacles for long-term manned space missions. Previous studies have demonstrated that astronauts on 4-6 months missions aboard the ISS experience femoral and vertebral bone loss of about 0.9-1.6% per month (Lang *et al.*, 2004). Bone loss and the corresponding loss of strength could increase the risk of fractures and pose a risk to mission safety. Exposure to GCR and solar particles presents a significant but poorly understood risk for carcinogenesis and degenerative diseases (Durante and Cucinotta, 2008). Together with microgravity, radiation might have a synergistic effect on bone cells resulting in dysfunction.

1.4.1 Bone remodeling

Bone is a dynamic tissue that constantly undergoes modeling and remodeling throughout lifespan. These modeling and remodeling processes are mainly executed by osteoclastic bone resorption followed by osteoblastic bone formation to maintain and renew its mineralized matrix (**Figure 1-7**).

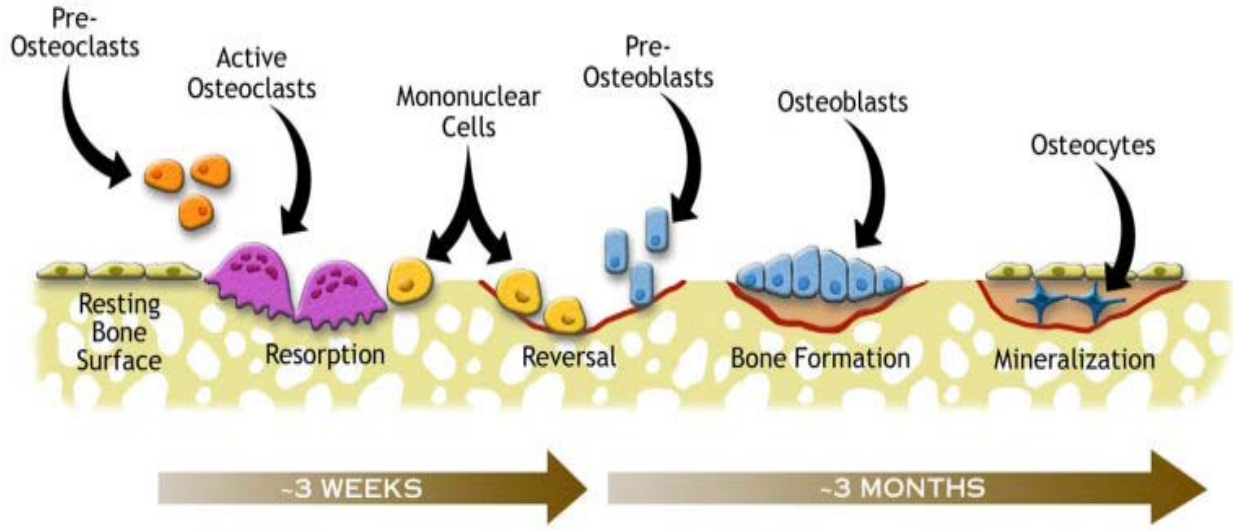

Figure 1-7 Bone remodeling cycle

Downloaded from http://www.ns.umich.edu/Releases/2005/Feb05/img/bone.jpg, 2010.

The remodeling process is regulated by systemic hormones including parathyroid hormone, calcitriol, growth hormone and some other hormones and factors; and by local factors such as growth factors, cytokines, and prostaglandins, which have been identified and are synthesized by osteoblasts (Hadjidakis and Androulakis, 2006). These hormones and factors affect both osteoblasts and osteoclasts in their replication, differentiation and activity.

Osteoblasts produce TGF-β (transforming growth factor beta) and deposit a latent form of TGF-β in bone tissue. The TGF-β superfamily comprises over forty members, such as TGF-βs, Nodal, Activin, and bone morphogenetic proteins (BMPs) (Guo and Wang, 2009). TGF-βs and BMPs have widely recognized roles in bone formation during mammalian development (Katagiri and Takahashi, 2002). Disruptions of TGF-β/BMP signaling implicate bone diseases including tumor metastasis and osteoarthritis (Siegel and Massague, 2003). TGF-β signaling promotes osteoprogenitor proliferation, commitment to the osteoblastic lineage and early differentiation (Chen *et al.*, 2012a). It has been recognized that TGF-β is involved in the pathogenesis of late radiation damage in the non-tumor bearing tissues of previously irradiated patients and thus its activity may modulate late post-radiation changes (Canney and Dean, 1990).

TGF-β1 is one of the isoforms of the TGF-β superfamily. It plays an important role in endochondral and intramembranous ossification. TGF-β1 deficient mice display reduced bone growth and mineralization (Janssens *et al.*, 2005). Ionizing radiation specifically induces the expression of TGF-β1, which is required for DNA repair, progression through cell cycle (**Figure 1-6**) (Mukherjee *et al.*, 2010), inflammation in early stage, and later development of radiation damage such as fibrosis (Martin *et al.* 1997; O'Malley *et al*. 1999).

BMPs are multifunctional growth factors and play an important role in bone formation (Wan and Cao, 2005; Weston *et al.*, 2000). BMPs activate Smad proteins and those Smads are phosphorylated and translocate into the nucleus where they regulate their target genes such as Runx2 (Runt-related transcription factor 2) to control mesenchymal precursor cell differentiation.

Runx2 is an important transcription factor that regulates osteoblast and chondrocyte differentiation and can be viewed as a marker gene for the BMP signaling pathway. Differentiation along the osteoblast lineage has been shown to depend on Runx2 and Osterix (Osx) regulation (**Figure 1-8**) (Nakashima *et al.*, 2002). Runx2 or Osx knockout mice show no bone formation (Nakashima *et al.*, 2002; Tsuji *et al.*, 2004), while Runx2 is a master regulator that acts upstream of Osterix (Nakashima *et al*. 2002). Osterix is expressed as early as mesenchymal cells are committed to enter the osteoblast lineage, and expression of Osterix becomes stronger as osteoblast differentiation occurs.

1.4.2 Radiation induces bone loss

In *in vivo* studies with a mouse model, prolonged and profound loss of trabecular or/and cortical bone has been found after acute radiation exposure to a dose of 2 Gy, which represents both a typical dose fraction in cancer radiotherapy and the cumulated space radiation exposure for an exploratory mission (Hamilton *et al.*, 2006; Lloyd *et al.*, 2008). Studies also show that significant differences in the induction of bone loss in an animal model were observed between radiation qualities of therapeutic and space-relevant sources (Hamilton *et al.* 2006). There is evidence showing that therapeutic irradiation can cause bone damage in cancer patients, which results in increased bone resorption and decreased bone mineral density, and this damage has a good chance in increasing the risk of bone fracture (Edwards *et al.*, 2011; Guise, 2006).

1.4.3 Osteoblasts and bone formation

Osteoblasts are specialized cells of mesenchymal origin, responsible for bone formation and support of osteoclast differentiation. Bone formation includes a complex process that contains the proliferation of primitive mesenchymal cells, differentiation into osteoblast precursor cells, maturation of osteoblasts, formation and mineralization of extracellular matrix, and finally some cells gradually flatten and become quiescent lining cells (**Figure 1-8**).

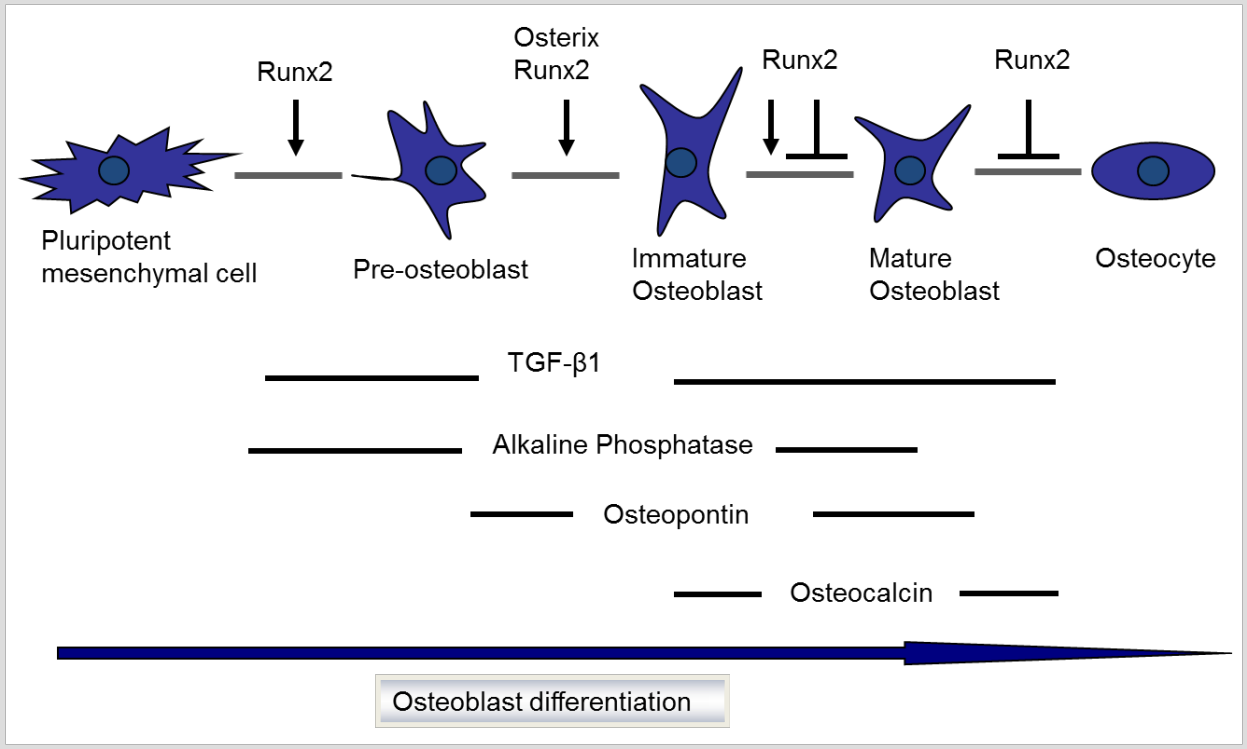

Figure 1-8 Genes involved in osteoblast differentiation

Runx2 directs pluripotent mesenchymal cells to the osteoblast lineage but inhibits osteoblast maturation. Osx also takes charge of osteoblast differentiation, and different proteins are produced at the consecutive stages of this process. Graph is modified from (Komori, 2010).

The differentiation of osteoblasts into mature bone cells is regulated by several bone derived growth factors such as TGF-β1, and by the transcription factors Osx and Runx2. Those factors cause the appearance of markers of differentiated osteoblasts, including expression of alkaline phosphatase (ALP) and Type I collagen (the major organic component of mineralized bone matrix) (**Figure 1-9**).

In addition, increased expression of bone matrix components such as osteopontin is an early marker of osteoblast differentiation. The main characteristic of functional, mature osteoblasts is their ability to deposit extracellular matrix that mineralizes (Aubin, 1998b). The mineralized nodules are composed of inorganic hydroxyapatite ($Ca_{10}(PO_4)_6(OH)_2$) and organic components including type I collagen. These nodules can be visualized by using staining methods such as Alizarin red S staining.

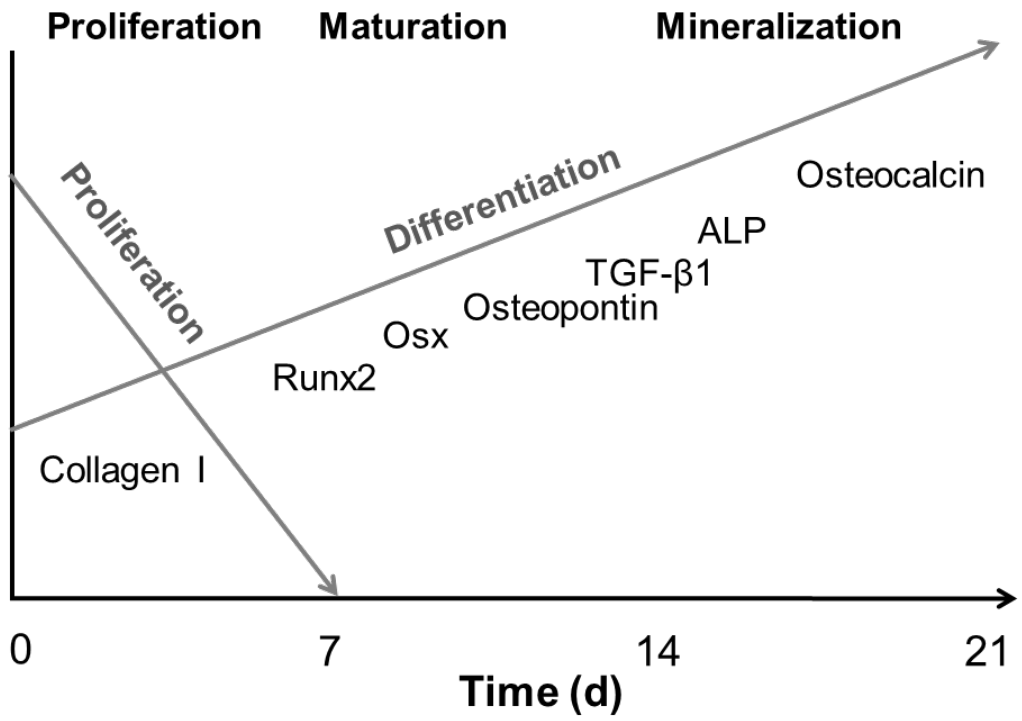

Figure 1-9 The relationship between osteoblast proliferation and differentiation during their development

During osteoblast differentiation, a series of genes like Runx2, Osx and the cytokine TGF-β1 are expressed. Runx2 and Osterix (Osx) are transcription factors. Collagen I, ALP, Osteopontin and Osteocalcin are secreted and they encode parts of the extracellular matrix (ECM) or enzymes that are important for production of ECM. Graph is modified from (Owen *et al.*, 1990).

During osteoblast mineralization, osteocalcin appears as a later marker. Some of them become embedded in the matrix and differentiate into osteocytes. This is likely been mediated by local factors produced during the resorption process performed by osteoclasts.

1.4.4 Effect of radiation exposure on osteoblastic differentiation and mineralization

Osteoblasts respond to local and systemic stimuli and multiple stresses like exposure to ionizing radiation (Dare *et al.*, 1997; Sakurai *et al.*, 2007). Ionizing radiation induces DNA damages which result in detrimental effects on cells. There is a great controversy on the effects of radiation on osteoblast differentiation, whether it is inhibited, reduced, delayed or stimulated.

An inhibition of differentiation of osteoblasts and osteoblast progenitors after radiation exposure has been described both *in vitro* (Szymczyk *et al.*, 2004) and *in vivo* (Sawajiri *et al.*, 2003). There is evidence that radiation at doses of 2 and 4 Gy reduces ALP and collagen type I along the osteoblasts' differentiation (Sakurai *et al.*, 2007). At dose of 4 Gy, exposure of mouse calvarial osteoblasts to X-rays delayed the mineralization of bone matrix *in vitro* (Park *et al.*, 2012). X-ray exposure at 1 or 2 Gy stimulated differentiation mouse calvarial osteoblasts, resulting in enhanced production of mineralized extracellular matrix (Park *et al.*, 2012). This stimulation was associated with increasing the levels of bone specific markers such as ALP, TGF-β1 and Runx2.

The influence of dose and radiation quality on the extent of ionization effects in osteoblasts have to be clarified and determined. Furthermore, the cellular mechanism behind the effects of ionizing radiation on osteoblast differentiation and mineralization needs to be further addressed.

1.4.5 p53 and osteoblast differentiation

p53 is mainly considered as a negative regulator of osteoblastogenesis by negatively regulating bone development and growth; and it suppresses the development of bone neoplasia (Chen *et al.*, 2012b; Liu and Li, 2010; Schwartz *et al.*, 1999). P53 negatively regulates osteoblast differentiation and function by repressing the expression of Osterix via BMP-Smad, BMP-p38 MAPK, or IGF (insulin-like growth factor)-MAPK pathway. Some studies show that p53 null mice have a high bone mass phenotype, and osteoblasts depleted of p53 have accelerated differentiation and favor osteoclast differentiation under the control of Osterix (Liu and Li, 2010). Mdm2 mediates inhibition of p53 function which is prerequisite for Runx2 activation, osteoblast differentiation and proper skeletal formation (Lengner *et al.*, 2006; Yang *et al.*, 2005); and cells depleted of Mdm2 have elevated p53 activity and a reduced level of Runx2 expression. Furthermore, p53 also negatively regulates osteoblast-dependent osteoclastogenesis. There is evidence showing that $p53^{(-/-)}$ osteoblasts have an enhanced ability to favor osteoclast differentiation, in association with an increase in expression of macrophage-colony stimulating factor, which is under the control of Osterix (Wang *et al.*, 2006a).

1.5 Aim of the thesis

In space, astronauts lose bone mass. A decreased bone density can also be observed in patients after radiotherapeutic treatment. However, little is known about osteoblast differentiation after exposure to space-relevant radiation. In order to increase the knowledge of the effects of space-relevant radiation on osteoblasts, this study was aimed at analyzing the cellular effects of irradiation with different qualities in the pre-osteoblast cell line OCT-1.

Hence first, the cell killing ability of OCT-1 cells by different radiation qualities was assessed by the colony forming ability test. To compare the killing effect of different radiation types, the RBE for OCT-1 cell killing by space relevant ionizing radiation was determined. For comparison of the radiation sensitivity of pre-osteoblasts with an earlier development stage, the RBE values for mesenchymal stem cells C3H10T1/2 were analyzed.

After the initial sensing of DNA damage, cell cycle checkpoint activation allows cells to repair the ionizing radiation induced DNA damage. Therefore, OCT-1 cell cycle regulation was analyzed after exposure with different radiation qualities. In order to address the role of p53 in ionizing radiation induced cell cycle blocks, cyclic pifithrin-α was applied.

In order to study the effects of radiation exposure during the osteoblast differentiation and function, OCT-1 cells were cultured in both standard medium and osteogenic induction medium. Firstly, cellular effects including cellular senescence, survival, repair kinetics and proliferation were compared after irradiation for cells cultured in presence or absence of osteogenic induction supplement. Secondly, the extracellular matrix produced by osteoblasts was analyzed after ionizing radiation exposure. As p53 can influence bone remodeling and is usually activated in response to ionizing radiation exposure, its role in the modulation of OCT-1 cell differentiation after exposure to X-rays was analyzed by means of the reversible chemical inhibition of p53 with cyclic pifithrin-α.

2. Materials and Methods

2.1 Materials

2.1.1 Laboratory equipments

The equipment used for this study is listed in **Table 2-1**.

Table 2-1 Laboratory equipments

Instrument	Designation	Supplier
Centrifuge	Multifuge 3 S-R	Thermo Scientific, Schwerte, Germany
Real-time Thermocycler	DNA Engine Opticon2 System	BioRad Ltd., Munich, Germany
Dosimeter	UNIDOSwebline	PTW, Freiburg, Germany
Fluorescence microscope	Axiovision 135	Carl Zeiss AG, Oberkochen, Germany
Flow cytometer	FACScan	Becton Dickinson, Heidelberg, Germany
Fluorescence microplate reader	Lambda fluoro 320	MWG Biotech, Ebersberg, Germany
Fluorescence microscope	Zeiss Axio Imager M2	Göttingen, Germany
Imager	ImageQuant LAS 4010 version 1.2	GE Healthcare, München, Germany
Incubator	Heraeus Jubilee Edition	Heraeus Instruments, Hanau, Germany
Laminar flow hood	Herasafe	Thermo Scientific, Schwerte, Germany
Light microscope	Axiovision 35	Carl Zeiss AG, Oberkochen, Germany
Microelectrophoresis	Bioanalyzer 2100	Agilent Technologies, Santa Clara CA, USA
MiniCycler	Biozym Diagnostik	Biozym, Oldendorf, Germany
pH-meter	Sartorius	Sartorius, Göttingen, Germany

Table 2-1 Laboratory equipments (Continued)

Instrument	Designation	Supplier
PhosphorImager	Storm 860 Molecular Imager	GMI Inc., Minnesota, USA
Water Bath	Aqualine AL 12	Lauda, Königshofen, Germany
X-ray generator	Gulmay RS225	X-strahl, Surrey, United Kingdom

2.1.2 Consumable materials, reagents and kits

Consumable materials are shown in **Table 2-2**. **Table 2-3** displays the used reagents and kits.

Table 2-2 Consumables

Item	**Supplier**
Chamber slide™ 16 well	Nunc, Wiesbaden, Germany
Cryo Tube™ Vials 1.8 ml	Eppendorf Ltd., Hamburg, Germany
Falcon tubes 15 ml	Nunc, Wiesbaden, Germany
Falcon tubes 50 ml	Nunc, Wiesbaden, Germany
Pasteur pipettes	Brand, Wertheim, Germany
Petri dishes ∅ 3 cm and 6 cm	Nunc, Wiesbaden, Germany
Pipet tips (10, 100, 1000 µl)	Eppendorf Ltd., Hamburg, Germany
Powder-free Latex Exam Gloves	Kimberly Clark, Neenah, WI, USA
Safe-Lock tubes 0.5 ml; 1.5 ml; 2.0 ml	Eppendorf Ltd., Hamburg, Germany
Sterile filter 0.22 µm	Millipore Corp., Bedford, USA
Strip well plate 12 × 8 well	Corning Costar, New York, USA
Tissue Culture flask 25 cm^2 and 80 cm^2	Nunc, Wiesbaden, Germany

Table 2-3 Reagents and kits

Item	Supplier
Alizarin red S	Sigma Aldrich, Steinheim, Germany
Amphotericin B (250 µg/ml)	PAN Biotech, Aidenbach, Germany
Ascorbic Acid	Merck, Darmstadt, Germany
Bisbenzimide ($C_{27}H_{28}N_6O$ •3HCl •3H_2O)	Sigma Aldrich, Steinheim, Germany
Bovine Serum Albumin (BSA)	Sigma Aldrich, Steinheim, Germany
ß-Glycerolphosphate	Merck, Darmstadt, Germany
ß-Mercaptoethanol	Sigma Aldrich, Steinheim, Germany
Cellular Senescence Assay	Millipore, Germany
Crystal violet	Merck, Darmstadt, Germany
Dexamethasone	Sigma Aldrich, Steinheim, Germany
4‘,6-Diamidino-2-phenylindole	Sigma Aldrich, Steinheim, Germany
Ethanol	Merck, Darmstadt, Germany
Fetal Bovine Serum (FBS)	Biochrom AG, Berlin, Germany
Formaldehyde 37%	Merck, Darmstadt, Germany
iScript™ cDNA synthesis kit	Bio-Rad, Munich, Germany
L-Glutamine (200 mM)	PAN Biotech, Aidenbach, Germany
Mounting medium	Invitrogen, California, USA
Neomycin/Bacitracin	Biochrom AG, Berlin, Germany
One-Step RT-PCR Kit	Invitrogen, Carlsbad, USA
OsteoImage™ mineralization assay	Lonza, Walkersville, USA
Penicillin/ Streptomycin	PAN Biotech, Aidenbach, Germany
Pifithrin-α, Cyclic	Sigma Aldrich, Steinheim, Germany
Platinum SYBR Green qPCR Supermix	Invitrogen, California, USA
Prolong gold antifade reagent	Thermo Scientific, Langenselbold, Germany
Propidium iodide	Invitrogen, Carlsbad, USA
RNA 6000 Nano Assay	Thermo scientific, Langenselbold, Germany
Ribonuclease (RNAse)	Calbiochem, La Jolla, USA
RNAse-Free Dnase Set	QIAGEN, Hilden, Germany
Rneasy Plus Mini Kit	QIAGEN, Hilden, Germany
Triton X-100	Sigma Aldrich, Steinheim, Germany
Trypsin/EDTA (0.025% trypsin, 0.01% EDTA)	PAN Biotech, Aidenbach, Germany

2.1.3 Buffers, solutions and culture medium

Buffers and solutions were prepared according to **Table 2-4**. Cell culture medium, which is shown in **Table 2-5**, was completed by adding FBS (fetal bovine serum) and glucose in order to provide growth factors and antibiotics to reduce the risk of contamination with bacteria and fungi.

Table 2-4 Buffers and solutions

Item	Reagent	Storage
Alizarin red S Solution	2 g Alizarin red S in *aqua dest*. pH 4.1 – 4.3, adjusted by 1 mol/l HCl	Room temperature
Bisbenzimide	10 µmol/l bisbenzimide in PBS (Phosphate buffered saline)	-20 °C, protected from light
Blocking buffer	0.5 g BSA 50 ml PBS	4 °C
Crystal Violet staining solution	0.5 g Crystal Violet 50 ml 37% formaldehyde (FA) stock solution 500 ml tap water	Room temperature
DAPI staining solution	0.1 µg/ml DAPI in PBS	-20 °C
Freezing medium	70% Culture medium 20% (v/v) FBS 10% (v/v) DMSO	4 °C
FA fixation solution	10 ml 37% FA stock solution in 90 ml PBS	4 °C
Lysis buffer	10 mmol Tris (pH 8.0) 50 mmol NaCl 0.5 mol EDTA 2% N-lauryl sarcosyl 0.1 mg/ml proteinase E and O	4 °C
PBS 5×	80 g NaCl 2 g KCl 14.4 g Na_2HPO_4 2 g KH_2PO_4 2 L *aqua dest.* pH 7.2	-20 °C

Table 2-4 Buffers and solutions (Continued)

Item	Reagent	Storage
PBS 1×	100 ml PBS 5× 400 ml autoclaved *aqua dest*.	4 °C
Propidium iodide (PI) staining solution	50 µg/ml RNAse A 0.1% (v/v) Triton X-100 20 µg/ml PI in PBS	4 °C
Tris/Borate/EDTA (TBE)	45 mmol/l Tris (pH 8.2) 45 mmol/l boric acid 1 mmol/l EDTA	Room temperature

Table 2-5 Culture medium

Item	Reagent	Storage
Basal Medium Eagle Medium (BME)	500 ml BME 50 ml FBS 5 ml Penicillin / Streptomycin 5 ml L-Glutamine 3.5 ml 17% Glucose 5 ml Amphotericin	4 °C
α-minimum essential medium (α-MEM)	500 ml α-MEM 50 ml FBS 5 ml Penicillin / Streptomycin 5 ml L-Glutamine 5 ml Amphotericin 10 ml 17% Glucose	4 °C
Osteogenic induction (OI) medium	Culture medium BME 50 µmol/l L-Ascorbic acid 10 mmol/l β-Glycerophosphate 100 nmol/l Dexamethasone	4 °C

2.1.4 Softwares

The computer programs used to edit and evaluate data are shown in **Table 2-6**.

Table 2-6 Software

Item	Purpose / use	Supplier
2100 Expert Software for Bioanalyzer	Assessment of integrity of RNA	Agilent Technologies, Karlsbrunn, Germany
Flowing Software version 2.5.0	Cellular DNA content calculation in different cell cycle phases	Free online software, http://www.flowingsoftware.com
Image Pocessing and Analysis in Java (ImageJ)	Image analysis	Free online software, http://rsbweb.nih.gov/ij/ download.html
Opticon 2	For real-time PCR detection	Bio-Rad, Munich, Germany
Relative Expression Software Tool – Multiple Condition Solver (REST-MCS©) - version 1	Determination of relative expression levels of investigated genes	W. Pfaffl & G.P. Horgan, Technical University (TU) Munich, Germany
Sigma Plot 12.0	Data analysis and graphing software	SPSS, Munich, Germany

2.1.5 Cell lines

OCT-1 cells were originally isolated from the calvaria of transgenic CB6F1 (C57BL/6 × BALB/c) mice carrying the SV40 large T antigen under the control of the bone-specific osteocalcin promoter (Chen *et al.*, 1995). They have the ability to form mineralized bone nodules after osteogenic induction. OCT-1 cells were used to study the differentiation process of osteoblast-like cells after exposure to ionizing radiation.

C3H10T1/2 cells were established in 1973 from 14- to 17-day-old C3H mouse embryos (Reznikoff *et al.*, 1973). These cells can undergo multiple differentiation pathways: chondrogenesis, osteogenesis, myogenesis and adipogenesis (Denker *et al.*, 1999; Shea *et al.*, 2003).

2.1.6 Cell culture

The murine calvaria-derived pre-osteoblast cell line OCT-1 at a low passage number (below 20) was maintained in α-MEM medium supplemented with 10% FBS at 37 °C in a humidified atmosphere containing 5% CO_2. Cells were passaged every week and seeded at a density of 3×10^3 cells/cm^2 in 80 cm^2 cell culture flasks.

For cell freezing, 1×10^6 cells in freezing medium were pipetted in cryotubes and frozen at -80 °C in a box containing 100 % isopropanol, assuring a decrease in temperature of 1 °C per minute (min). After 24 h, the cryotubes were transferred into the liquid nitrogen container for long term storage.

C3H10T1/2 cells were seeded at a density of 5×10^3 cells/cm^2 in 80 cm^2 cell culture flasks and maintained in BME culture medium supplemented with 10% FBS in a humidified atmosphere at 37 °C.

2.1.7 Inhibitor experiments

In order to study Mdm2, interactions of p53 and Mdm2 or p53-Mdm2 pathway, there are some chemicals are applied currently, for example Nutlin-3 (Mdm2 antagonist; inhibits Mdm2-p53 interaction) (Vassilev *et al.*, 2004), cyclic pifithrin-α (reversible inhibitor of p53-mediated apoptosis and p53-dependent gene transcription) (Sohn *et al.*, 2009), and cyclic pifithrin-α (cyclized form of cyclic pifithrin-α) which is more stable than cyclic pifithrin-α (Meschini *et al.*, 2010). Cyclic pifithrin-α was applied in this study by adding into the culture medium at a concentration of 30 nmol/l 2 h before radiation exposure.

2.1.8 Osteogenic induction

To induce osteoblast differentiation, cells were seeded at a density of 5×10^3 cells/cm^2 and cultured for 3 days. The medium was then changed to osteogenic induction (OI) medium according to **Table 2-5**. OI medium was changed every 3 or 4 days.

2.1.9 Radiation exposure

In this work, murine cells were exposed to different radiation qualities. X-rays were used as sparsely ionizing reference radiation for comparison with heavy charged particles.

2.1.9.1 X-irradiation

X-ray exposure was performed at German Aerospace Center (DLR) in Cologne, Germany. OCT-1 cells in the early exponential growth phase were placed on a horizontal plate in the X-ray generator RS225 and exposed to X-rays (200 kV, 15 mA) at the focus-object distance of 455 mm and with the copper filter (0.5 mm), yielding a dose rate of 1 Gy/min, determined by using the dosimeter UNIDOS webline. The irradiation chamber was preheated to 37 °C and kept at this temperature during irradiation. Control cells were treated similarly but without X-irradiation (mock irradiation).

2.1.9.2 Heavy ion irradiation

High-LET heavy ion irradiation was performed at the GSI Helmholtzzentrum für Schwerionenforschung GmbH located in Darmstadt, Germany or at the "Grand Accélérateur National d'Ions Lourds" (GANIL) in Caen, France (**Figure 2-1**). Cells were seeded at an initial density of 5×10^3 cells/cm^2 in 25 cm^2 cell culture flasks 2 days prior to exposure to heavy ions. For lead ion exposure, lumox™ dishes with a 50 µm polytetraethylene foil as growth surface were applied. Characteristics of the applied beams are shown in **Table 2-7**. Dosimetry was performed by the staff at the accelerator facilities (Hellweg *et al.*, 2011). Dose rates were adjusted to ~1 Gy/min. To convert fluence (F) to the absorbed dose (Gy), the following **Equation 2-1** was applied.

$$\text{Dose[Gy]} = 1.6 \times 10^9 \times \text{LET[keV/µm]} \times \text{F[P/cm}^2\text{]} \qquad \textbf{Equation 2-1}$$

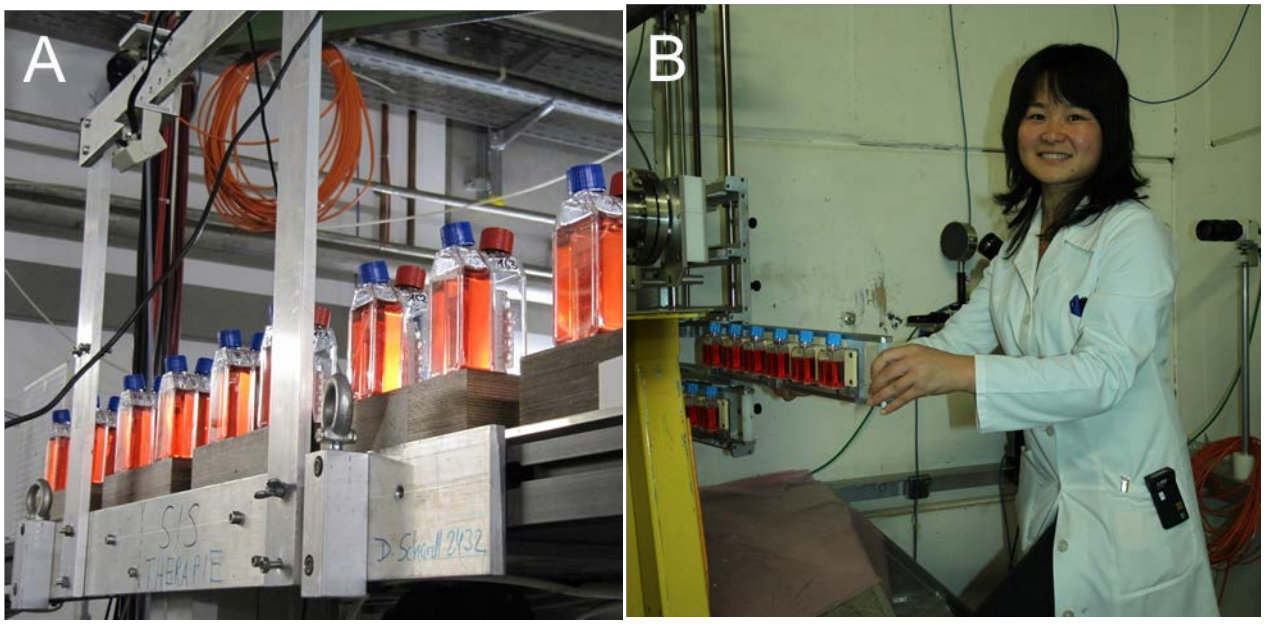

Figure 2-1 Experiment setup for heavy ion irradiation at GSI in Darmstadt (A) and GANIL in Caen, France (B)

Table 2-7 Characteristics of heavy ion irradiation

Ion	Location	Energy (MeV/n)	Energy on target[a] (MeV/n)	LET (keV/µm)	Average hits per cell nucleus	Dose range (Gy)
X-rays	DLR	0.2	0.2	0.5 – 3		0.5 – 12.0
^{13}C	GANIL	75	71	34	3.6 – 56.8	1.4 – 21.8
^{16}O	GANIL	95	91	51	0.9 – 21.3	0.5 – 12.1
^{13}C	GANIL	35	28	75	0.3 – 7.1	0.2 – 6.3
^{22}Ne	GANIL	80	75	92	0.2 – 5.4	0.2 – 5.7
^{48}Ti	GSI	1000	996	108	0.2 – 12.6	0.3 – 15.4
^{56}Fe	GSI	1000	997	150	0.3 – 2.3	0.5 – 3.9
^{58}Ni	GSI	1000	985	175	0.2 – 2.4	0.5 – 4.8
^{64}Ni	GSI	1000	985	175	0.5 – 4.0	0.9 – 7.7
^{36}Ar	GANIL	95	85	272	0.07 – 1.4	0.2 – 3.7
^{58}Ni	GANIL	75	56	905	0.2 – 2.1	2.0 – 23.6
^{209}Pb	GANIL	29	20	9674	0.009 – 0.6	1.0 – 62.0

[a] Effective irradiation energy at the cell monolayer after the energy losses in two detectors, the exit window, air (GANIL: 1 cm, GSI: 100 cm) and the bottom of the culture vessel (1200 mm polystyrene).

Immediately prior to irradiation, flasks were completely filled with serum free α-MEM or BME. Flasks were irradiated in an upright position at room temperature. Control samples were sham-irradiated by subjecting them to the same conditions, but without being irradiated.

2.1.9.3 Cell survival determination

Cellular survival was determined by the colony forming assay as established by Puck and Markus (Puck *et al.*, 1956). Cells were seeded and irradiated in 25 cm^2 flasks. The cell number to be seeded was determined according to the plating efficiency (PE) and the expected survival in order to obtain ~50 colonies per Petri dish. Immediately after radiation exposure, cells were trypsinized and plated in six Petri dishes (∅ 6 cm) per dose. Mock-irradiated cells were used as a control. After 10-12 days incubation time, culture medium was removed and they were gently washed with 1× PBS. The resulting colonies were fixed and stained with crystal violet solution. Next, dishes were washed with tap water and air dried overnight. Resulting colonies with more than 50 daughter cells were considered as survivors.

The survival fractions (S) were calculated by dividing the PE of irradiated cells (PE_{irr}) by the PE of mock-irradiated cells ($PE_{control}$) according to the **Equations 2-2** and **2-3**.

$$PE = \frac{\text{Colonies counted}}{\text{Cells seeded}} \qquad \textbf{Equation 2-2}$$

$$S = \frac{PE_{irr}}{PE_{control}} \qquad \textbf{Equation 2-3}$$

The resulting dose-effect curves are described by the following **Equation 2-4** and are characterized by the parameters D_0 and n (single hit multi target model) (**Figure 2-2**).

$$S = 1 - (1 - e^{D/D_0})^n \qquad \textbf{Equation 2-4}$$

(D: dose; D_0: reciprocal value of the slope within the linear part of the curve;
n: extrapolation number, obtained by extrapolating the exponential section of the curve to the abscissa.)

All data were compared by means of the t-test and fitted using a least squares linear regression analysis of ln $S_D/S_{D=0}$ versus dose. S_D and $S_{D=0}$ represent the surviving fractions of the irradiated and non-irradiated cells, respectively.

The RBE of different radiation qualities is described by the **Equation 2-5**. The absorbed dose (D) of a test radiation (D_{Test}) is compared to a reference radiation dose (D_{Ref}) that is assumed to cause the same biological effect. In order to determine the RBE for cell killing by heavy ions, X-rays (200 kV) were used as the reference radiation. The D_0 of the survival curves was used as measure of the cell killing effect.

$$RBE = \frac{D_{Ref}}{D_{Test}} \qquad \textbf{Equation 2-5}$$

(D_{ref} is the D_0 value of the X-ray survival curve; D_{test} is the D_0 of the tested radiation)

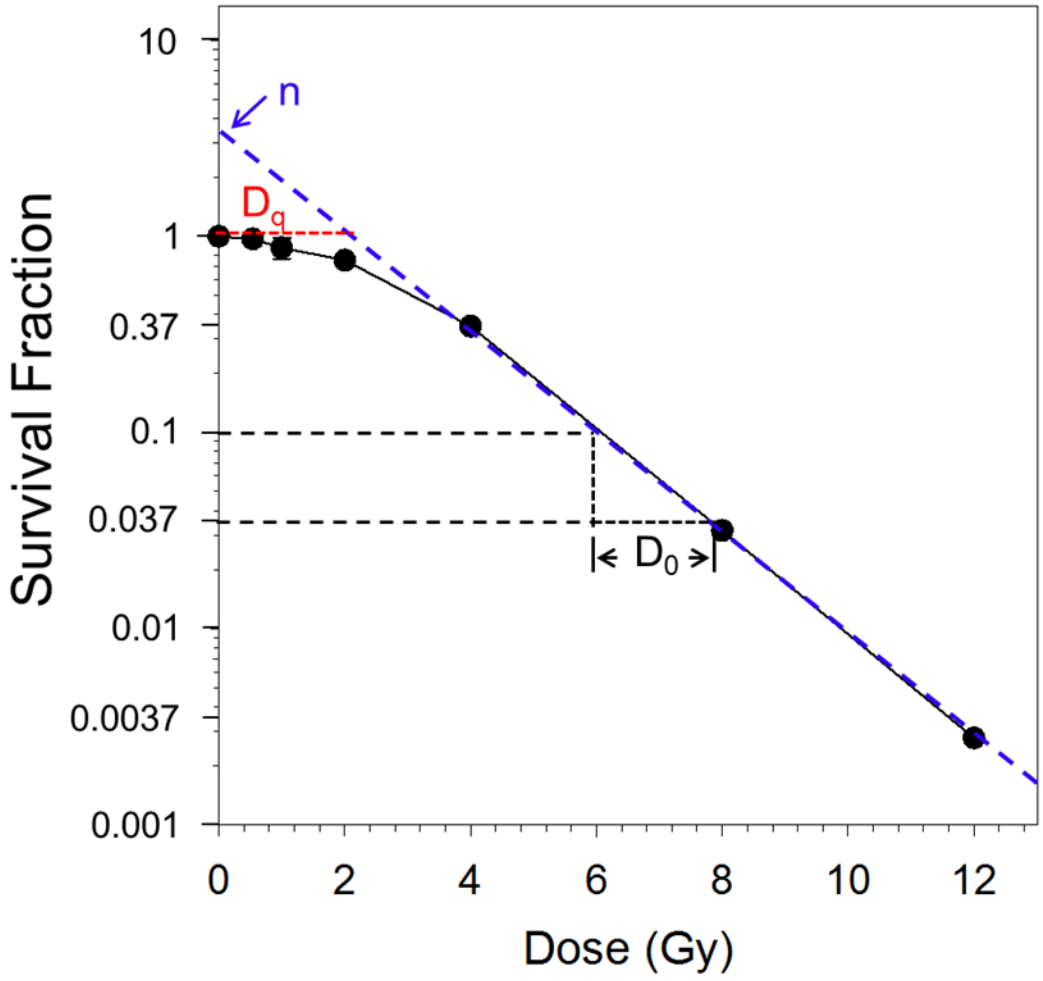

Figure 2-2 Single hit multi target model of a survival curve for mammalian cells exposed to ionizing radiation

The survival fraction is plotted on a logarithmic scale against dose on a linear scale. D_0 is the reciprocal of the curve slope (k) in the exponential part of the curve (D_0 = 1/k). The extrapolation number n results from extrapolation of the exponential part of the curve to the y-axis. The intersection of this extrapolated curve with the 100% survival line is the quasi-threshold dose D_q. This dose is required to inactivate all but the last target and can be defined by: - ln(n) = D_q/D_0.

2.1.9.4 DNA repair kinetics

Cells were seeded at a density of 5 × 10^3 cells/cm^2 in 25 cm^2 flasks and cultured for 3 days allowing about 80% confluence, and medium was changed with standard culture (SC) or OI medium. Cells were then incubated for 1, 2 or 3 weeks. SC or OI medium was refreshed twice a week. After the indicated time points, all flasks cells with freshly changed SC medium were irradiated and incubated for repair at 37 °C. After certain

incubation time periods, they were washed with cold PBS, kept on ice for 4 h, trypsinized and re-suspended in serum free medium at a concentration of 1×10^6 cells/ml. Then the cell suspension was mixed with an equal volume of 1% agarose; pipetted into 3-mm diameter glass tubes, and placed on ice to allow for solidification. The solidified cell-agarose suspension was extruded from the glass tubes and cut into 10 cylindrical blocks containing about 1×10^5 cells/block. The blocks were then placed in lysis buffer and incubated first at 4 °C for 45 min and then at 50 °C for 16-18 h. After agarose block washing for 1 h at 37 °C in a buffer containing 10 mmol/l Tris (pH 8.0) and 0.1 mol/l EDTA, treatment for 1 h at 37 °C in the same buffer, at pH 7.5, with 0.1 mg/ml Rnase A, followed. The asymmetric field inversion gel electrophoresis (AFIGE) was applied (DiBiase *et al.*, 2000). This method is a modification of field inversion gel electrophoresis which uses periodically reversal of electric field directions (180 degree change). AFIGE was carried out in 0.5% agarose in the presence of 0.5 mg/ml ethidium bromide, in 0.53 × TBE at 10 °C for 40 h. During this time, cycles of 1.25 V/cm for 900 s in the direction of DNA migration alternated with cycles of 5.0 V/cm for 75 s in the reverse direction. AFIGE gels stained with ethidium bromide were imaged using a PhosphorImager (Molecular Dynamics).

To determine DNA damage, the fraction of activity released (FAR) was calculated. To estimate an equivalent dose (Deq) for each FAR value, dose response curves were generated and utilized (Windhofer *et al.*, 2007; Wu *et al.*, 2008).

The FAR as a measure of DNA DSBs in irradiated and non-irradiated samples were plotted (**Figure 2-3**) against the dose. From this graph, the equivalent doses (Deq) were derived. Repair kinetics were plotted as Deq versus time.

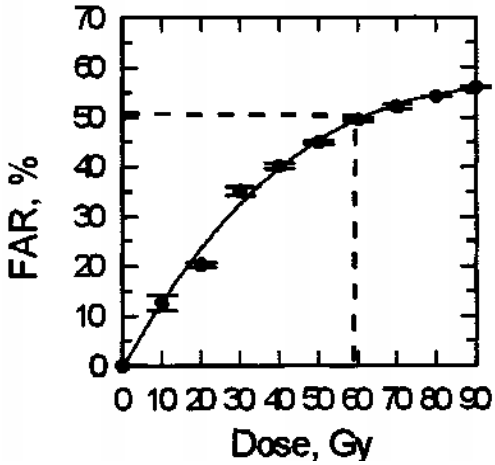

Figure 2-3 Example of a dose effect curve for DNA DSB induction determined by AFIGE

The fraction of activity released (FAR) as a measure of DNA DSBs in X-irradiated exponentially growing wild-type DT40 cells was determined immediately after irradiation. A dose of 60 Gy results in a FAR of 50 % (Wang *et al.*, 2001).

2.1.10 Senescence-associated β-galactosidase assay

The expression of senescence-associated β-galactosidase (SA-β-gal) was determined by cytochemical staining. OCT-1 cells were seeded at a density of 3 × 10^3 cells/cm^2 in Petri dishes (∅ 3 cm) and cultured for up to 6 days in SC and OI medium. After an incubation time of 6 days, cells were washed once with cold PBS and fixed in 70% ethanol for 15 min at room temperature (pH 6.0). After fixation, the cells were stained with freshly prepared 2 ml 1 × SA-β-gal detection solution (X-gal solution, staining solution A (contains potassium ferrocyanide, potassium ferricyanide) and staining solution B (contains sodium phosphate dibasic, citric acid monohydrate)) over night at 37 °C. For long-term storage of the stained samples at 4 °C, the complete staining solution was removed and the cells were overlaid with 70% glycerol in PBS. The stained cell monolayer was visualized under the light microscope Axiovision 135 and pictures were taken with the camera MRc5.

2.1.11 Proliferation analysis

OCT-1 cells were plated at a density of 3 × 10^3 cells/cm^2 (n= 8/ treatment group) in strip well plates and irradiated after 24 h. After the serial incubation time points, cells were fixed with 0.1 ml 3.5% FA in PBS per well at 4 °C for 30 min and stained with 0.1 ml

bisbenzimide Hoechst 33342 per well (10 µmol/l) for 15 min, protected from light. Cellular DNA content was then measured with the Lambda plate reader by reading the bisbenzimide fluorescence using the excitation/emission filter combination 360/40 + 460/40 nm with the optics in bottom position.

2.1.12 Cell cycle analysis

2.1.12.1 Sample preparation

To analyze cell cycle regulation, cells were seeded at a density of 5×10^3 cells/cm^2 two days ahead in order to obtain exponentially growing cells at the time of radiation exposure. After irradiation, cells were incubated for up to 96 h. Then cells were harvested by gentle trypsinization followed by immediate mixing with ice-cold 100% ethanol (with a final ethanol concentration of 75%) and fixation over night at -20 °C.

Propidium iodide (PI) was used for DNA content/cell cycle analysis. PI passes through a permeabilized cell membrane and intercalates into the major groove of double-stranded DNA and produces a highly fluorescent adduct with a broad excitation peak at 538 nm and fluorescence emission centered around 619 nm. It can be excited by the 488 nm argon laser of the flow cytometer. RNAse is used for optimal DNA resolution since PI can also bind to double-stranded RNA.

After fixation, ethanol was diluted with 8 ml PBS and the cells were centrifuged at 500 × g for 5 min. The supernatant was removed, and the cell pellets were gently mixed in the PI staining solution and incubated at 37 °C for 30 min.

2.1.12.2 Flow cytometric analysis

Measurement of cellular DNA content and the analysis of the cell cycle were performed by flow cytometry. A flow cytometer enables the fast and differentiated analysis of a heterogeneous cell population with respect to fluorescence intensity, cell size, shape and internal complexity. The principle of the cell cycle analysis by PI staining is that the stained material has incorporated an amount of dye proportional to the content of DNA. Initially, a fluorescent dye that binds the DNA is added to a suspension of permeabilized single cells or cell nuclei. The stained material is then measured in the flow cytometer and the emitted fluorescence signal yields an electronic pulse with a height proportional

to the total fluorescence emission from the cell. Thereafter, these fluorescence intensities are considered to be a measure of the cellular DNA content. The distribution of cells in the various cell cycle phases was identified by this determination of the relative cellular DNA content.

The distinct phases of cellular division in a proliferating cell population are: the G1 (cells are active, growing and receptive to signals to begin DNA synthesis), S (DNA synthesis phase), G2 (cells are actively preparing for mitosis and contain twice the amount of DNA) and M phase (Mitosis occurs in the M phase which results in cell division and normal DNA content). G2 and M phases could not be discriminated based on both of them having the identical amount of DNA.

The thoroughly suspended cells are directed through a very thin capillary to separately pass a laser beam. In direction of the beam, a photodiode converts forward scattered light into electrical impulses (called FSC, forward scatter). At right angle to the laser beam, four sensors behind optical filters detect the sideward scattered light (called SSC, side scatter) and fluorescence signals (FL-1 to FL-3). The PI stained events were detected in the FL2-H channel. The results were displayed as histogram (one-parameter-dependency) and topographically as a dot plot (two-parameter-dependency). Flow cytometric analysis with 10,000 events counting was performed.

2.1.12.3 Cell cycle data evaluation

The results were analyzed with Flowing Software 2.5.0 for flow cytometry data analysis. A dot plot of FSC and SSC from the raw data was created, and the region of intact cells was inserted (**Figure 2-4 A**). The SSC-PI plot was created for the SSC on the y-axis versus the fluorescence signal PI on the x-axis and linked to the FSC-SSC plots (**Figure 2-4 B**). A histogram was created and linked to the SSC-PI plots (**Figure 2-4 C**). Only cells gated in Figure 2-4 B were displayed in a histogram of the fluorescence signal in FL-2 (FL2-H). G1, S and G2/M phases were defined by markers in this histogram. The percentage of cells in G1, S and G2/M phases was calculated from the number of events within the three histogram markers defined by the fluorescence signal.

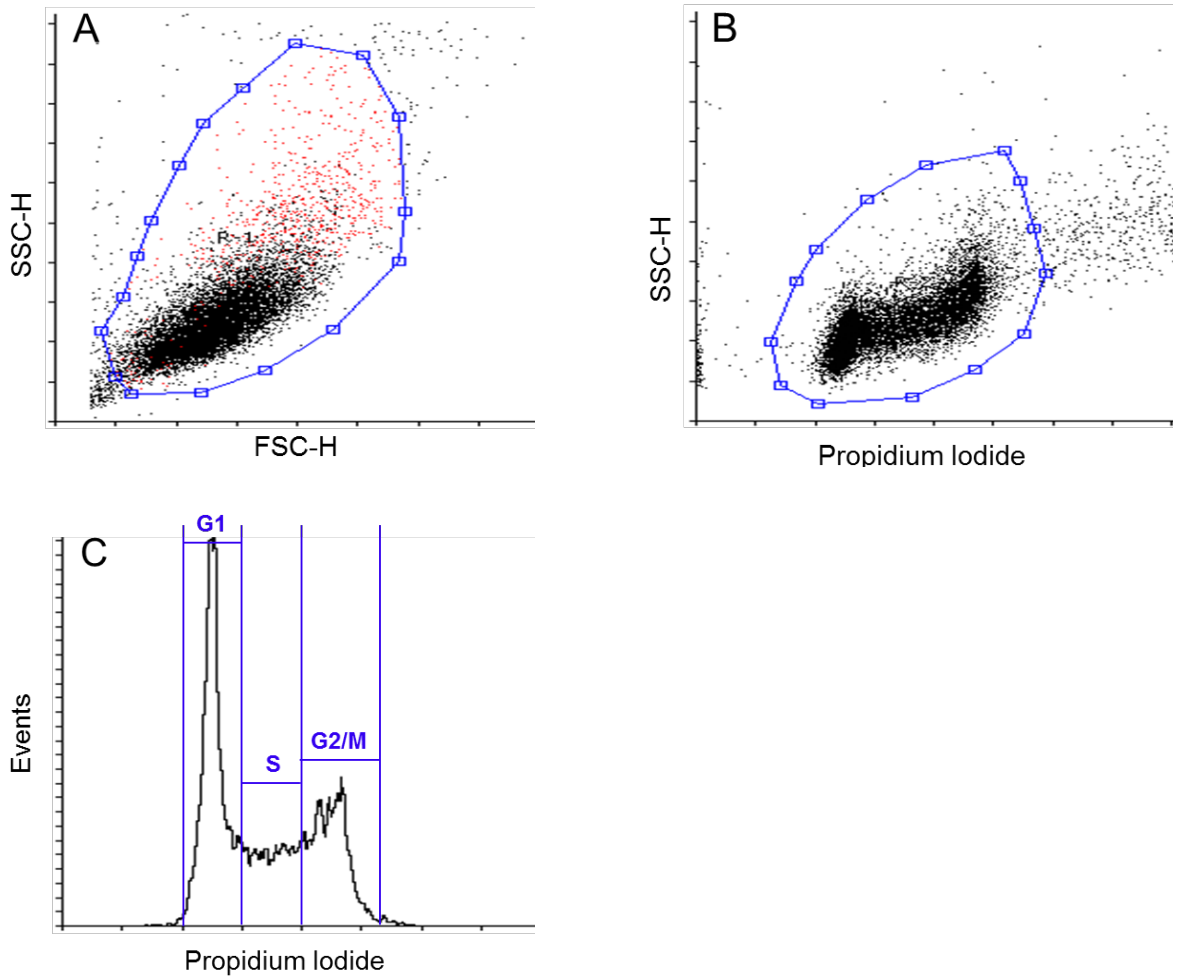

Figure 2-4 Cell cycle flow cytometry data analysis

The region of living and single cells was set manually in the FSC-H/SSC-H dot plot (A) and the PI-SSC dot plot (B). Markers for the cell cycle phase were defined in the propidium iodide fluorescence histogram showing the gated cells (C). Markers and regions were set by means of untreated control samples.

2.1.13 Gene expression analysis

Reverse transcription real-time quantitative polymerase chain reaction (RT-qPCR) was applied for the gene expression analysis. The basic goal of qPCR is to precisely measure specific nucleic acid sequences even in a very small quantity. If no reagents are limiting, 2^n copies of the target DNA fragment can be obtained after n PCR cycles. In addition, real-time PCR can read the fluorescence signal during this amplification.

Because DNA polymerase cannot utilize RNA as a template, the conversion of mRNA to DNA is needed before and can be achieved using the enzyme reverse transcriptase.

Changes in mRNA expression after exposure to ionizing radiation were analyzed. The examination of gene expression profiles was performed using a two-step real-time RT-qPCR method after RNA isolation and quality control.

2.1.13.1 RNA Isolation

Cells were seeded in 25 cm^2 flasks or in Petri dishes (∅ 6 cm) for culturing up to 21 days under standard or osteogenic conditions. Culture medium was refreshed every 3-4 days.

Total cellular RNA was collected by using the RLT buffer of the Rneasy Plus Mini Kit. Syringes, needles and 1.5 ml Eppendorf tubes were pre-cooled at -20 °C. Medium was removed from the culture vessels completely before adding 600 µl RLT buffer (containing 10 µl/ml β-mercapto-ethanol). Lysed cells were then collected by using a cell scraper. To homogenize, the cell lysate was passed 5 times through a 20-gauge needle (0.9 mm diameter). Samples were immediately frozen at -80 °C.

Total cellular RNA was isolated using an Rneasy Plus Mini kit according to the manufacturer's specifications (QIAGEN, Hilden, Germany). The isolated RNA was eluted with 30 µl RNAse free water. The integrity of RNA was then assessed by using the lab-on-chip Bioanalyzer 2100. Only samples with RNA integrity numbers (RIN) higher than eight were used for downstream applications (**Figure 2-5**).

2.1.13.2 Reverse transcription

The reverse transcription (RT) was performed in a final volume of 20 µl containing 500 ng RNA, using the iScript™ cDNA Synthesis Kit. A mock reverse transcription control (RT-) was produced with RNA without reverse transcriptase. The RT was run in the MiniCycler™ with the following program: 25 °C for 5 min, followed by synthesis at 42 °C for 30 min, denaturation at 85 °C for 5 min and 4 °C for 5 min. After the RT program was finished, samples were kept in -20 °C.

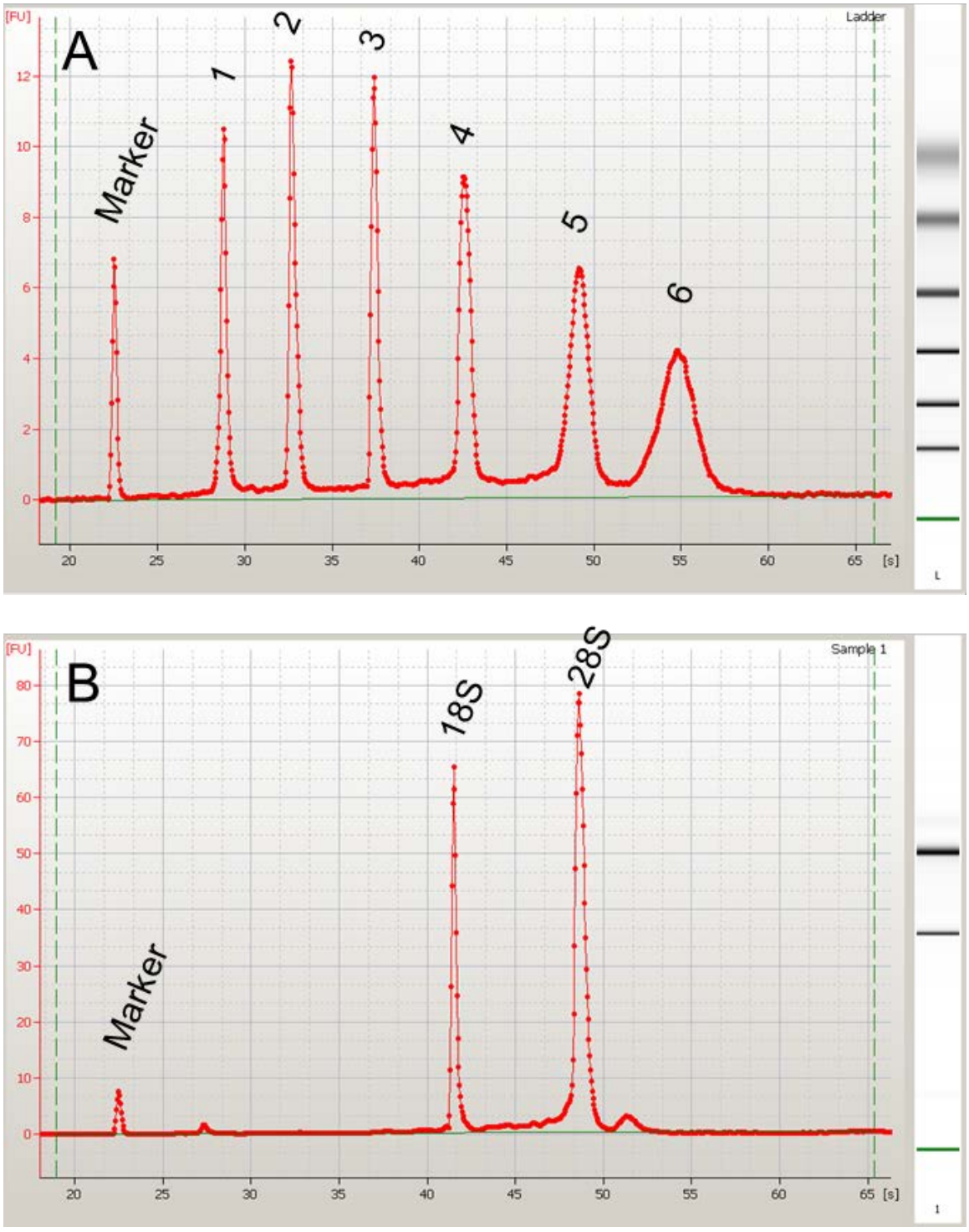

Figure 2-5 Electropherogram analysis

The electropherograms result from micro-electrophoresis of a RNA ladder (a) and an intact RNA sample (b) using the Bioanalyzer. FU, fluorescence units, s, seconds. The seven characteristic regions of the ladder and 3 regions in the sample are marked (Schroeder *et al.*, 2006).

2.1.13.3 Realtime qPCR

qPCR was performed by using a SYBR Green based detection system. Fluorescence of SYBR Green-DNA complexes was measured by the DNA Engine Opticon2 System during cycling.

The reaction mix had a total volume of 25 µl and contained ready to use cocktail 1 × reaction mix (Platinum® SYBR® Green qPCR SuperMix-UDG), 0.2 µmol/l specific forward and reverse primer, 20 ng cDNA, and RNAse free water to fill up to the final volume of 25 µl.

The PCR conditions were optimized for the specific primers. The primer sequences are given in **Table 2-8**.

The amplification was performed under following conditions: a single step of pre-denaturation at 50 °C for 30 min; initial denaturation at 94 °C for 2 min; 44 cycles of 94 °C for 15 s, specific primer annealing temperature (T_A) for 30 s, 72 °C for 30 s, plate reading, 78 °C for 20 s and then plate reading was performed; afterwards melting temperature was measured by reading every 0.2 °C for 3 sec from 95 °C to 60 °C.

Table 2-8 Primer sequences for PCR of cell cycle regulating genes and reference genes

Gene		Sequence	Annealing temperature (T_A) (°C)	Gene bank accession
B2M	Forward Reverse	CCG TCT ACT GGG ATC GAG AC GCT ATT TCT TTC TGC GTG CAT	59.1	NM_009735
CDKN1A	Forward Reverse	TTG CAC TCT GGT GTC TGA GC TCT GCG CTT GGA GTG ATA GA	59.1	NM_007669
GAPDH	Forward Reverse	GTG GAC CTC ATG GCC TAC AT TGT GAG GGA GAT GCT CAG TG	59.2	NM_008084
Mdm2	Forward Reverse	CGG CCT AAA AAT GGT TGC AT TTT GCA CAC GTG AAA CAT GAC A	57.4	NM_010786
TP53	Forward Reverse	TGA AAC GCC GAC CTA TCC TTA GGC ACA AAC ACG AAC CTC AAA	56.0	NT_096135

Threshold cycle (C_t) values were calculated using the Opticon2 software (**Figure 2-6**). For each primer set, the standards (by a series of cDNA dilutions), a no template control (NTC), and the mock reverse transcription control RT- were included.

Beta-2-microglobulin (B2M) and glyceraldehyde-3-phosphate dehydrogenase (GAPDH) were chosen as reference genes for contrasting function and abundance in various tissues and cells with significant differences in gene expression levels.

The authenticity of the PCR products was verified using melting curve analysis (**Figure 2-7**).

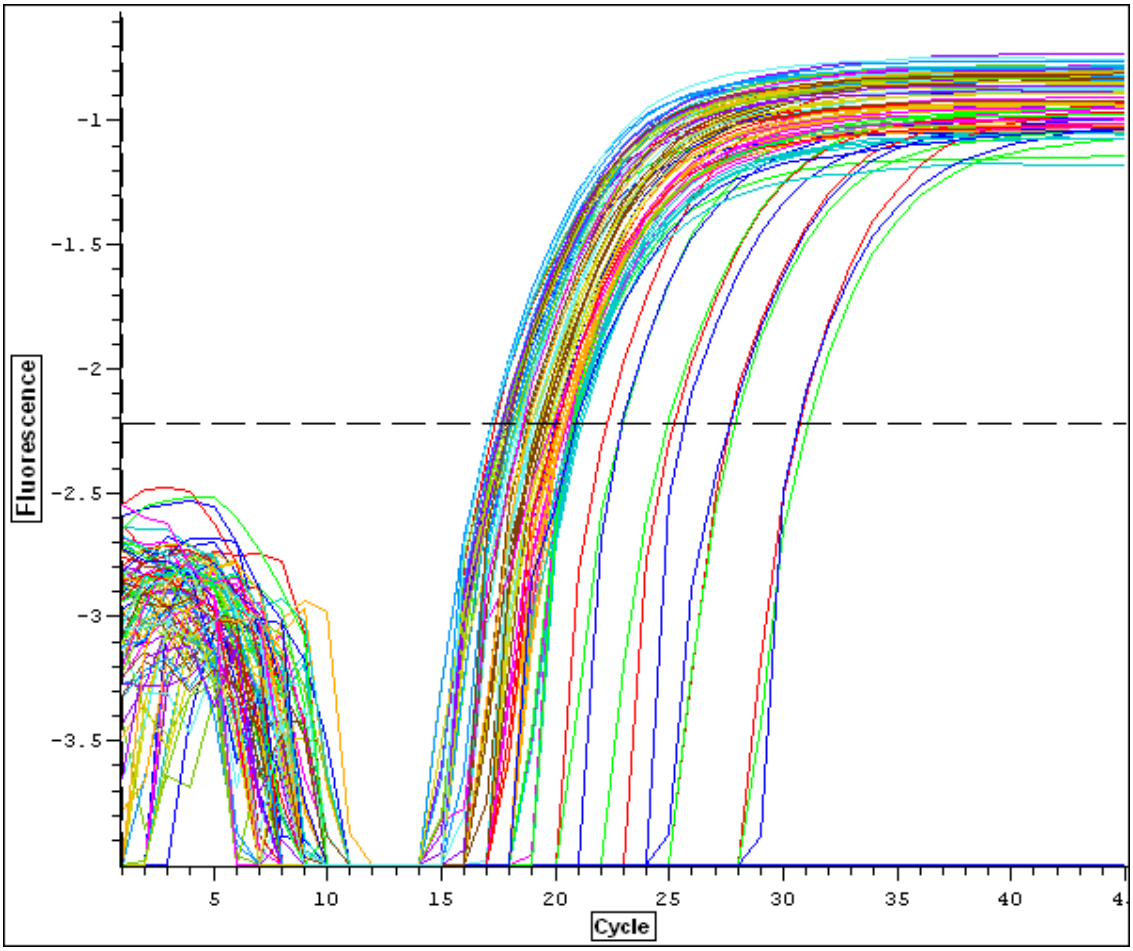

Figure 2-6 Real time qPCR amplification plots

Real time qPCR amplification plots of B2M (samples of ^{56}Fe experiment, LET 150 keV/µm). The fluorescence is increasing with the PCR cycle. The number of the cycle during which the threshold was crossed is the C_t value. The threshold was set manually in the early exponential phase of the DNA amplification plots, above the background fluorescence of the first 10-15 PCR cycles (dotted line).

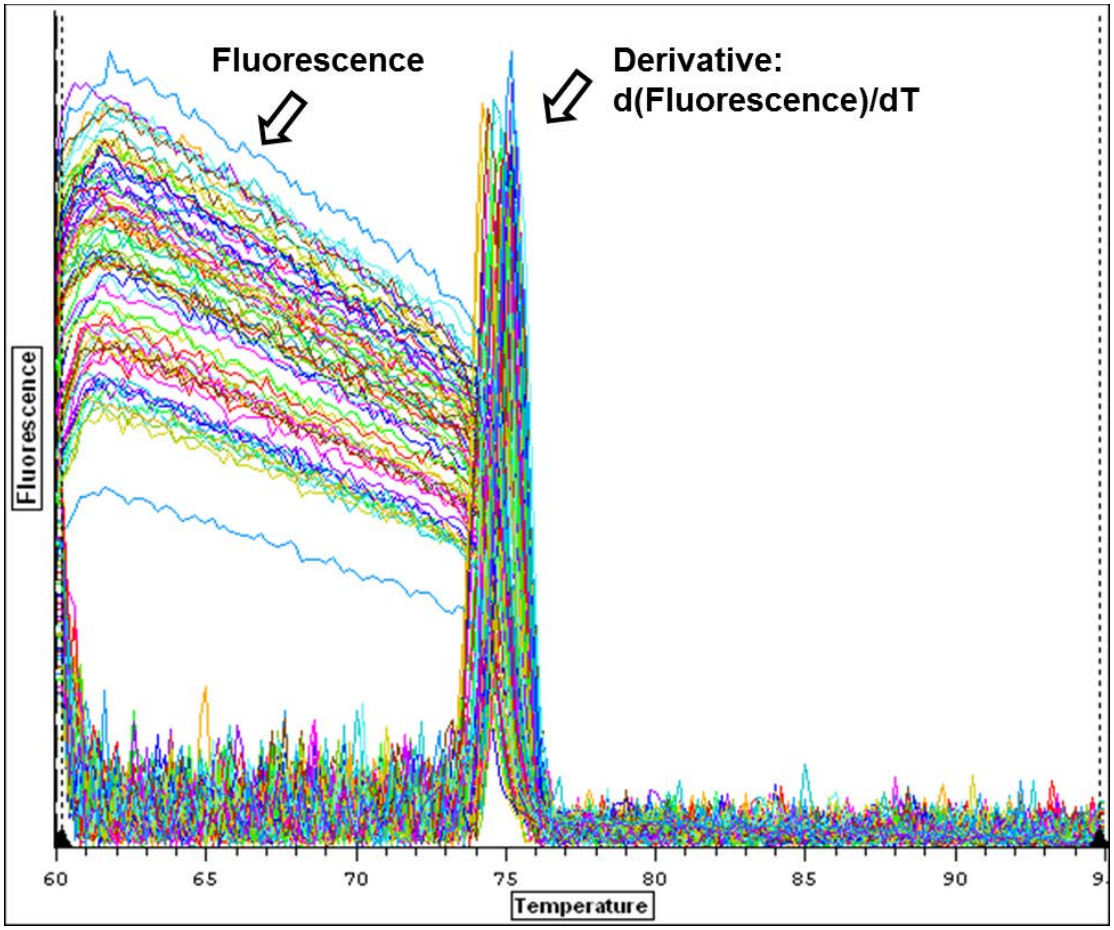

Figure 2-7 Melting curves of real time PCR

Melting curves of real time PCR products of B2M (samples of ^{56}Fe experiment, LET 150 keV/µm). The fluorescence is decreasing during heating and dissociation of the DNA. The first derivative curves of fluorescence show a single, sharp peak, suggesting that only one specific PCR product was generated.

2.1.13.4 Relative quantification of gene expression levels

Relative quantification of gene expression was based on calculation of the efficiency-corrected ΔC_t for the gene of interest in relation to references genes. The C_t values were corrected for the efficiency of the qPCR reaction (EFF). The qPCR efficiency was determined using a dilution series of a pool of cDNA from all samples (2-3 µl per sample) of the experiment. The slope of the resulting standard curve (**Figure 2-8**) was used to calculate qPCR efficiency according to **Equation 2-6** (Rasmussen, 2001).

$$EFF = 10^{-1/slope} \qquad \textbf{Equation 2-6}$$

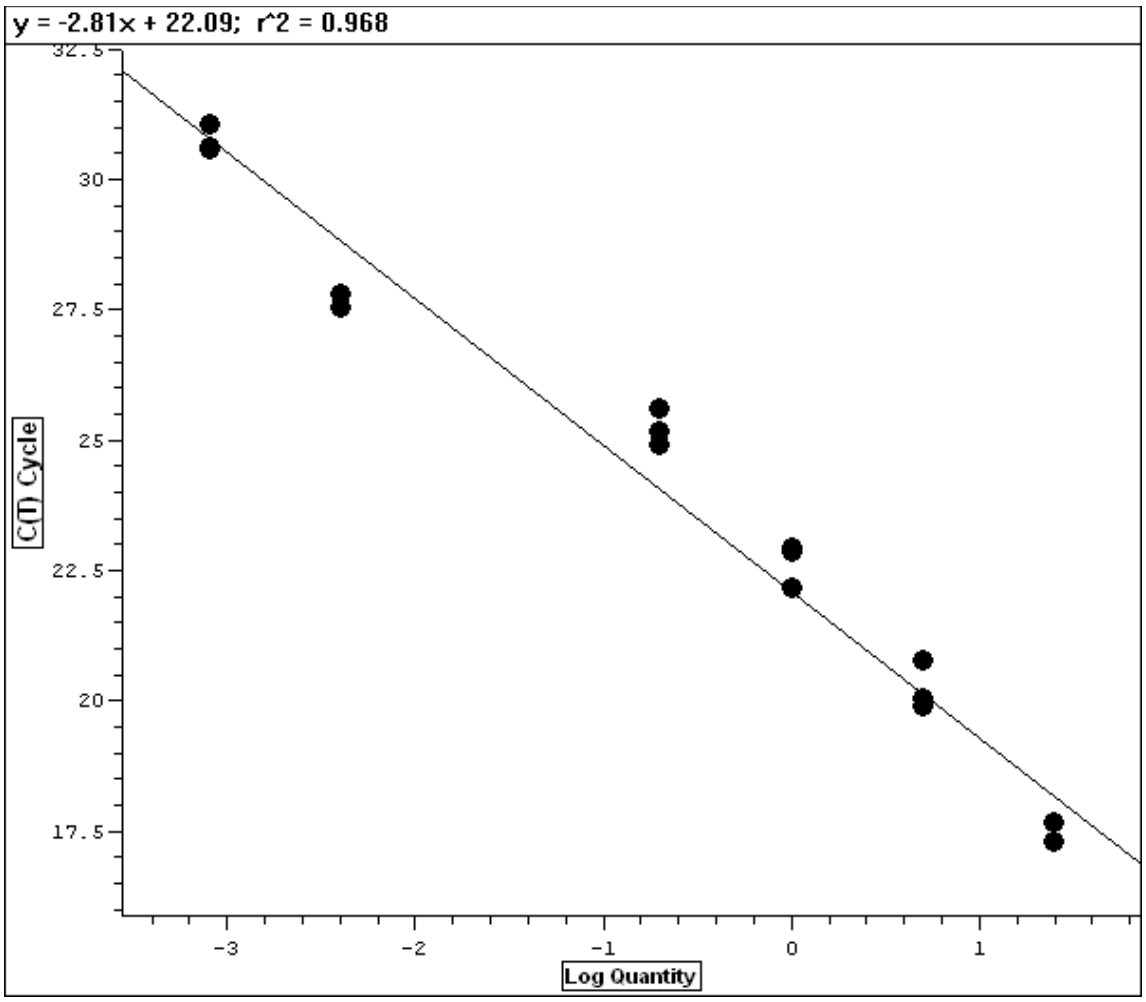

Figure 2-8 Real time PCR standard curve

Real time PCR standard curve of B2M (samples of ^{56}Fe experiment, LET 150 keV/µm). The slope of the standard curve is -2.81, and the regression coefficient r^2 is 0.968.

The mean C_t values were calculated from triplicate measurements. Relative quantification was performed by measuring the difference in copy numbers between two samples that had been normalized to an endogenous reference gene (housekeeping gene). Changes in gene expression levels of specified transcripts are measured and described in arbitrary units relative to the level of reference transcripts within the same sample.

Relative expression levels of all investigated genes were determined using the REST-MCS© software (Pfaffl *et al.*, 2002). This software normalizes target gene expression against the expression of the reference genes B2M and GAPDH according to **Equation 2-7**

and performs a pair wise fixed reallocation randomization test as significance test. Reference genes were selected by using BestKeeper software (Pfaffl *et al.*, 2004).

$$\text{Regulation} = \frac{(E_{\text{Target}})^{\Delta Ct_{\text{target}}(\text{Mean}_{\text{control}} - \text{Mean}_{\text{sample}})}}{(E_{\text{Reference}})^{\Delta Ct_{\text{Reference}}(\text{Mean}_{\text{control}} - \text{Mean}_{\text{sample}})}} \qquad \textbf{Equation 2-7}$$

2.1.14 Assessment of extracellular matrix mineralization

2.1.14.1 Alizarin red S staining

OCT-1 cells were seeded at a density of 3×10^3 cells/cm^2 into Petri dishes (∅ 6 cm^2) 3 days before irradiation. The cells were irradiated as described in 2.1.9 and a medium change (SC/OI medium) was performed afterwards. The cells were then cultured for up to 21 days. Since the calcium usually co-precipitates with the phosphate ion also under *in vitro* culture conditions, mineralized matrix can be visualized histochemically via Alizarin red S staining reaction with the calcium portion to form a chelate (Wang *et al.*, 2006b). To estimate the amount of mineralized tissue formed in each culture, fixed cultures were stained with Alizarin red S solution. After the incubation time, cells were washed once with PBS and fixed in 70% ethanol for 20 min at room temperature. The cells were rinsed in *aqua bidest.*, then stained with 2% Alizarin red S (pH 4.2) for 20 min, and followed by rinsing twice with *aqua bidest.*, extensively washed with ethanol to mitigate the non-specific staining, and then immediately scanned with the ImageQuant^{TM} LAS 4010 (trans-illumination, 1 s exposure time).

2.1.14.2 Quantification of mineralized extracellular matrix

In order to quantify the mineralized extracellular matrix stained with Alizarin red S, Image J was used. The mineralized material was measured by analyzing the red saturation of the surface area. In each image, five measurements were taken in different areas within the image. The same area size and position were applied for each image. The arithmetic means of five measurements were calculated and plotted by using Sigma Plot 12.0.

2.1.15 Immunofluorescence staining

In order to visualize TGF-β1, Runx2, p53 and Mdm2 protein expression, immunofluorescence staining of irradiated cells was performed.

Cells were seeded in chamber slides (16 wells) at a density of 5×10^3 cells/cm^2. Then cells were incubated at 37 °C for 48 h under standard cell culture conditions. After treatment with ionizing radiation and/or with the p53 inhibitor cyclic pifithrin-α, the cells were fixed for immunofluorescence analysis. For multiple time-points, observed samples were fixed and stored at 4 °C until all samples were ready.

For staining, chamber slides were first washed 3 times with 0.2 ml 1 × PBS per well. In the following, cells were permeated for 10-15 min on ice with 0.1 ml of 0.5% Triton X-100 with 1% BSA in PBS. Then cells were blocked with 0.2 ml 50% FBS in PBS for 1 h at room temperature (alternative: overnight at 4 °C) and followed by incubation with the primary antibody (**Table 2-9**) for 1 h at room temperature (alternative: overnight at 4 °C), preventing drying out by sealing the chamber slides with parafilm.

Table 2-9 Primary antibodies

Antigen	Product code	Species	Supplier	Working dilution	Cross reactivity
TGF-β1	sc-146	Rabbit	Santa Cruz Biotechnology	1:200	Mouse, rat, human, *Xenopus laevis*
RUNX2	sc-10758	Rabbit	Santa Cruz Biotechnology	1:200	Mouse, rat, human
p53	PAB421	Mouse	Millipore	1:500	Human, monkey, mouse, rabbit, rat
Mdm2	MAB3776	Mouse	Millipore	1:500	Human, mouse, rat

After 3 times washing with 0.2 ml PBS with 1% BSA, the secondary antibody (**Table 2-10**) was diluted and incubated on a shaker (30 RPM (Revolutions per minute)) for 1 h in the dark. After 3 times washing with 1% BSA PBS solution, DAPI-solution was added and the slides were incubated at 37 °C for 15 min. The chamber wall was removed from the slide. A cover glass was then fixed with mounting medium on the slide.

The samples were investigated under a fluorescence-microscope (Zeiss Axio Imager M2) (Excitation/Emission: Cy5, 646 nm/664 nm; FITC, 495 nm/517 nm; DAPI, 360 nm/460 nm).

Table 2-10 Secondary antibodies

Antibody conjugate	Product code	Species	Supplier	Working dilution
Cy5 anti-mouse IgG	PA45010	Goat	GE Healthcare	1:250
FITC anti-rabbit IgG	SC-2090	Donkey	Santa Cruz Biotechnology	1:250
FITC anti-mouse IgG	821 462	Sheep	Boehringer	1:250

2.1.16 Statistical analyses

X-irradiation experiments were performed ≥3 times. Heavy ion experiments were performed according to beam time availability. Standard errors were calculated to account for differences in the number of replicates and the repetition of experiments. Means, standard errors, and significance levels (t-tests) were calculated with Microsoft® Office Excel 2010. Results are presented as mean ± standard error (SE). Statistical significance between different samples was determined with two-tailed Student's t-tests. In the result section, significant differences between two treatments are represented by the probability (p) of the assumption that the null hypothesis is true (*, $p < 0.05$; **, $p < 0.01$; ***, $p < 0.001$).

3. Results

This study was aimed at determining the effects of ionizing radiation on bone forming osteoblast cells.

Firstly, the effects of different qualities of ionizing radiation on pre-osteoblasts were determined. Cell killing by different ionizing radiation qualities was assessed indirectly by determining the cellular survival after irradiation. To compare the cell killing effect of exposure to energetic heavy ions to that of the reference radiation, low-LET X-rays, the relative biological effectiveness (RBE) for reducing the reproductive survival fraction to 37% was calculated.

After ionizing radiation exposure, in order to survive and maintain the genomic stability, cell cycle checkpoints can be activated and will allow cells to repair the ionizing radiation induced DNA damage, mediate cell fate including differentiation. Therefore, in this study, cell cycle regulation was analyzed. The influence of different radiation qualities was compared on equal survival level for cell cycle arrest and mRNA expression of the cell cycle regulator CDKN1A. The encoded protein p21 is one of the transcriptional targets of p53 which can respond to radiation induced DNA damage. In the following, the role of p53 in cell cycle regulation after irradiation was also studied by applying cyclic pifithrin-α.

The influence of ionizing radiation on OCT-1 osteogenic differentiation was analyzed by determining the calcium deposition of cells cultured in OI medium up to 21 d after radiation exposure. In order to study the impact of the OI medium on the radiation response of osteoblasts, cellular survival, repair kinetics and proliferation were addressed. Furthermore, early differentiation was investigated by visualizing the markers TGF-β1 and Runx2 shortly after irradiation; the role of p53 in radiation-induced bone cell differentiation was also examined by applying its reversible inhibitor cyclic pifithrin-α.

3.1 Effects of ionizing radiation on the cellular survival of pre-osteoblasts

In order to identify the survival ability of pre-osteoblasts after exposure to ionizing radiation, the colony forming ability of OCT-1 cells was determined. The survival level after exposure to space relevant radiation with a large range of linear energy transfer (LET) was compared to that after exposure to X-rays.

For comparison of the radiosensitivity of pre-osteoblasts and mesenchymal stem cells, the survival ability of C3H10T1/2 cells after exposure to selected radiation qualities was determined. These cells can also differentiate into osteoblasts, but are not yet committed to the osteoblast lineage.

3.1.1 Cellular survival of OCT-1 cells after exposure to different radiation qualities

After exposure to ionizing radiation, clonogenic survival of OCT-1 cells was determined using the colony forming ability assay as established by Puck and Marcus (1956).

The results show that radiation with different LET reduces the cellular survival fraction in a dose-dependent manner (**Figure 3-1**).

After X-ray exposure, the survival curve shows an initial shoulder region. In this dose range, DNA repair can eliminate potentially lethal damage. The shoulder is followed by an exponential decrease.

The survival curves after exposure to densely ionizing heavy ions show no or only a very slight shoulder prior to the exponential decrease of survival with radiation dose. The slope of the curves depends on the radiation quality (LET) (**Figure 3-1**). Up to an energy loss of 150 keV/µm, the slope decreases with LET (**Figure 3-1 A**); at higher LETs, the slope increases sharply (**Figure 3-1 B**).

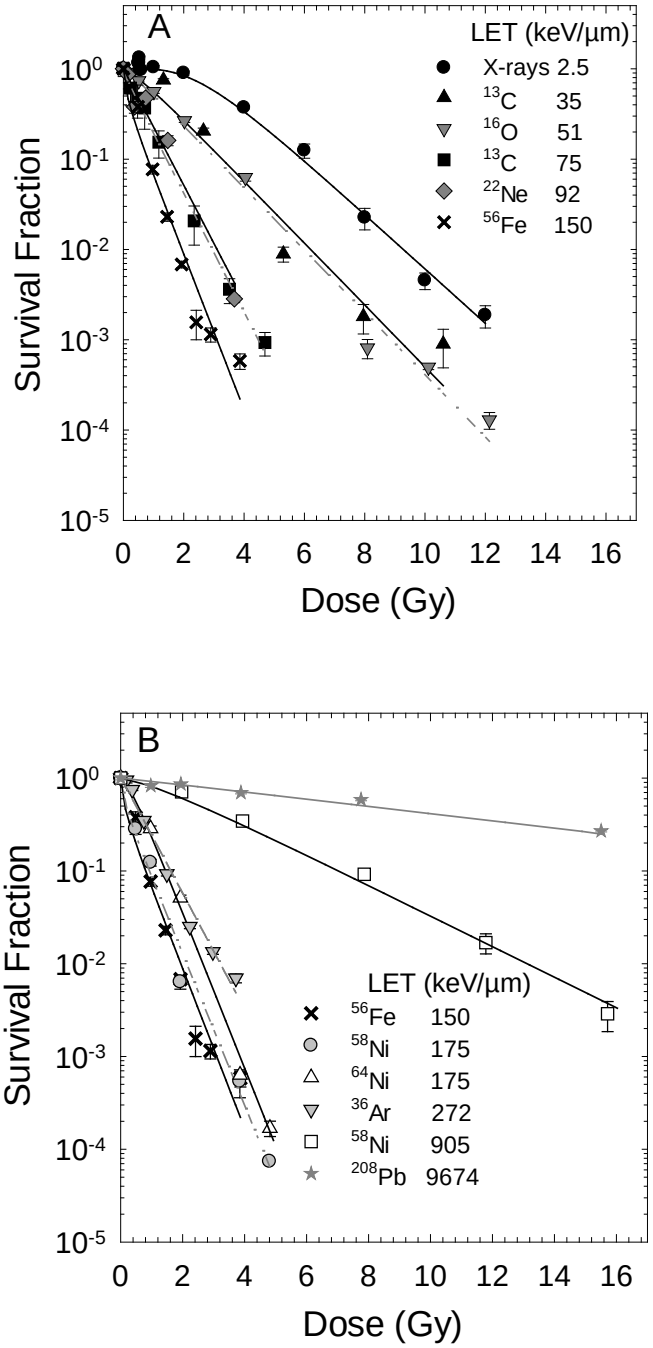

Figure 3-1 Survival curves of OCT-1 cells exposed to low-LET X-rays or high-LET accelerated charged particles

Survival curves of OCT-1 cells exposed to low-LET X-rays (5 independent experiments with each 6 replicates) or high-LET accelerated charged particles (1 independent experiment with each 6 replicates). Survival curves were fitted according to the equation $S = 1-(1-e^{D/D_0})^n$. D, dose; D_0, reciprocal value of the slope within the linear part of the curve; n, number of targets. Curve slopes increase up to LET values of approximately 150 keV/µm (A) and then decrease (B).

3.1.2 Relative efficiency of OCT-1 cell killing by different radiation qualities

In order to compare the survival curves resulting from exposure of OCT-1 cells to different radiation qualities, three parameters of the dose-effect curves were calculated.

In this context, the extrapolation number n was obtained by extrapolating the exponential portion of the curve to the y-axis. X-rays display a higher n value with 6.37, compared to all other tested radiation qualities (0.63-1.31).

D_q is the quasi-threshold dose required to inactivate all but the last targets (Hall 2000). For X-rays and ^{58}Ni ions (LET 905 keV/µm), the D_q values are 2.66 Gy and 0.63 Gy, respectively. The D_q values of other radiation qualities are mostly around 0 Gy (**Table 3-1**).

D_0 is defined as 37% survival dose in the linear section of the survival curve. The D_0 for OCT-1 cells after X-ray exposure was 1.44 Gy. When LET values increased up to 150 keV/µm, D_0 values decreased down to a value of 0.48 Gy. The D_0 increased for heavy ions with an LET above 150 keV/µm, reaching a value of 11.44 Gy for lead ions with an LET of 9674 keV/µm (**Table 3-1**).

The RBE for killing of OCT-1 pre-osteoblasts by the investigated radiation qualities was calculated using the D_0 of the survival curves. X-rays were used as reference radiation.

The RBE increases from 1.00 for X-rays to 3.03 for ^{56}Fe ions with augmenting LET up to 150 keV/µm, and then decreases to 0.13 for ^{208}Pb ions with an LET of 9674 keV/µm (**Table 3-1**). This reflects that radiation qualities with an LET of about 150 keV/µm are most effective in killing pre-osteoblast cells. The RBE values plotted on a linear scale against LET on a logarithmic scale reveal a distinct peak of around 3.0 at an LET of about 150 keV/µm (**Figure 3-2**).

Table 3-1 Parameters of the survival curves (n, D_q, D_0, $D_{1\%}$) and RBE of different ion species in OCT-1 cells (sorted from smallest to largest LET)

Ion species	Energy (MeV/n)	LET in H_2O (keV/µm)	n	D_q (Gy)	D_0 (Gy)	$D_{1\%}$ (Gy)	RBE (D_0)
X-rays	0.2	0.3-3	6.37 ± 2.61	2.66 ± 0.69	1.44 ± 0.09	6.62	1.00
^{13}C	75	35	1.12 ± 0.67	0.15 ± 0.70	1.30 ± 0.15	6.00	1.10
^{16}O	95	51	1.11 ± 0.28	0.13 ± 0.31	1.30 ± 0.06	5.98	1.11
^{13}C	35	75	1.19 ± 0.19	0.14 ± 0.13	0.79 ± 0.04	3.62	1.83
^{22}Ne	80	92	1.08 ± 0.23	0.05 ± 0.14	0.64 ± 0.05	2.94	2.26
^{56}Fe	1000	150	0.63 ± 0.35	-0.22 ± 0.21	0.48 ± 0.05	2.19	3.03
^{58}Ni	1000	175	0.68 ± 0.28	-0.20 ± 0.17	0.52 ± 0.04	2.39	2.77
^{64}Ni	1000	175	1.31 ± 0.34	0.15 ± 0.13	0.54 ± 0.02	2.47	2.68
^{36}Ar	95	272	1.03 ± 0.18	0.02 ± 0.14	0.81 ± 0.05	3.73	1.78
^{58}Ni	75	905	1.29 ± 0.32	0.63 ± 0.60	2.48 ± 0.12	11.42	0.58
^{208}Pb	29	9674	1.00 ± 0.04	0.05 ± 0.49	11.44 ± 0.41	52.68	0.13

Note. D_0 values were calculated according to the equation $S = 1-(1-e^{D/D_0})^n$, where D is the dose; D_q, the quasi-threshold dose for a given cell population and radiation quality that indicates the width of the shoulder of the survival curve; D_0, the reciprocal value of the slope within the linear part of the curve; D_0, the 37% cellular survival dose within the linear part of the curve; $D_{1\%}$, the 1% cellular survival dose within the linear part of the curve and n, the number of targets. RBE was calculated from D_0 by applying the equation RBE = $D_{0\ reference}$ / $D_{0\ test}$. X-rays were used as reference radiation. RBE ($D_{1\%}$) is equal to RBE (D_0).

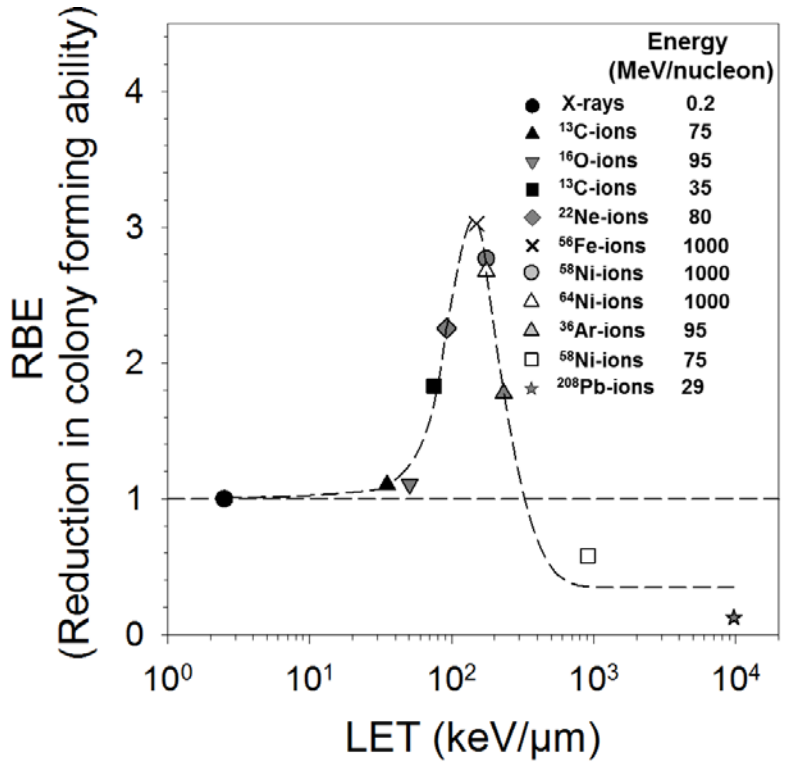

Figure 3-2 Relative efficiency of OCT-1 cell killing by different radiation qualities

The RBE values were calculated from D_0 of the survival curves resulting from colony forming ability tests after exposure of OCT-1 cells to accelerated HZE particles. 200 kV X-rays were used as reference radiation for RBE calculation.

3.1.3 Cellular survival of C3H10T1/2 cells after exposure to different radiation qualities

As for OCT-1 cells, the survival of C3H10T1/2 cells after exposure to different ionizing radiation qualities was determined by means of the colony forming ability test. Also in C3H10T1/2 cells, the LET of the heavy ion beam influences the course of the survival curves.

After X-ray exposure, the survival curve shows a similar initial shoulder region as for OCT-1 cells, which is followed by an exponential decrease of the survival fraction.

After irradiation with ^{13}C (LET 35 keV/µm), ^{16}O (51 keV/µm) and ^{13}C ions (75 keV/µm), the survival curves are decreasing exponentially with almost no shoulder. The slope of the curves augments when LET increases (**Figure 3-3**).

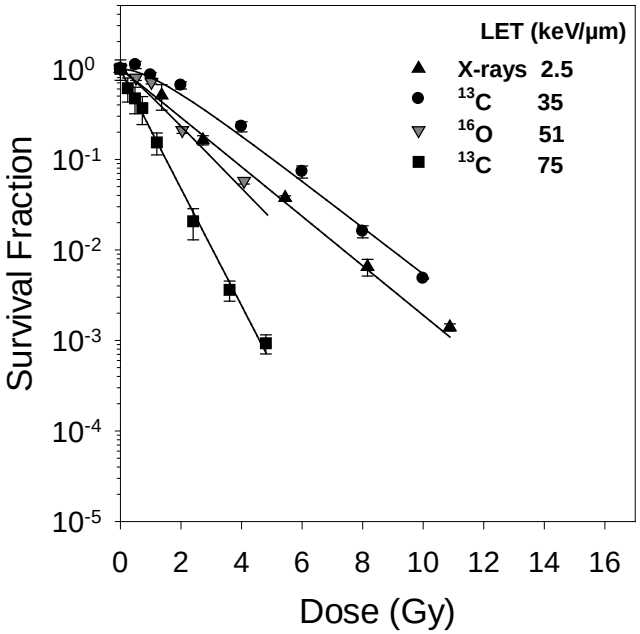

Figure 3-3 Survival curves of C3H10T1/2 cells

Survival curves of C3H10T1/2 cells exposed to low-LET X-rays (3 independent experiments with each 6 replicates) or high-LET accelerated charged particles (1 independent experiment with 6 replicates each).

3.1.4 Relative efficiency of C3H10T1/2 cell killing by different radiation qualities

In order to compare the survival curves for different radiation qualities and to determine the RBE for C3H10T1/2 cell killing, the parameters n, D_q and D_0 were calculated (**Table 3-2**).

Table 3-2 Parameters of the survival curves (n, D_q, D_0, $D_{1\%}$) resulting from exposure of C3H10T1/2 cells to different radiation qualities and RBE

Ion species	Energy (MeV/n)	LET in H_2O (keV/µm)	n	D_q (Gy)	D_0 (Gy)	$D_{1\%}$	RBE (D_0)
X-rays	0.2	0.3 – 3	1.88 ± 0.39	1.05 ± 0.39	1.66 ± 0.10	7.66	1.00
^{13}C	75	35	1.01 ± 0.08	0.01 ± 0.13	1.64 ± 0.03	7.55	1.01
^{16}O	95	51	1.04 ± 0.14	0.07 ± 0.20	1.50 ± 0.08	6.93	1.11
^{13}C	35	75	0.93 ± 0.08	-0.05 ± 0.06	0.67 ± 0.02	3.09	2.48

The survival curve after X-ray exposure has a relatively high n value of 1.88, whereas the heavy ion survival curves have the n values of ~ 1. The D_q values of X-ray and ^{13}C (35 keV/µm), ^{16}O and ^{13}C (75 keV/µm) ion survival curves, are 1.05, 0.01, 0.07 and -0.05 Gy, respectively. The D_0 for X-rays is 1.66 Gy; and for heavy ions, the D_0 value decreases when LET increases.

The RBE values, which were calculated as described before, increase from 1.00 to 2.48 as the LET increases from 3 to 75 keV/µm (**Table 3-2**).

3.1.5 Comparison of relative killing efficiency in C3H10T1/2 and OCT-1 cells

To compare the RBE for killing of C3H10T1/2 and OCT-1 cells by different radiation qualities, the LET-RBE curves were plotted together. The result revealed that for both cell lines, an LET dependence of cell survival ability exists, and both cell lines show a comparable extent of relative cell killing effectiveness for the tested radiation qualities (**Figure 3-4**).

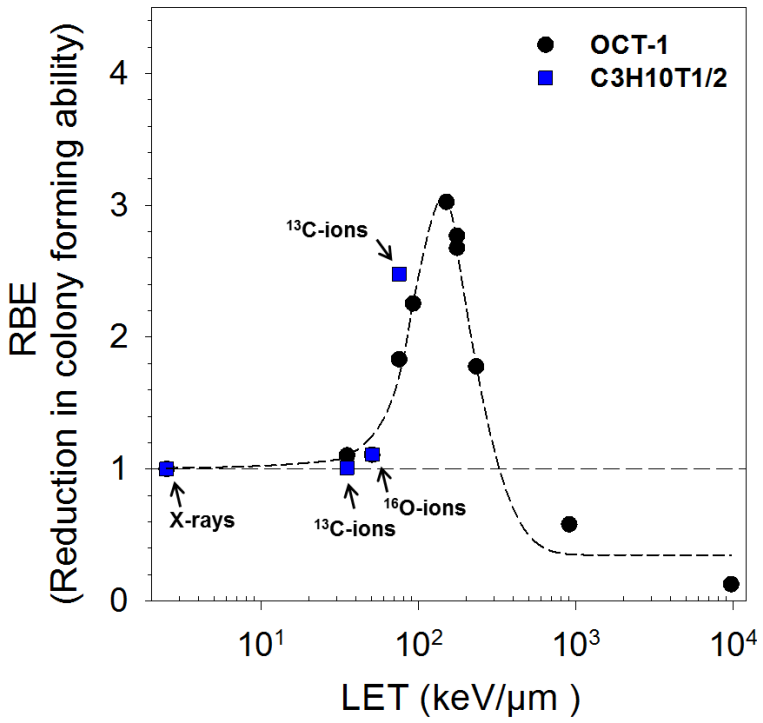

Figure 3-4 Comparison of the LET dependence of the RBE for reduction in colony forming ability calculated from D_0, for OCT-1 and C3H10T1/2 cells

200 kV X-rays were used as reference radiation for RBE calculation. For OCT-1 cell exposures, the heavy ions are designated in Figure 3-2. The heavy ions C3H10T1/2 cells were exposed to are indicated in the graph.

3.2 Cell cycle progression after irradiation with X-rays and heavy ions

In the previous subchapter, survival as a late endpoint of the cellular radiation response was analyzed, showing its dose and radiation quality dependence in OCT-1 cells.

Earlier steps after radiation exposure include the activation of cell cycle check-points in response to DNA damage. Only after successful repair during such a cell cycle arrest, survival with reproductice integrity can be achieved. Therefore, the cell cycle progression after exposure to different radiation qualities was assessd.

OCT-1 cells were exposed to X-rays and different heavy charged particles: ^{13}C-ions (35 keV/µm), ^{13}C-ions (75 keV/µm), ^{22}Ne-ions (92 keV/µm), ^{48}Ti-ions (115 keV/µm), and ^{64}Ni-ions (175 keV/µm). A summary of all applied radiation qualities is shown in **Table 2-7.** After irradiation, the cells were harvested as described before and stained with propidium iodide before they were subjected to flow cytometry to analyze the cell cycle progression.

3.2.1 Cell cycle progression after X-ray and heavy charged particle exposure

After radiation exposure, the fraction of OCT-1 cells in G2/M phase was significantly higher than non-irradiated control, reflecting the radiation dose of X-rays and heavy ions (**Figure 3-5 A-F**). For X-ray and heavy ion irradiation, the maximal cell cycle perturbation is observed at around 8-12 h after exposure. The G2/M percentage of OCT-1 cells exhibits a clearly higher peak after exposure to ^{22}Ne-ions and ^{64}Ni-ions compared to X-irradiation (**Figure 3-5 D F**). The block persists longer and is higher after ^{64}Ni-ion exposure with doses of 2, 4 and 8 Gy, resulting in 32.9%, 47.4% and 65.2% of the cell population accumulating in the G2/M phase after 72 h (**Figure 3-5 F**).

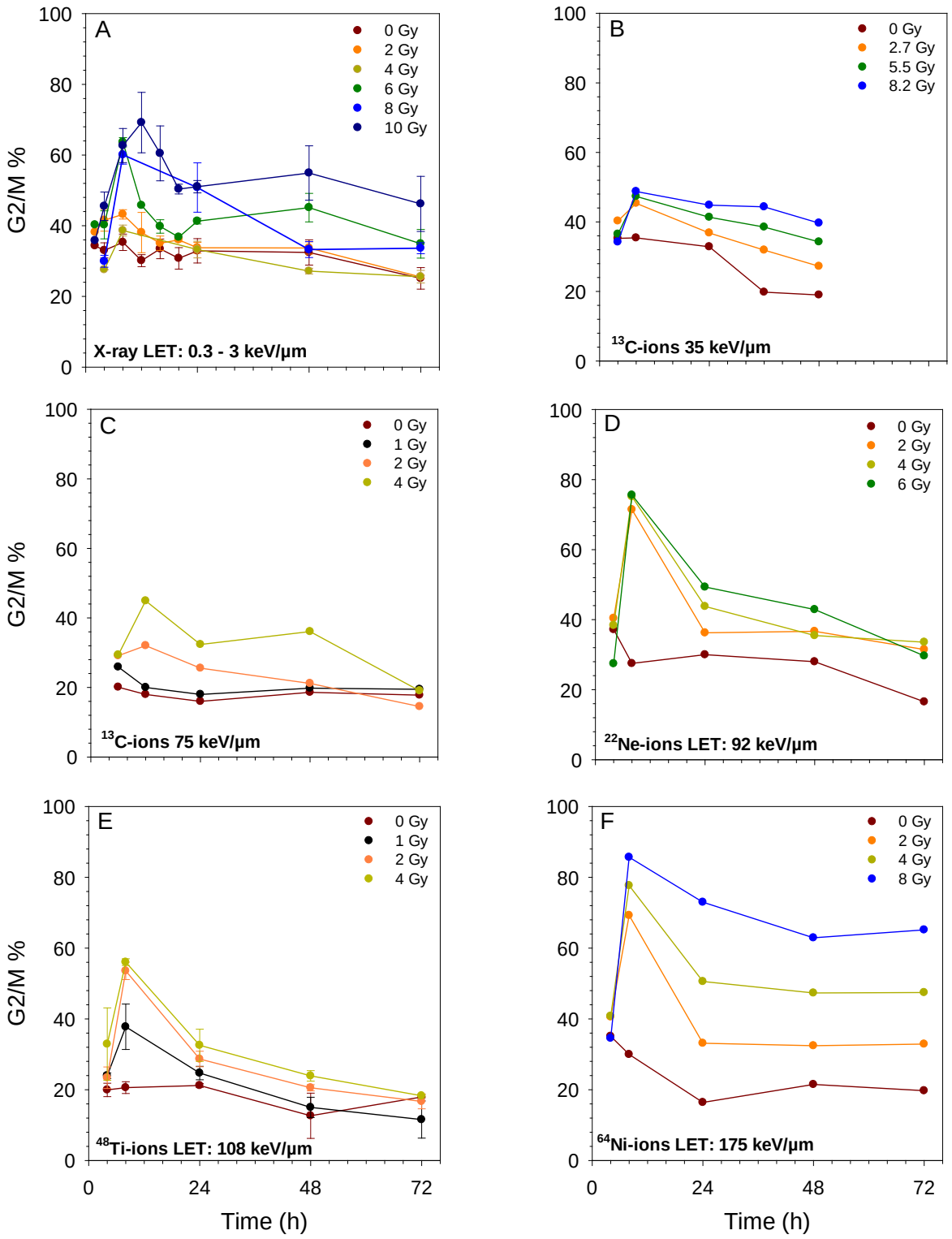

Figure 3-5 Accumulation of OCT-1 cells in the G2/M phase after irradiation

Comparison of the accumulation of cells in the G2/M phase of the cell cycle after exposure of OCT-1 cells to high- or low LET radiation. Cells were fixed and analyzed up to 72 h after exposure to X-rays (A), ^{13}C-ions (LET 35 keV/µm) (B), ^{13}C-ions (LET 75 keV/µm) (C), ^{22}Ne-ions (D), ^{48}Ti-ions €, and ^{64}Ni-ions (F).

3.2.2 Comparison of cell cycle progression at 1% cellular survival level

In order to compare the influence of different radiation qualities on cell cycle regulation, RBE values for cell killing were classified in four categories:

I, 0 < RBE ≤1;

II, 1 < RBE ≤ 2;

III, 2 < RBE ≤ 3; and

IV, RBE >3.

Within each category, one representative radiation quality was selected as follows: a, X-rays with an LET of 0.5-3 keV/µm; b, ^{13}C-ions, 75 MeV/n; c, ^{22}Ne-ions, 80 MeV/n; d, ^{56}Fe-ions or ^{64}Ni-ions, 1000 MeV/n (**Figure 3-6**). Doses resulting in 1% survival levels were: 10, 5.5, 3.8, and 1.9 Gy, respectively (**Figure 3-7 A B**).

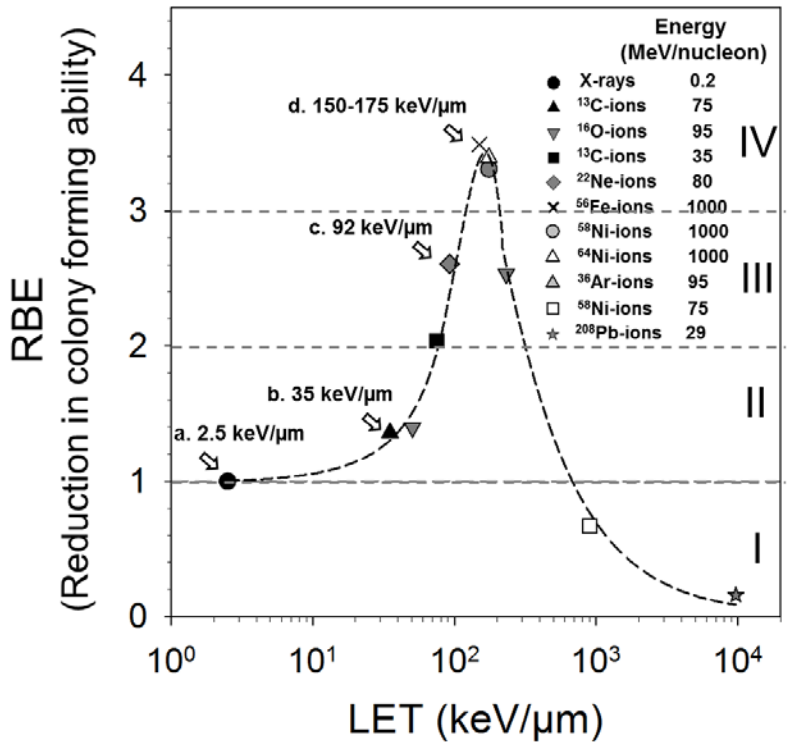

Figure 3-6 RBE categories for cell cycle analysis

RBE values were classified in four categories: I, 0 < RBE ≤1; II, 1 < RBE ≤ 2; III, 2 < RBE ≤ 3; and IV, RBE > 3. Four radiation qualities with an LET of 0.5-3 keV/µm; 35 keV/µm; 92 keV/µm and 150 -175 keV/µm were selected from those four categories.

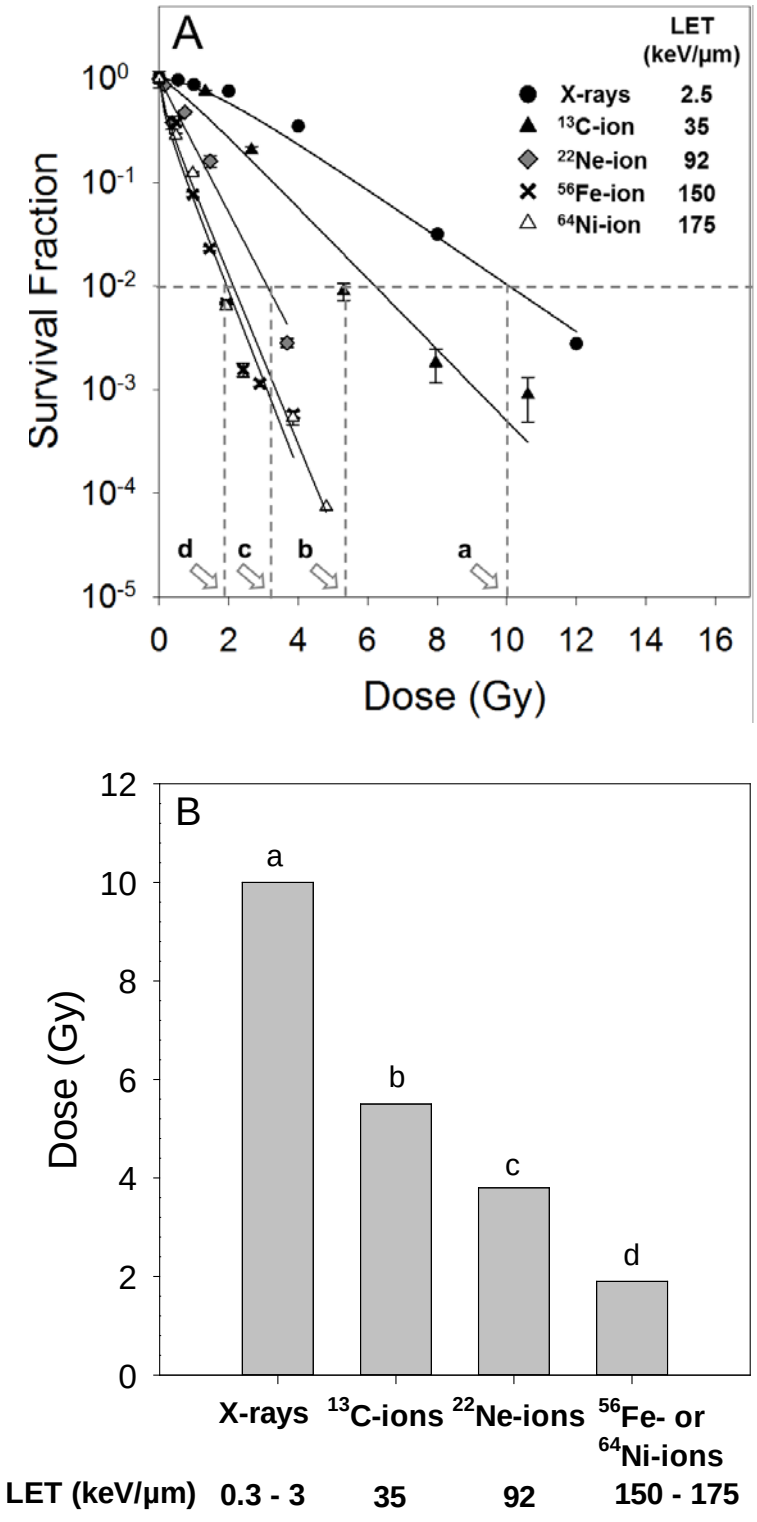

Figure 3-7 Calculated 1% cellular survival dose

The dose resulting in 1% cellular survival was calculated from the survival curves of the selected radiation qualities (A), and plotted in bar chat (B).

Cell cycle progression of exponentially growing OCT-1 cells was analyzed by flow cytometry up to 48 h after radiation exposure for the doses leading to 1% cellular survival.

An increase in the G2/M peak was observed as early as 4 h after radiation exposure for all investigated doses. Changes were even more pronounced 8 h after radiation exposure. 8 h after X-ray exposure, 62% of the cells were captured in G2/M phase. The percentages of cells triggered to arrest in G2/M phase after irradiation with carbon, neon and nickel ions were 47%, 81% and 78%, respectively (**Figure 3-8 B**). The amount of cells in the G2/M phase decreased 24 h after exposure and a certain amount of cells became polyploidy. 48 h after irradiation, even more polyploidy cells appeared (**Figure 3-8 A**).

The G2/M arrest was more pronounced after exposure to heavy ions with an LET of 150-175 keV/µm, compared to X-ray exposure. After carbon ion exposure, the cell accumulation in the G2/M phase was less distinct than after X-irradiation.

A comparison based on the same absorbed dose (4 Gy) reveals similar kinetics for high-LET neon and nickel ions, except for a slower decrease in G2/M arrested cells after 24 h compared to the 1 % survival dose.

For low-LET radiation, exposure to the same absorbed dose results in a stronger G2/M arrest after carbon ion exposure compared to X-irradiation. 48 h after X-irradiation, the percentage of cells in G2/M reaches normal values, while it is still slightly elevated after carbon and neon ion exposure, and clearly increased after nickel ion irradiation.

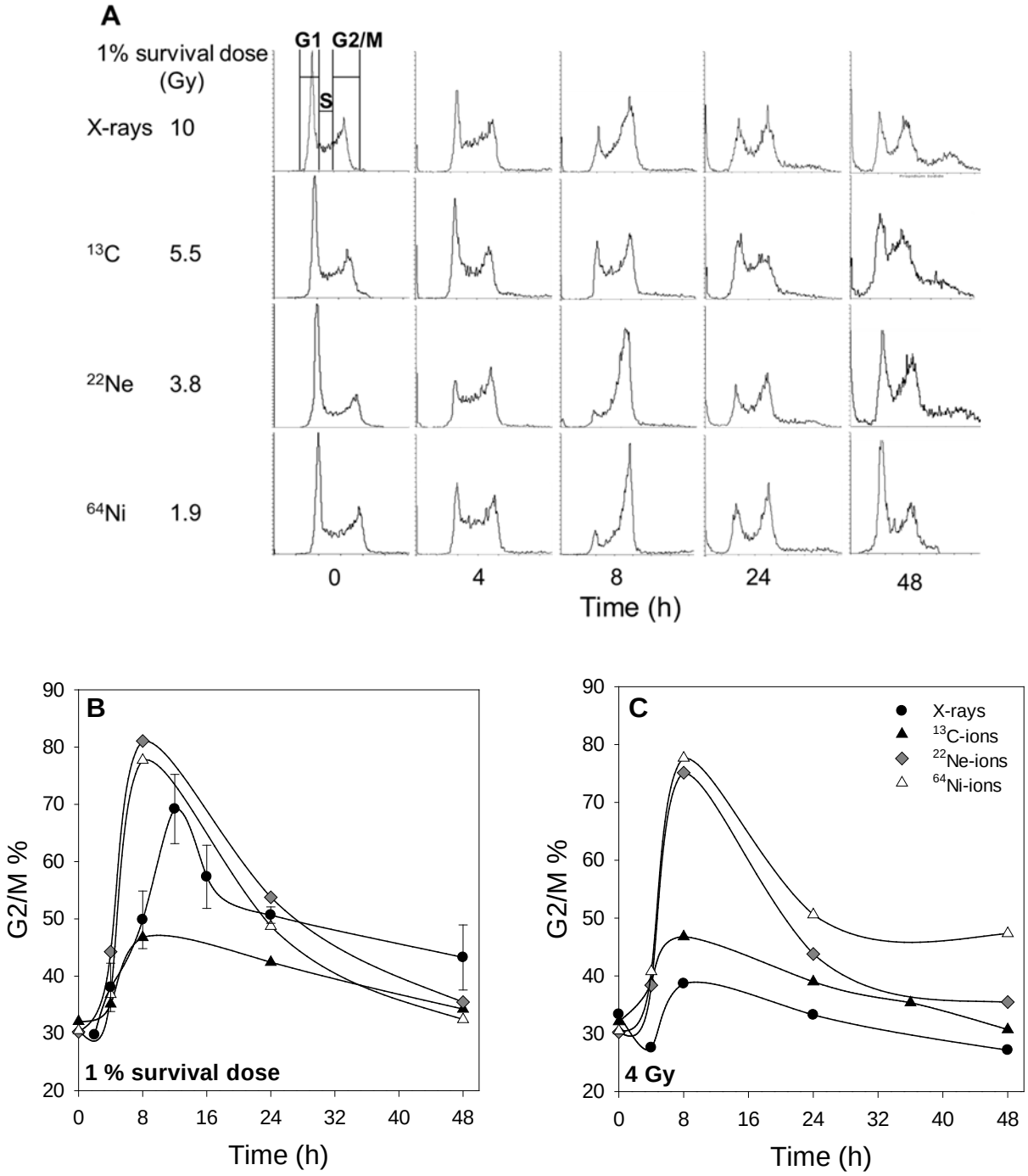

Figure 3-8 Cell cycle progression in OCT-1 cells after exposure to radiation doses resulting in 1% cellular survival and to 4 Gy

Cells were exposed to four different qualities radiation including X-rays, ^{13}C-, ^{22}Ne- and ^{64}Ni –ions at doses of 10, 5.5, 3.8 and 1.9 Gy and analyzed 4, 8, 24 and 48 h after irradiation. Histograms of propidium iodide fluorescence (A). The percentage of cells in G2/M phase was derived from the histograms (B). For comparison, the percentage of cells in G2/M phase after exposure to 4 Gy of the different radiation qualities is shown (C).

3.2.3 CDKN1A expression at mRNA level

To determine the possible mechanisms underlying the effects of ionizing radiation on cell cycle progression, the expression of a gene related to cell cycle regulation was evaluated: the mRNA levels of CDK inhibitor CDKN1A which encodes p21 were determined. $P21^{CDKN1A}$ is a mediator of p53-induced growth arrest which directly regulates CDK activity, and is expressed concomitantly with cellular senescence (Noda et al., 1994).

CDKN1A expression of OCT-1 cells was investigated with real-time RT-qPCR after exposure to low- and high-LET radiation at doses of 10, 5.5, 3.8, and 1.9 Gy. Expression analyses of CDKN1A mRNA revealed a significant time-dependent up-regulation compared to non-irradiated mock samples; and the up-regulation was much more evident after X-irradiation than after heavy ion exposure. The result show that by exposure to 10 Gy X-rays, CDKN1A was up-regulated 9.9-fold relative to the unirradiated control at the time-point 8 h; and up-regulated 4.1-fold at time 24 h. ^{13}C-, ^{22}Ne- and ^{64}Ni-ions exposure resulted in a 5.6-, 3.9-, 1.9-fold up-regulation 8 h post irradiation and 3.0-, 2.3-, 1.7-fold 24 h after irradiation (**Figure 3-9**).

At the same absorbed dose of 4 Gy, exposure to X-rays and carbon ions elicits comparable CDKN1A expression after 8 h. The expression level is lower after irradiation with 4 Gy high-LET neon and iron ions. The largest decrease in CDKN1A up-regulation 24 h after irradiation is observed after X-ray exposure. This decrease is less pronounced after heavy ion exposure, and the relative expression is still > 2 times higher compared to the unirradiated controls.

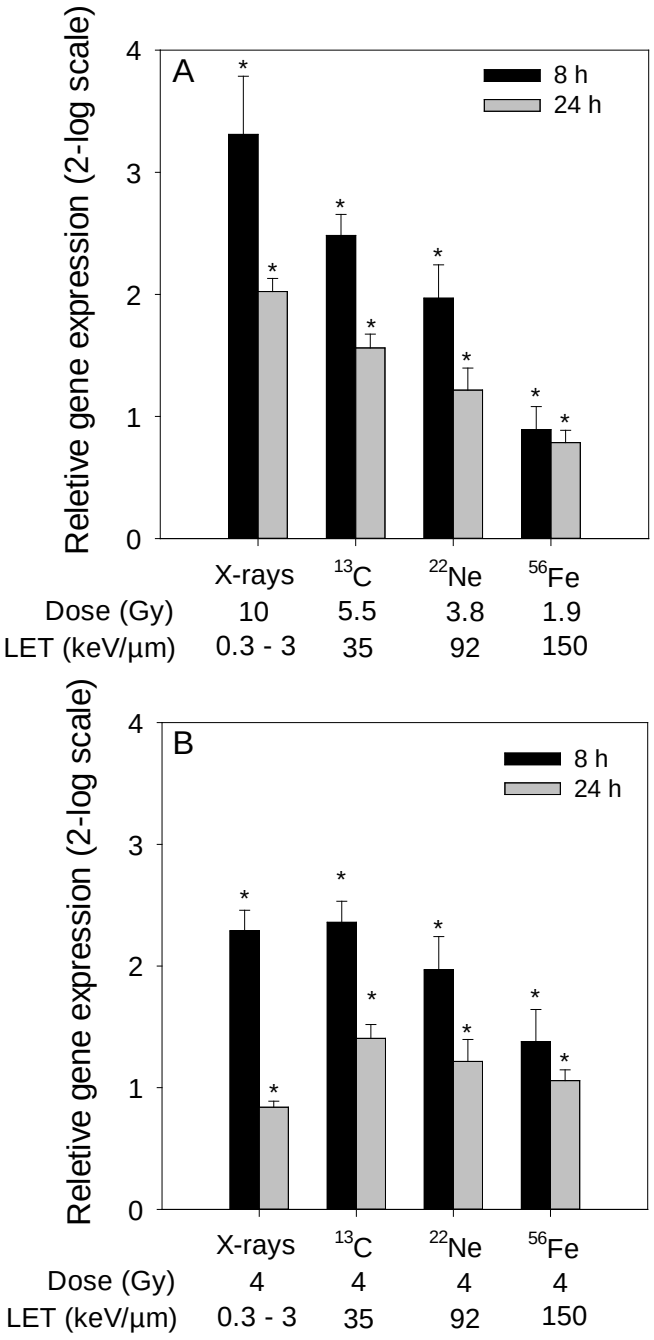

Figure 3-9 Effects of radiation exposure on CDKN1A mRNA levels

Cells were harvested 8 or 24 h after X-ray or accelerated charged particle (^{13}C, ^{22}Ne, ^{56}Fe) irradiation. CDKN1A mRNA levels were determined after exposure to the 1% survival doses (A) and for comparison, to the same absorbed dose of 4 Gy (B). Values represent normalized means of the replicates (n = 3) and are expressed relative to non-irradiated controls. CDKN1A gene expression was normalized against the expression of the reference genes B2M and GAPDH. *p < 0.05 using a log-transformed, one-sample t-test (n = 3) for comparison between irradiated samples and the 0 Gy control.

3.2.4 Role of p53 in X-ray-induced cell cycle arrest

As the expression of the p53 target gene CDKN1A was elevated after exposure to ionizing radiation and radiation exposure induced a G2/M arrest, the role of p53 in X-ray-induced cell cycle arrest in pre-osteoblasts was studied.

Therefore, the p53 inhibitor cyclic pifithrin-α (30 µM) was added to the culture medium 2 h before radiation exposure. OCT-1 cells were harvested at indicated time points after irradiation with X-rays at doses up to 10 Gy for cell cycle and gene expression analysis of TP53 and its target genes Mdm2 and CDKN1A.

3.2.4.1 Cell cycle progression

An accumulation of cells in G2/M phase appears as early as 4 h after X-ray exposure. For all investigated doses, the change was more pronounced around 8-16 h after radiation exposure. When radiation dose increases, the G2/M peak also increases. After 16-24 h, the G2/M blockage decreases. Cells 16 h after irradiation with 2 Gy seem to have started cycling again. For cells irradiated with 6 Gy, 48 h were of recovery time where necessary. After treatment with 10 Gy, even after 72 h a large part of the population was still in G2/M phase and a large amount of events displayed a higher than 2n DNA content, indicating polyploidy (**Figure 3-10 A**). These results demonstrate that X-rays induce a time- and dose- dependent cell cycle arrest of OCT-1 cells in G2/M phase.

When cells were treated with cyclic pifithrin-α (without X-irradiation), there was a slight but not significant difference in cell cycle phase distribution up to an incubation time of 72 h. When irradiated with 2, 6 and 10 Gy X-rays after the cyclic pifithrin-α treatment (2 h pre-incubation), there is a more pronounced induction of G2/M blockage compare to treated with X-rays alone (**Figure 3-10 B**).

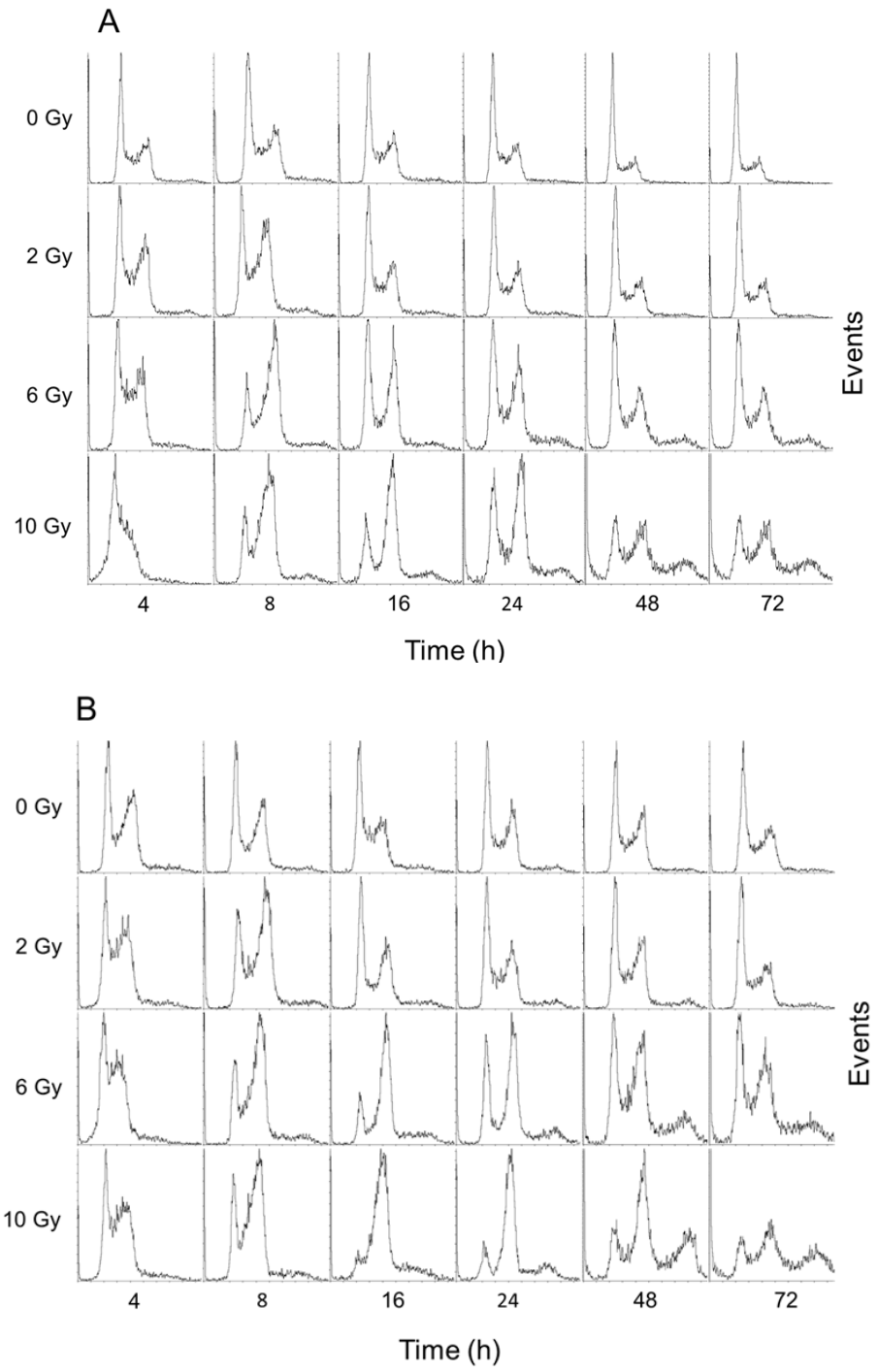

Figure 3-10 The effects of X-rays and/or cyclic pifithrin-α on cell cycle progression

Cells were harvested at various time points to determine the distribution of cells within the cell cycle phases by measuring the DNA content in propidium iodide stained permeabilized cells. Histograms of propidium iodide fluorescence intensity are shown for OCT-1 cells treated with 0, 2, 6, and 10 Gy X-rays only (A) and in the presence of cyclic pifithrin-α (2 h pre-incubation) (B) at the indicated time points.

As a measure of cell cycle delay, the fractions of cells captured in G2/M phase of the cell cycle were calculated as percentage of the population of intact single cells after exposure to different radiation doses (**Figure 3-11**). After X-irradiation with 2, 6 and 10 Gy, the percentage of cells in G2/M phase increases after an incubation time of 4 h (41.8%, 40.2% and 36.2%) and peaks after about 8 h (43.2%, 63.8% and 65.2%). 16 h after irradiation with 2 Gy X-rays, the percentage of cells in G2/M phase is comparable to the unirradiated controls. After exposure to 6 and 10 Gy X-rays, the cells stayed in G2/M cell cycle phase for a prolonged period compared to cells after lower doses (2 Gy) and remained there up to 48 h (6 Gy) and even longer than 72 h (10 Gy) (**Figure 3-11 A**).

In the presence of cyclic pifithrin-α, cells after X-irradiation exposure to 0, 2, 6 and 10 Gy, the percentage of cells in G2/M phase are 37.4%, 39.8%, 48.0% and 47.2%, and peaks after about 12 h (42.6%, 56.4%, 84.4% and 92.5%) (**Figure 3-11 B**).

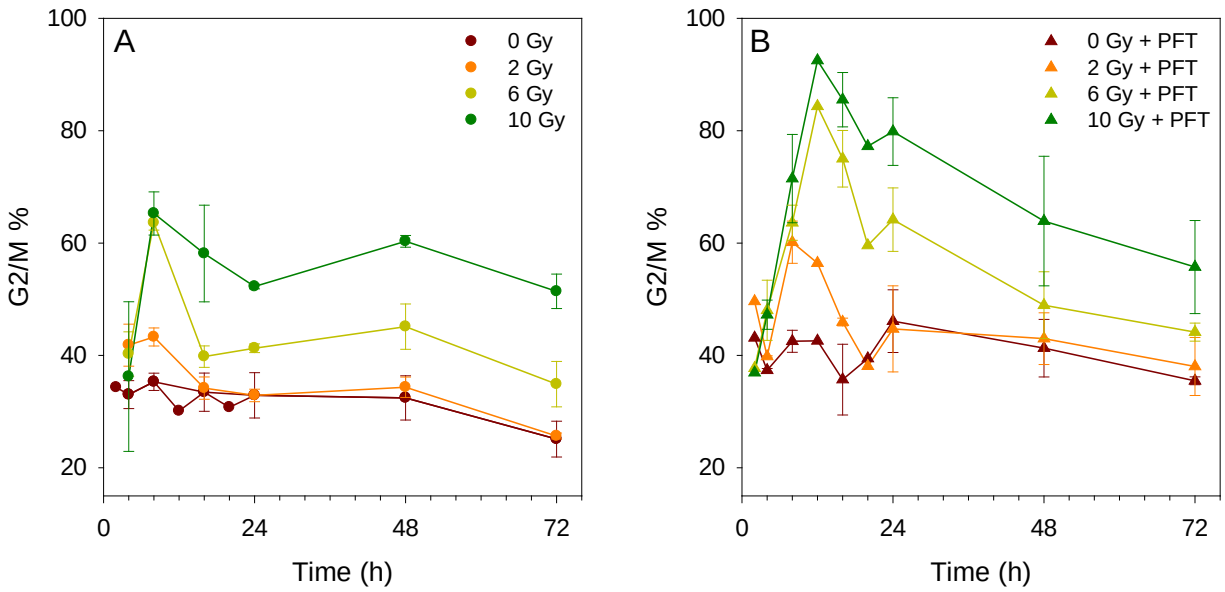

Figure 3-11 OCT-1 cells accumulated in G2/M phase

OCT-1 cells accumulated in G2/M phase after X-irradiation (A) and after X-irradiation in presence of cyclic pifithrin-α (B). Mean and SE of three independent experiments are shown. The percentage of cells in G2/M phase was determined by flow cytometric analysis of propidium iodide stained cells at various time points after irradiation.

3.2.4.2 CDKN1A, TP53 and Mdm2 mRNA level after X-ray exposure with and without p53 inhibition

In order to study the role of the p53 in the regulation of p21 and Mdm2 in response to exposure of OCT-1 cells to X-rays, p53 was suppressed by cyclic pifithrin-α and the mRNA level of TP53, CDKN1A and Mdm2 was determined by realtime RT-qPCR. TP53 encodes the tumor suppressor protein p53, CDKN1A the cell cycle regulating protein p21. Mdm2 is a negative feedback regulator of p53.

Cells were exposed to X-rays in absence or presence of cyclic pifithrin-α.

Treatment with cyclic pifithrin-α alone without irradiation resulted in an early up-regulation of CDKN1A and an early down-regulation of TP53 4 h after mock-irradiation (6 h after addition of pfithrin). The expression reaches normal levels 8 h after mock-irradiation. Mdm2 expression is not significantly altered in presence of cyclic pifithrin-α.

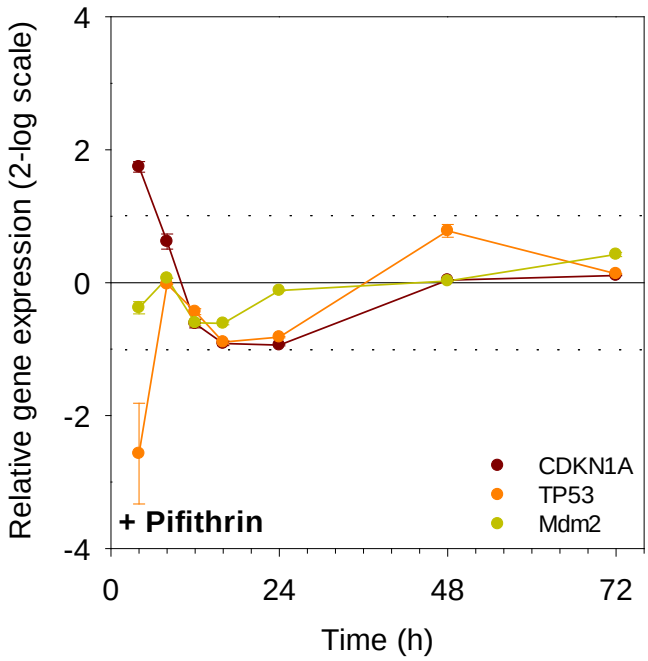

Figure 3-12 Gene expression kinetics of CDKN1A, TP53, and Mdm2

OCT-1 cells were pre-incubated with cyclic pifithrin-α 2 h and harvested at the indicated time points. Target gene expressions were normalized against the expression of the optimal combination of the housekeeping genes B2M and GAPDH. The solid line is the control without cyclic pifithrin-α and the dashed lines are the standard deviations of the samples in absence of cyclic pifithrin-α.

Exposure to 6 and 10 Gy X-rays increased the expression of CDKN1A as early as 4 h after irradiation. This enhancement increases until 8 h after irradiation. After 16-24 h, at the dose of 2 Gy, the not-significant transient CDKN1A upregulation decreased to the control level; for higher doses (6 and 10 Gy), the up-regulation decreased transiently then a second peak appeared after 48 hours (**Figure 3-13 A**).

No significant difference in TP53 mRNA expression was observed in the early time (up to 24 h) after irradiation. 48 h after exposure to X-rays at dose of 6 and 10 Gy in the presence of cyclic pifithrin-α a slight down-regulation was detected (**Figure 3-13 C D**).

The gene expression kinetics of Mdm2 after X-ray exposure was similar compared to CDKN1A, with an elevated expression at 8 h after irradiation, a decrease of this enhancement 16-24 h post exposure and a second increase with a smaller peak at 48 h (**Figure 3-13 E**).

The gene expression of CDKN1A, TP53 and Mdm2 of OCT-1 cells which were treated with cyclic pifithrin-α for 2 h before X-irradiation was also analyzed. For CDKN1A, 4 and 8 h after X-irradiation, the mRNA expression was up-regulated for all the doses compared to the unirradiated control. This elevated expression is more pronounced after 2 Gy irradiation in presence of cyclic pifithrin-α compared to the samples treated with radiation only (**Figure 3-13 B**).

TP53 mRNA expression was relatively consistent up to 24 h after irradiation, but TP53 mRNA was down regulated 48 h after exposure to X-rays in presence of cyclic pifithrin-α (**Figure 3-13 D**).

Mdm2 was also partially differentially regulated after irradiation in presence of cyclic pifithrin-α compared to after irradiation alone. 4 h after irradiation with dose of 10 Gy, the mRNA expression was up-regulated. After 8 h, this up-regulation peaked. This was also the case for the doses 2 and 6 Gy (**Figure 3-13 F**). The second peak after 48 h is missing in presence of cyclic pifithrin-α.

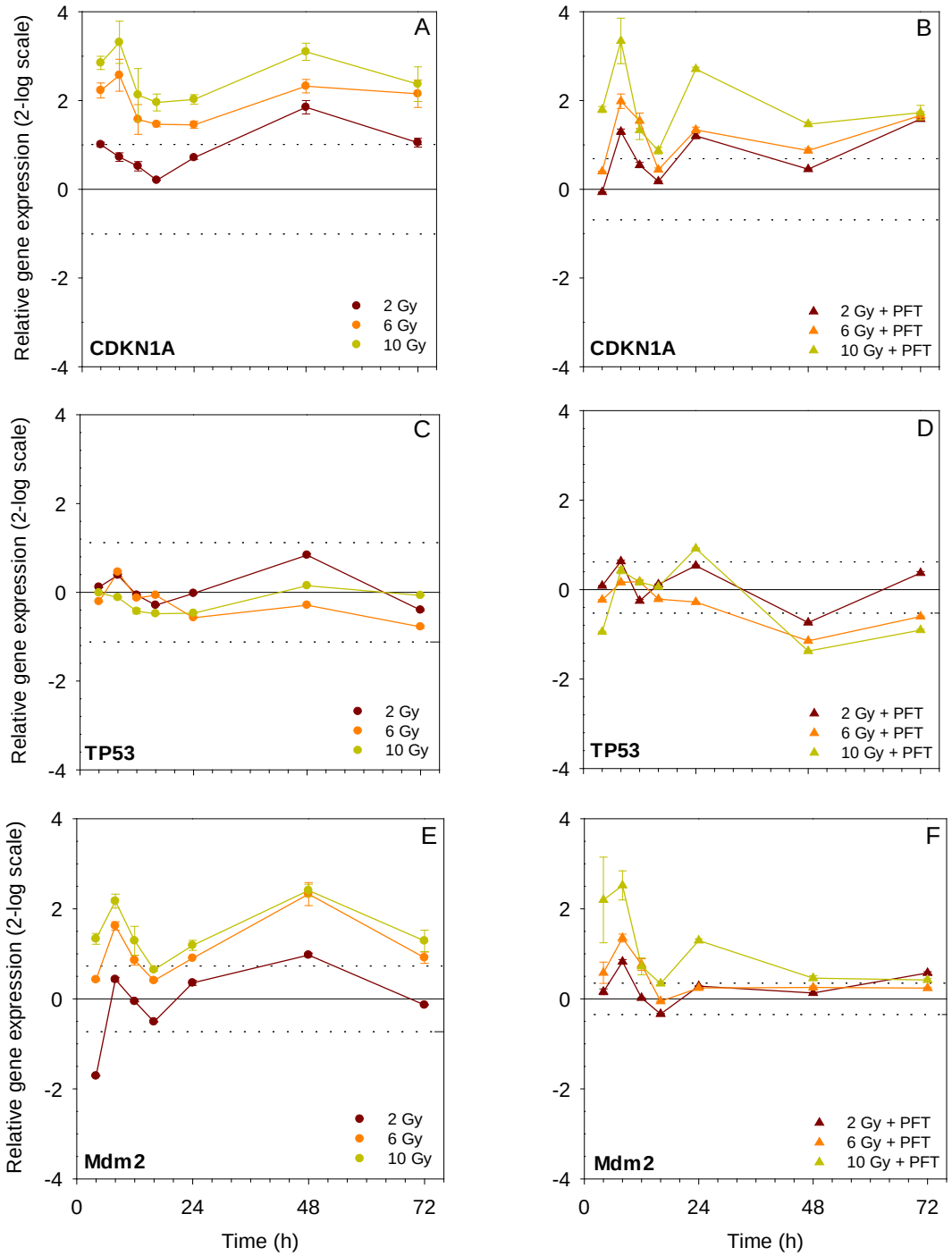

Figure 3-13 Gene expression kinetics of CDKN1A, TP53, and Mdm2

OCT-1 cells were exposed to X-rays (A, C, E) or treated with cyclic pifithrin-α 2 h before, during and after X-irradiation (B, D, F) and harvested at the indicated time points. Target gene expressions were normalized against the expression of the optimal combination of the housekeeping genes B2M and GAPDH. The solid line is the unirradiated control without (A, C, E) or with cyclic pifithrin-α (B, D, F) and the dashed lines are the standard deviations of the unirradiated samples.

3.2.5 Effects of radiation on p53 and Mdm2 expression

In order to visualize p53 (**Figure 3-14, 3-15**) and Mdm2 (**Figure 3-16, 3-17**) content and intracellular localization after X-irradiation, immunofluorescence staining was performed.

The immunofluorescence staining of p53 and Mdm2 in OCT-1 cells after X-ray exposure shows that a 2 h pretreatment with cyclic pifithrin-α resulted in only a very slight decrease in Mdm2 expression (**Figure 3-17 A**) but not p53 expression (**Figure 3-15 A**). After irradiation combined with cyclic pifithrin-α pre-incubation, the expression of p53 was almost vanished (**Figure 3-15 B**) and the same effect on Mdm2 was found (**Figure 3-17 B**).

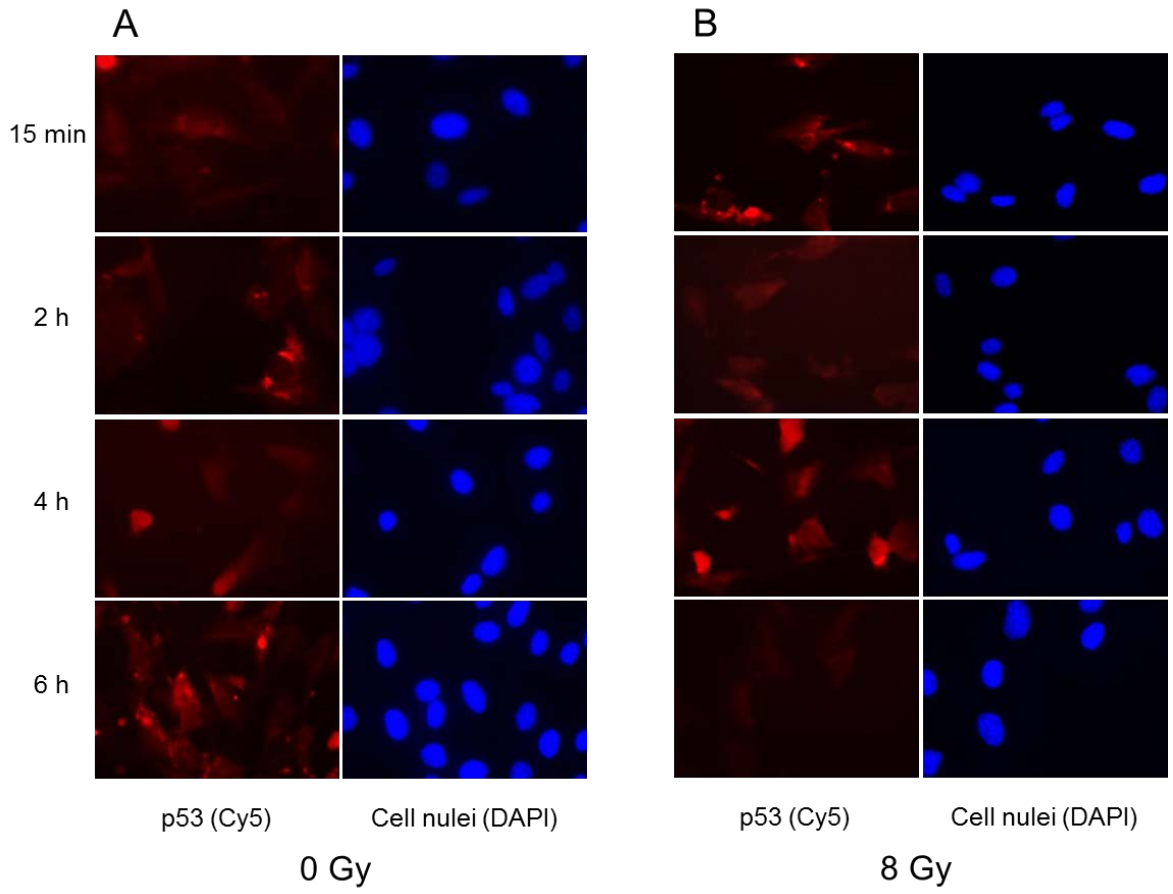

Figure 3-14 Immunostaining of p53 in OCT-1 cells after X-irradiation

The staining was performed with fixed cells using polyclonal rabbit anti-p53 antibody 0.25, 2, 4 and 6 h after exposure to 8 Gy X-rays (B). The unirradiated samples are shown as controls (A). p53 was visualized by Cy5 by fluorescence microscopy. On the right side of the figures, the DAPI stained cell nuclei are shown. (object lens magnification: 63 ×)

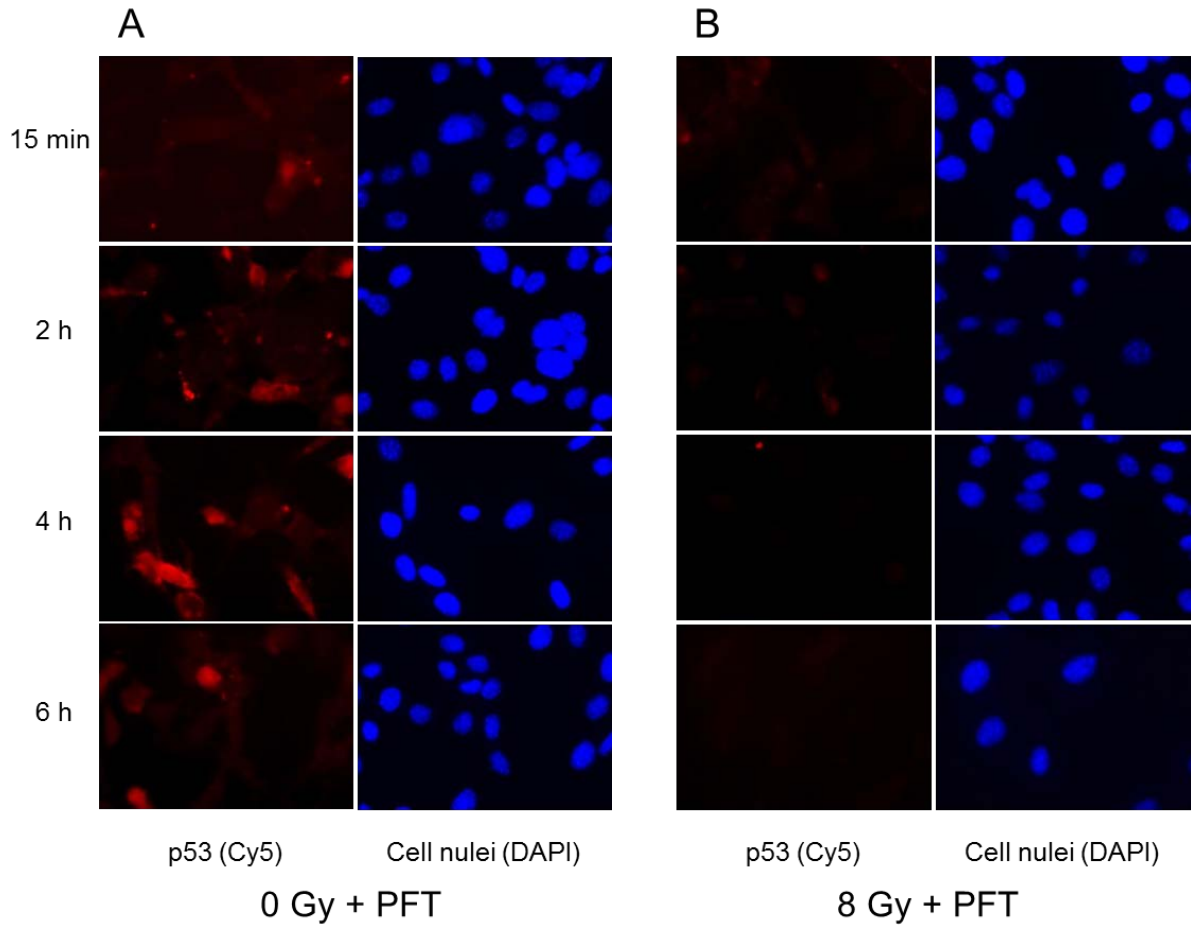

Figure 3-15 Immunostaining of p53 in OCT-1 cells after X-irradiation in presence of cyclic pifithrin-α

The staining was performed with fixed cells using polyclonal rabbit anti-p53 antibody 0.25, 2, 4 and 6 h after exposure to 8 Gy X-rays with 2 h cyclic pifithrin-α pretreatment (B). The unirradiated samples are shown as controls (A). p53 was visualized by Cy5 by fluorescence microscopy. On the right side of the figures, the DAPI stained cell nuclei are shown. (object lens magnification: 63 ×)

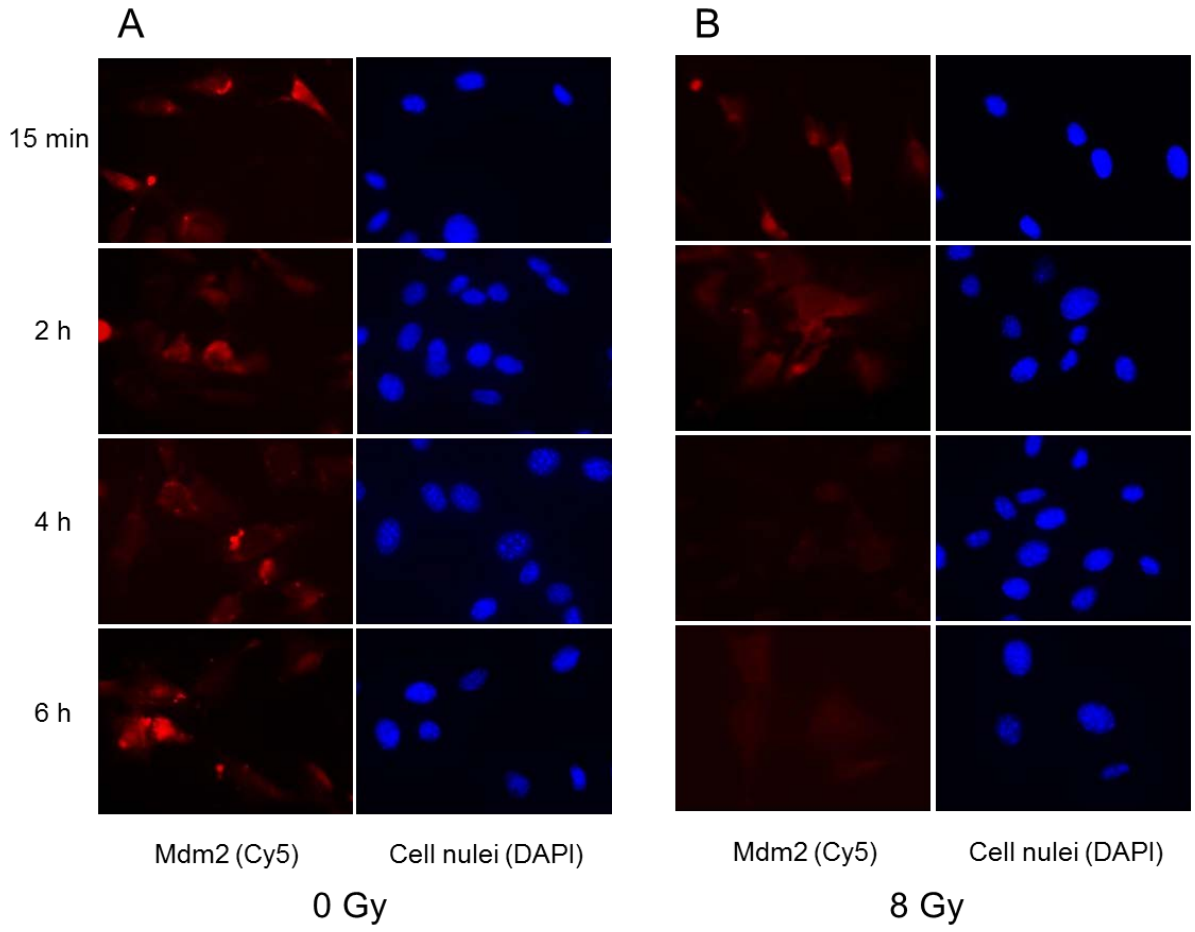

Figure 3-16 Immunostaining of Mdm2 in OCT-1 cells after X-irradiation

The staining was performed with fixed cells using polyclonal rabbit anti-Mdm2 antibody 0.25, 2, 4 and 6 h after exposure to 8 Gy X-rays (B). The unirradiated samples are shown as controls (A). Mdm2 was visualized by Cy5 by fluorescence microscopy. On the right side of the figures, the DAPI stained cell nuclei are shown. (object lens magnification: 63 ×).

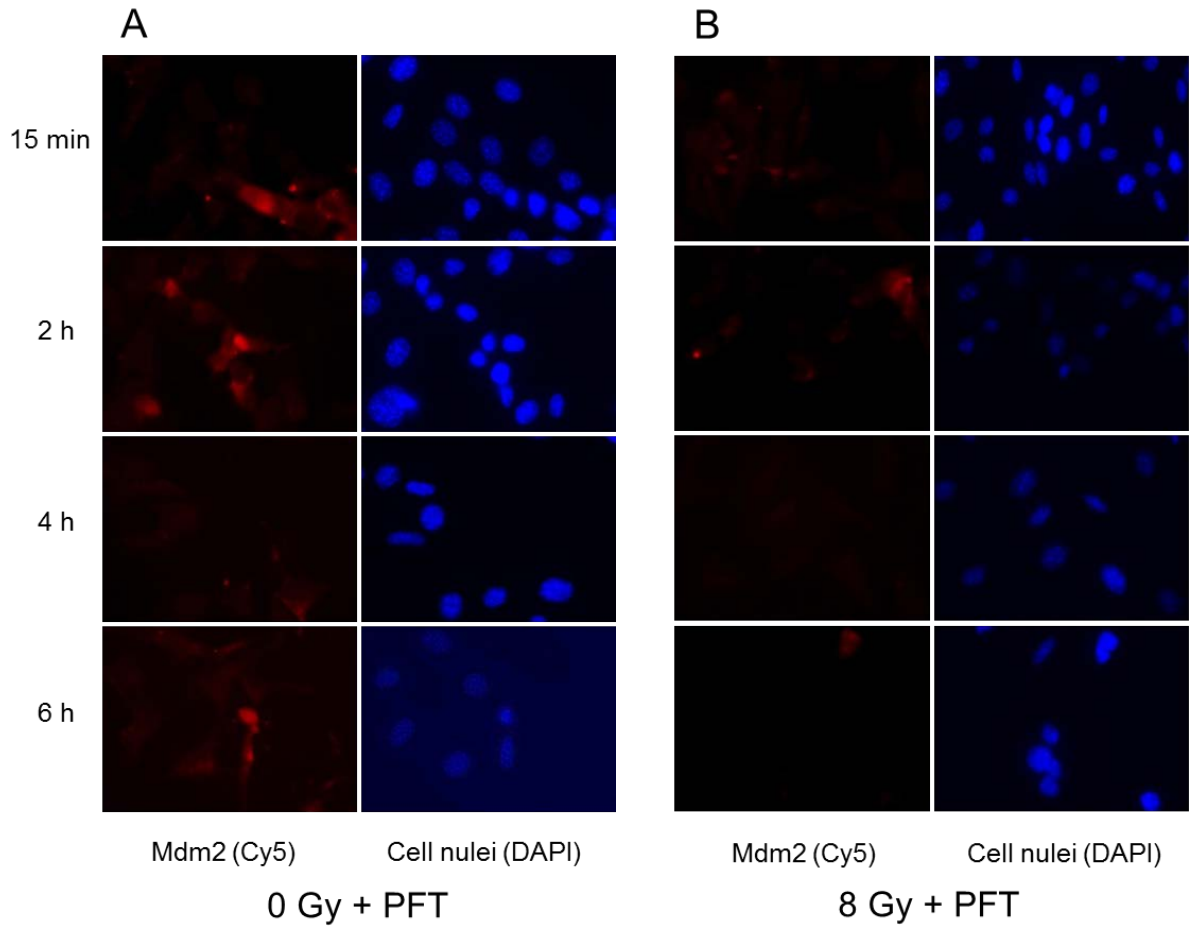

Figure 3-17 Immunostaining of Mdm2 in OCT-1 cells after X-irradiation in presence of cyclic pifithrin-α

The staining was performed with fixed cells using polyclonal rabbit anti-Mdm2 antibody 0.25, 2, 4 and 6 h after exposure to 8 Gy X-rays with 2 h cyclic pifithrin-α pretreatment (B). The unirradiated samples are shown as controls (A). Mdm2 was visualized by Cy5 by fluorescence microscopy. On the right side of the figures, the DAPI stained cell nuclei are shown. (object lens magnification: 63 ×).

3.3 Effects of ionizing radiation on cellular differentiation of pre-osteoblasts

As shown in the two previous subchapters, the hallmarks of the general cellular radiation response, cell death and cell cycle arrest, are present in pre-osteoblasts. In order to discover whether bone cell specific radiation responses exist, the effects of radiation exposure on osteogenic differentiation were analyzed.

OCT-1 cells can differentiate *in vitro* to bone-matrix producing, mature osteoblasts in presence of OI medium containing β-glycerophosphate, ascorbic acid, and dexamethasone. The influence of exposure to ionizing radiation on this differentiation process was analyzed by several approaches. After X-irradiation, OCT-1 cells were directed to mature osteoblasts by adding OI medium. For comparison, OCT-1 cells were also cultured under SC medium after irradiation.

Firstly, cell morphology, proliferation, senescence, extracellular matrix production, survival and repair ability were compared for cells that were cultivated in presence or absence of osteogenic induction supplements after radiation exposure.

Cell morphology and cellular senescence were analyzed 6 days after X-irradiation. After being cultured in OI medium for up to 21 days after X-irradiation, the production of mineralized extracellular matrix by OCT-1 cells was analyzed by using Alizarin red S staining and further quantified with ImageJ software.

Furthermore, the influence of osteogenic induction by incubation in OI medium on cellular survival, repair kinetics and proliferation of OCT-1 cells after X-irradiation was examined.

Finally, in order to identify possible contributors in the X-irradiation-modulated osteogenic differentiation process, the protein expression of TGF-β1 and Runx2 was analyzed by means of immunofluorescence staining.

3.3.1 Cell morphology after radiation exposure

The effects of ionizing radiation on cellular proliferation and morphology were assessed after exposure of OCT-1 cells to various X-ray doses (2, 4 and 8 Gy). After irradiation, cells were incubated for 6 d in SC or OI medium (**Figure 3-18**). Microscopic observations reveal some large and flat cells with the characteristic appearance of senescent cells 6 d after exposure to 8 Gy and cultivation in SC medium. This morphology is already observed after exposure to 4 Gy, if the cells were cultured in OI-medium.

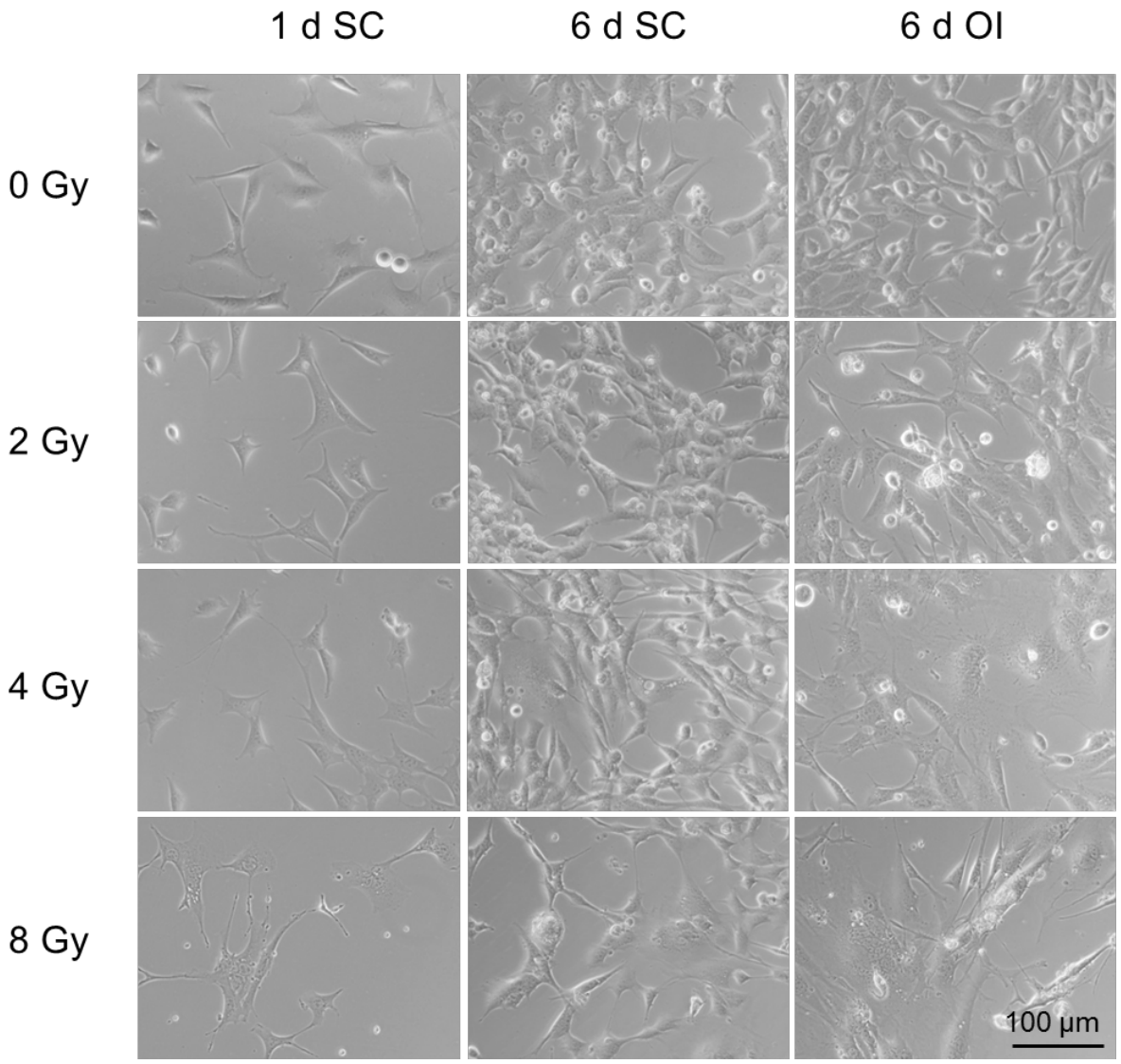

Figure 3-18 Morphology of OCT-1 cells after X-ray exposure

After cell seeding, cells were cultured for 1 d and exposed to 2, 4 and 8 Gy X-rays. After radiation exposure, the cells were incubated for up to 6 d under SC or OI medium. Photographs were taken 1 d and 6 d after X-ray exposure at the same magnification (object lens magnification: 20 ×).

3.3.2 Senescence of OCT-1 cells after X-ray exposure

As OCT-1 cells showed senescent morphology after X-irradiation (4-8 Gy in Figure 3-17), an established senescence marker was analyzed. Several markers can identify senescent cells in culture and *in vivo*. In this experiment, senescent cells were identified by detecting the activity of senescence-associated β-galactosidase (SA-β-gal). SA-β-gal catalyzes the hydrolysis of X-gal, which results in the accumulation of distinct blue-green colored substrate in senescent cells.

OCT-1 cells were cultured for 6 d under standard or osteogenic conditions. The level of X-gal increased after exposure to 8 Gy in both SC and OI medium (**Figure 3-19**). However, SA-β-gal was slightly higher in irradiated cells under osteogenic conditions. Under these conditions some OCT-1 cells show an increased cell size and a distinctive flat morphology. Interestingly, a diffuse low level X-gal staining was also present in cells cultured under both standard and osteogenic conditions without irradiation.

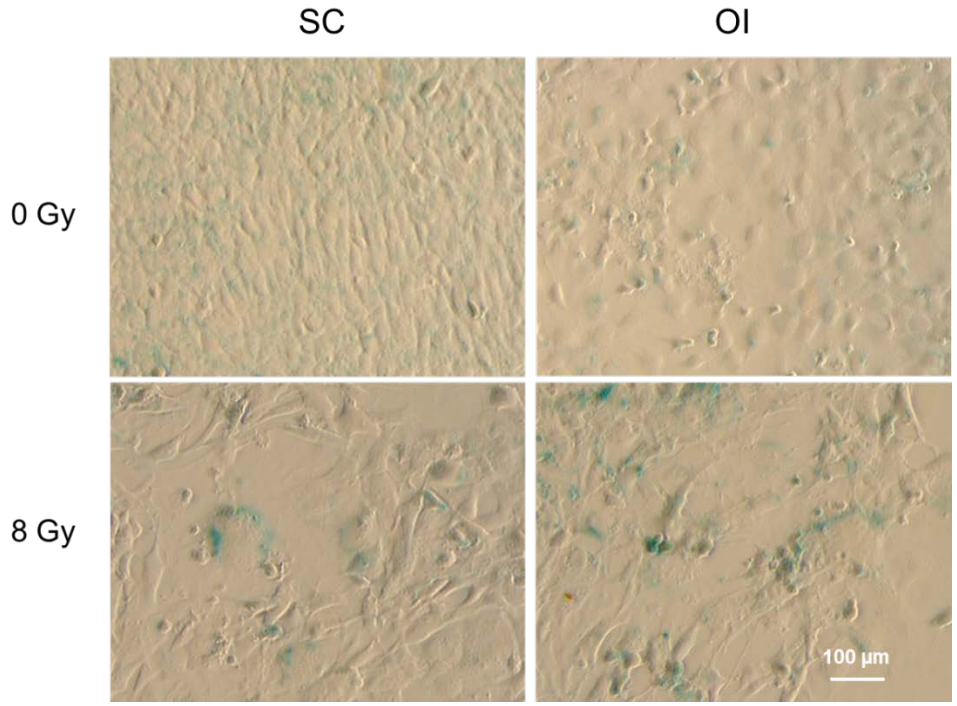

Figure 3-19 Senescence staining of OCT-1 cells after X-ray exposure

OCT-1 cells were cultured for 6 d under standard and osteogenic conditions after X-irradiation. After fixation, X-gal staining was performed. OCT-1 cells converted this substrate of senescence-associated β-galactosidase (SA-β-gal). Senescent cells were detected after exposure to 8 Gy regardless of cultivation in SC or OI medium.

3.3.3 Effects of irradiation on production of mineralized matrix by OCT-1 cells

3.3.3.1 Effects of X-irradiation on calcium deposition

The effects of radiation exposure on differentiation of bone cells were investigated by determining their ability to deposit mineralized extracellular matrix under *in vitro* culture conditions using the Alizarin red S staining. After X-irradiation, cells were cultured in OI medium for 7, 10, 14 and 21 d (**Figure 3-20**). After Alizarin red S staining, the deposited calcium, which co-precipitates with phosphate to form bone nodules, appears as accumulation of red material in the petri dishes. Calcium precipitation was observed in brightly red color already 10 d after exposure to X-rays for doses above 4 Gy. At 10 Gy, the increase in agglomerated extracellular matrix was higher than at lower doses. With increasing incubation time, the calcium precipitation augmented dose-dependently.

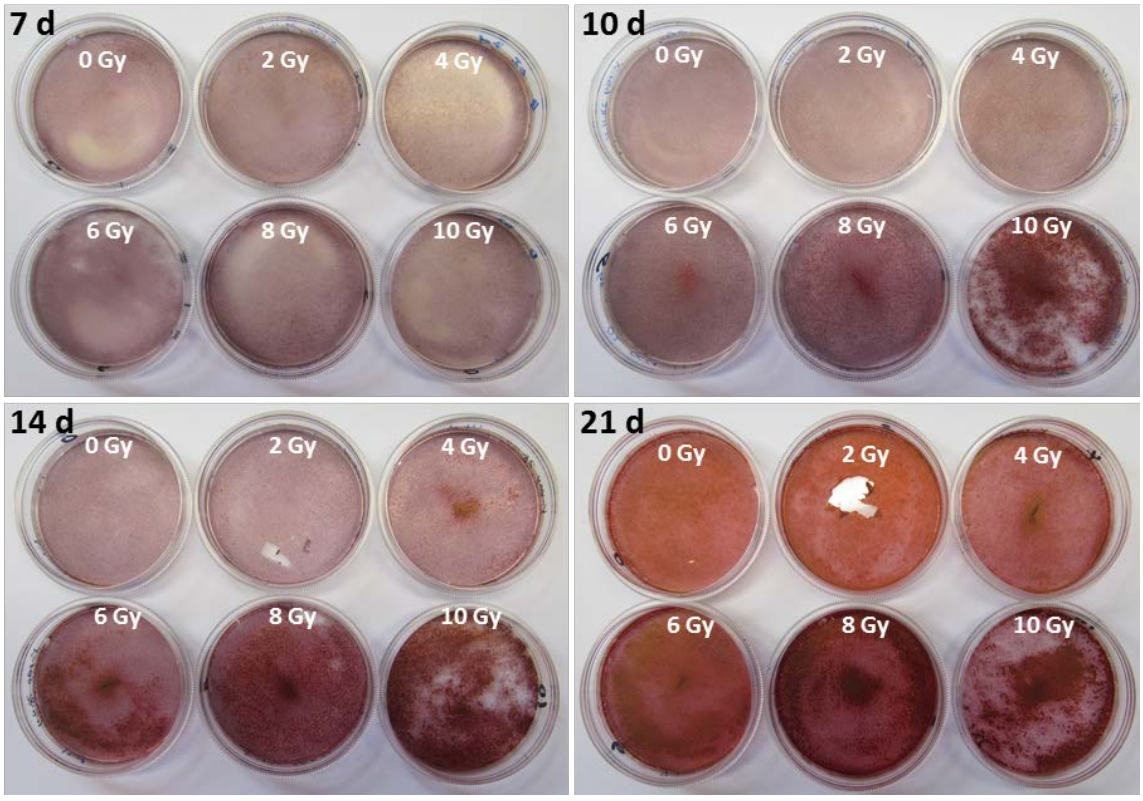

Figure 3-20 Deposition of mineralized extracellular matrix by OCT-1 cells after X-irradiation

After X-ray exposure with different doses (0, 2, 4, 6, 8 and 10 Gy) and incubation in OI medium for 7, 10, 14 and 21 d, the cells were fixed after the incubation time and stained with Alizarin red S.

3.3.3.2 Quantification of calcium deposition

OCT-1 cells were exposed to X-rays irradiation with doses of 2, 4, 6, 8 and 10 Gy and the deposited calcium was visualized by Alizarin red S staining. To quantify the calcium deposition of OCT-1 cells, images of the cell layer were taken and analyzed using ImageJ software. The resulting red color saturation were plotted (**Figure 3-21**). With increasing incubation time, calcium deposition increased after exposure to all tested doses and also after mock-irradiation (**Figure 3-21 A**). On day 7, there was no difference for the tested doses. After irradiation, deposition of mineralized extracellular matrix started already at day 10 and further increased dose-dependently at day 14. Without X-ray exposure, there is no increase until after day 14.

21 d after X-irradiation, the staining reveals that an almost equal amount of calcium was deposited in all samples (**Figure 3-21 B**).

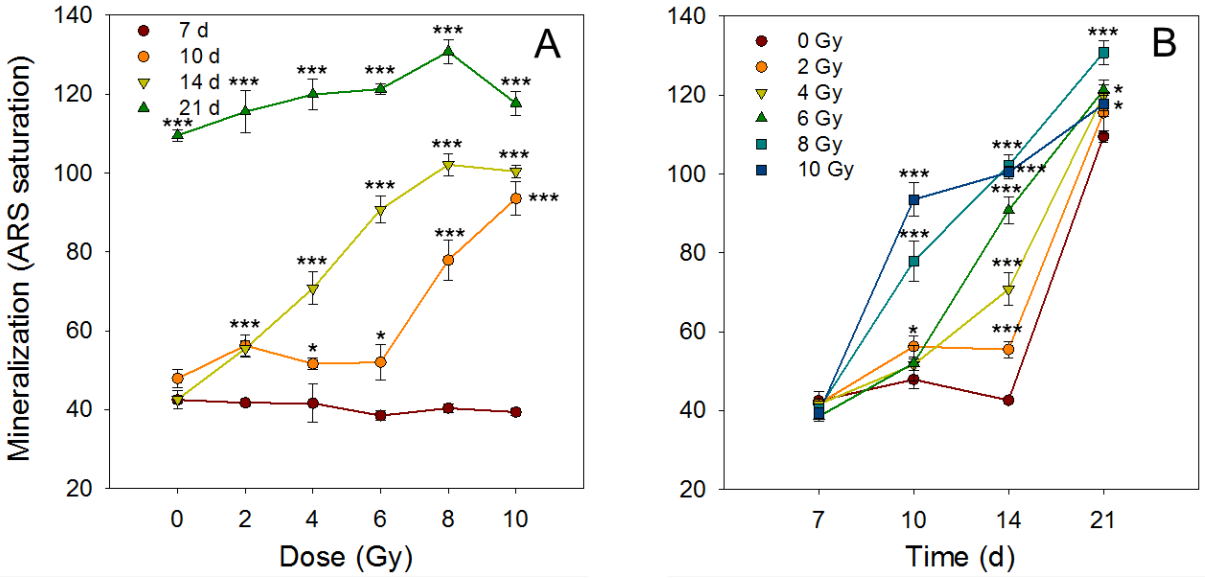

Figure 3-21 Calcium deposition by OCT-1 cells after X-ray exposure

For the dose-dependence of calcium deposition, significant differences of the mineralization of 10, 14, 21 d to 7 d post-irradiation incubation were addressed (A). For the kinetics of calcium deposition after X-ray exposure, the significance of differences of the mineralization after exposure to 2, 4, 6, 8, 10 Gy in comparison 0 Gy was calculated (B). Data represent mean ± SE from 3 independent experiments with 5 measurements each. Statistical significance was determined with two-tailed Student's t-tests (*, p < 0.05; **, p < 0.01; ***, p < 0.001).

3.3.4 Effects of osteogenic differentiation medium on radiation effects in OCT-1 cells

To understand the influence of osteogenic induction by incubation in OI medium on survival, repair, and proliferation ability of OCT-1 cells after exposure to X-rays, colony forming ability, DNA DSB repair and growth were measured in cells that were seeded and cultured in OI and SC medium.

3.3.4.1 Survival after X-ray exposure

The survival curves after X-irradiation show a shoulder in the lower dose range for both conditions, OI and SC medium (**Figure 3-22**). Exposure to higher doses resulted in an exponential course of the survival curves. No significant differences could be detected for cellular survival under osteogenic culture conditions compared to standard conditions.

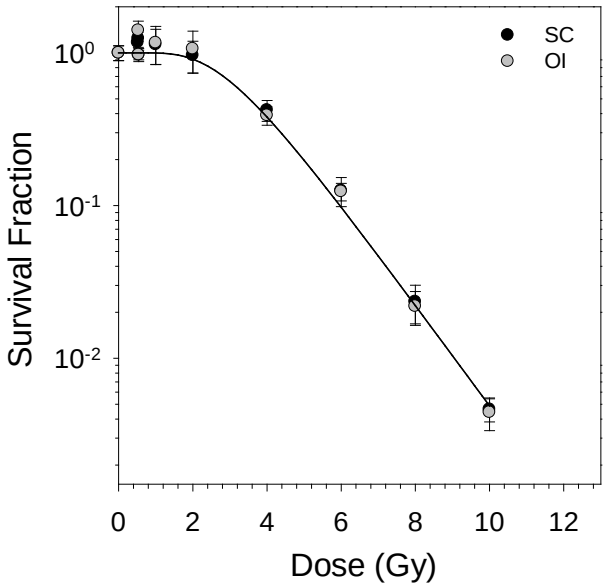

Figure 3-22 Survival after X-irradiation without or with osteogenic induction

After irradiation, OCT-1 cells were seeded and cultured in SC or in OI medium. Their survival curves were fitted with the equation $S = 1-(1-e^{D/D_0})^n$ with D, dose; D_0, reciprocal value of the slope within the linear part of the curve; n, number of targets. Data represent mean ± SE of three independent experiments with 6 replicates for each sample. Statistical significance was determined with the two-tailed Student's t-tests. No significant difference for incubation in SC or OI medium was found.

3.3.4.2 DNA repair kinetics

After cultivation of cells in SC/OI medium for up to 3 weeks, OCT-1 cells were exposed to X-rays. Directly afterwards, the DNA DSBs were analyzed using AFIGE. The fraction of activity released (FAR) is a measure of DNA DSBs. The equivalent dose (Deq) was estimated for each FAR value and dose response curves were generated. The repair kinetics after exposure to X-rays at single dose of 20 Gy were measured and plotted as Deq against time (**Figure 3-23 A B**).

The cells cultured in the SC medium for up to 3 weeks show similar repair kinetics for all pre-irradiation incubation periods. The DSBs decreased to a nearly basal level within 2 to 4 h (**Figure 3-23 A**). There is a similar effect in the cells cultured in OI medium (**Figure 3-23 B**). These results show that OI medium does not disturb the repair capacity.

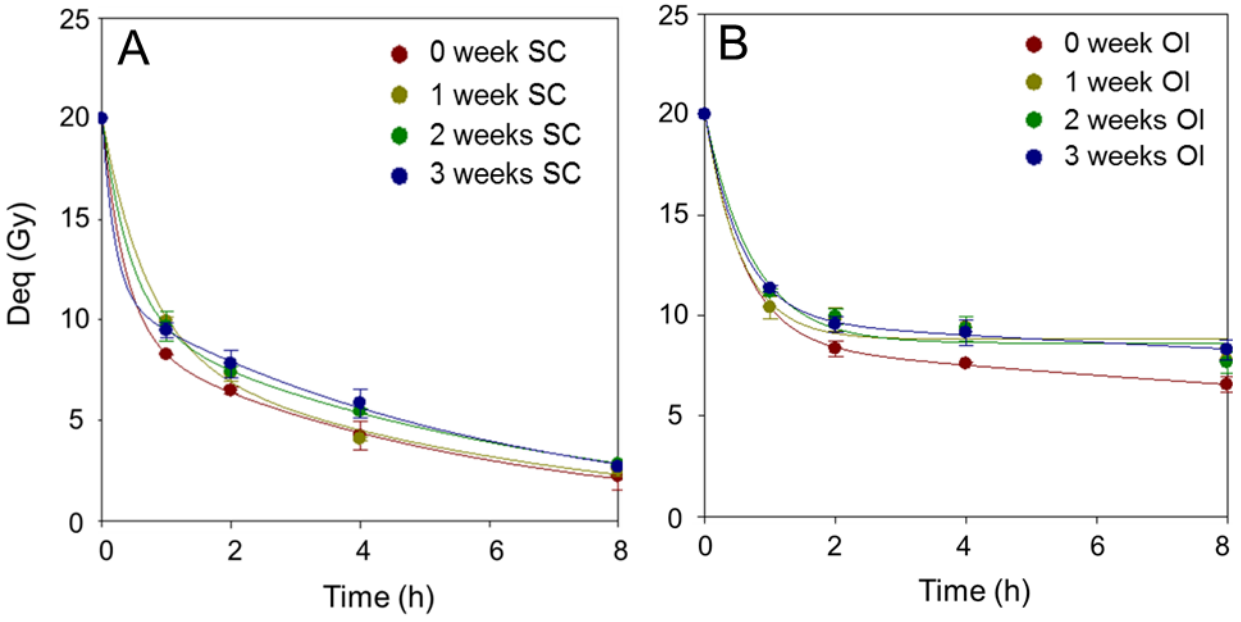

Figure 3-23 DNA double strand break (DSB) repair kinetics of OCT-1 cells after X-irradiation

Cells were cultured in SC (A) and OI (B) medium for up to 3 weeks and then exposed to X-rays. DSB were measured by AFIGE and the equivalent dose (Deq) was calculated. Data represent mean ± SE of 3 independent experiments with each 10 replicates. Statistical significance was determined with two-tailed Student's t-tests. No significant difference for incubation in SC or OI medium was found.

3.3.4.3 Cellular proliferation after radiation exposure

The effects of different radiation qualities on cell proliferation in absence or presence of OI medium were investigated by establishing growth curves based on DNA content of the cell layers. Cells were stained with bisbenzimide and resulting blue fluorescence of bisbenzimide-DNA complexes was measured.

X-irradiation caused a significant decrease in cell numbers under standard and osteogenic differentiation culture conditions (**Figure 3-24 A B**). Maximal DNA content of the cell layer was observed on day 5-6 after exposure to 1 and 2 Gy or after mock-irradiation. At this time, cells demonstrated a polygonal morphology (**Figure 3-18**). Exposure to 8 Gy resulted in a significantly lower increase of DNA content of the cell layer.

These results indicate that X-irradiation significantly slows down the proliferation of pre-osteoblast cells in a dose-dependent manner (at doses of 4 and 8 Gy). Compared to X-rays, cellular proliferation was significantly reduced after exposure to 4 Gy of titanium ions (LET 108 keV/µm) (**Figure 3-24 C D**). The presence of OI medium had no significant impact on cellular proliferation in comparison to growth in SC medium.

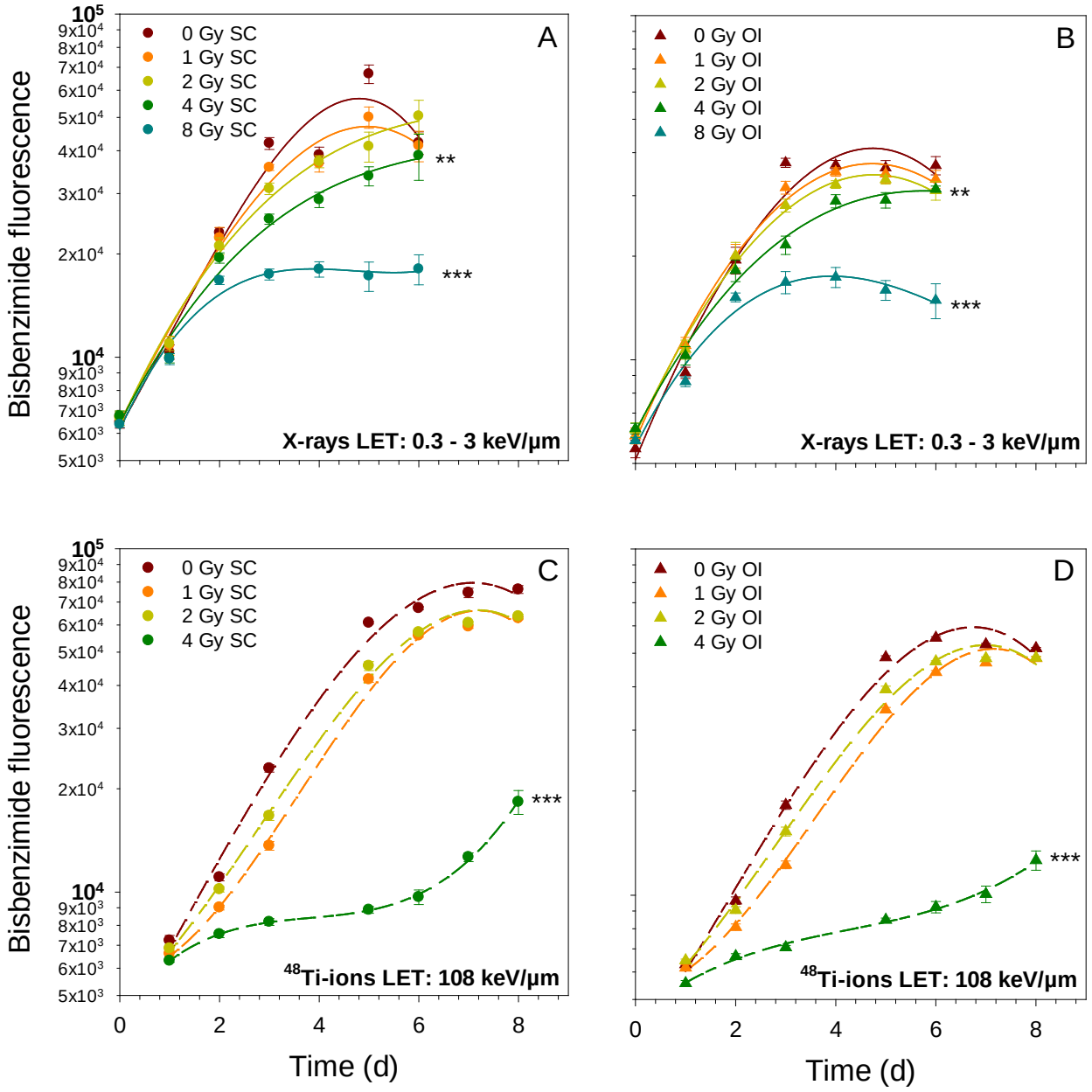

Figure 3-24 Proliferation of OCT-1 in absence or presence of OI medium after exposure to different radiation qualities

OCT-1 cells were exposed to 1, 2, 4 and 8 Gy X-rays (A, B) or 1, 2 and 4 Gy Ti ions (LET 108 keV/µm) (C, D). After radiation exposure, cells were subsequently cultured for up to 6 d or 8 d in SC and OI medium. The relative cell number was evaluated by measuring the fluorescence of the DNA intercalating dye bisbenzimide at excitation/emission wavelengths of 360 nm / 460 nm, respectively. Data represent mean ± SE of one (Ti) or 3 independent experiments (X-rays) with 8 replicates each. Statistical significance between irradiated and unirradiated samples was determined with two-tailed Student's t-tests (*, p < 0.05; **, p < 0.01; ***, p < 0.001).

3.3.5 Effects of radiation on pre-osteoblast differentiation

TGF-β1 and Runx2 play an important role in controlling osteoblasts' growth, early differentiation and also later mineralization of secreted extracellular matrix.

P53 takes part in the DNA damage response and repair, and also in the differentiation of bone cells. In order determine whether p53 plays a role in the effect of radiation of on OCT-1 cell differentiation, cells were treated with p53 inhibitor cyclic pifithrin-α (30 µM) 2 h before radiation.

To address the question whether radiation can influence the initiation of OCT-1 cell differentiation via p53 activation, TGF-β1 (**Figure 3-25, 3-26**) and Runx2 (**Figure 3-27, 3-28**) expression of OCT-1 cells after exposure to X-rays at a dose of 8 Gy was visualized by immunofluorescence staining in the presence or absence of cyclic pifithrin-α.

3.3.5.1 Effects of radiation on TGF-β1 expression

Figure 3-25 illustrates the immunofluorescence staining of TGF-β1 in OCT-1 cells. After exposure to 8 Gy X-rays, TGF-β1 expression increases after 15 min until 6 h (**A, B**). There are no obvious changes after treatment with cyclic pifithrin-α alone (**Figure 3-26 A**). Cells treated with cyclic pifithrin-α before X-irradiation show a decrease in TGF-β1 expression 2 h after irradiation which recovers only marginally at 4 and 6 h after exposure (**Figure 3-26 B**).

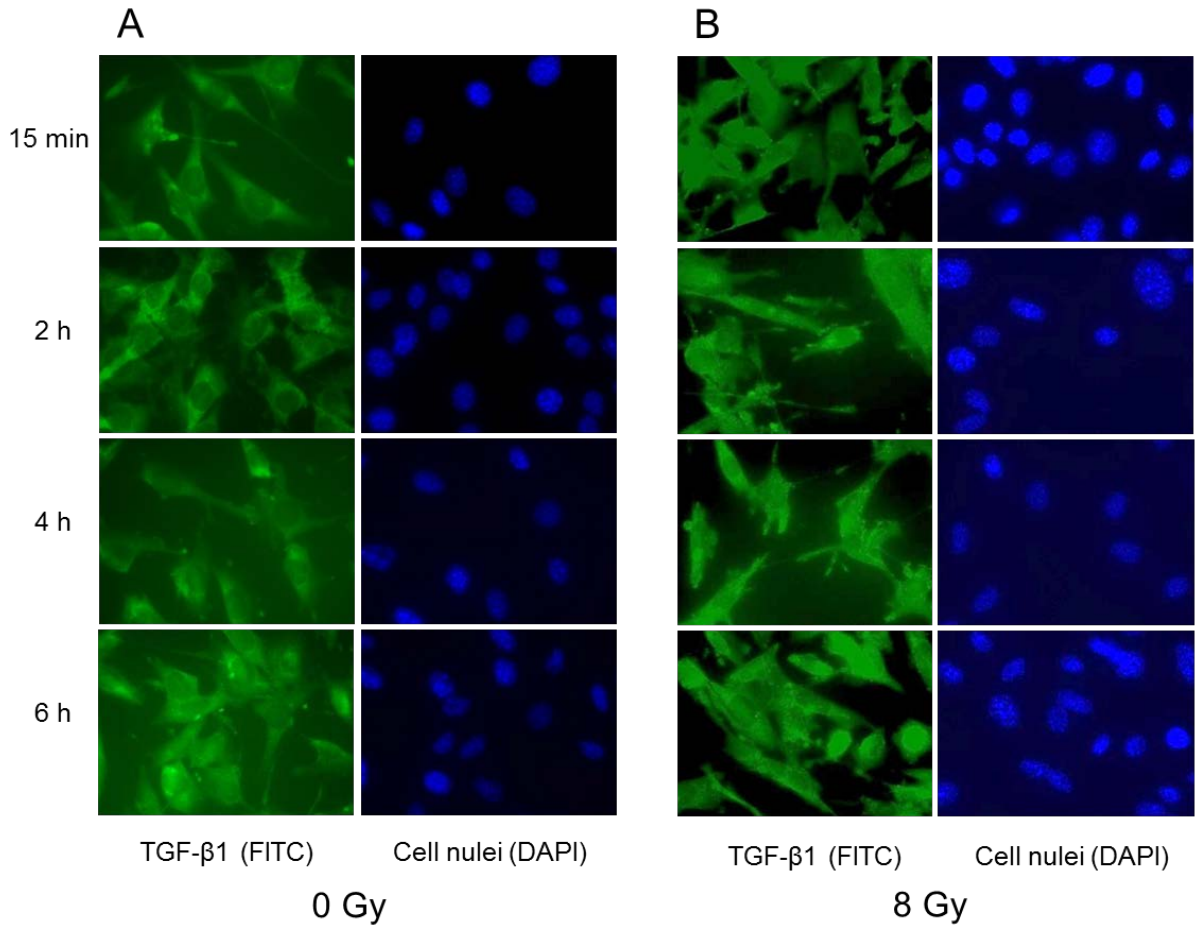

Figure 3-25 TGF-β1 expression in OCT-1 cells after X-ray exposure

The staining was performed with fixed cells using polyclonal rabbit anti-TGF-β1 antibody 0.25, 2, 4 and 6 h after exposure to 8 Gy X-rays (B). The unirradiated samples are shown as controls (A). TGF-β1 was visualized by FITC in the fluorescence microscope. On the right side of the figures show the DAPI stained cell nuclei (object lens magnification: 63 ×).

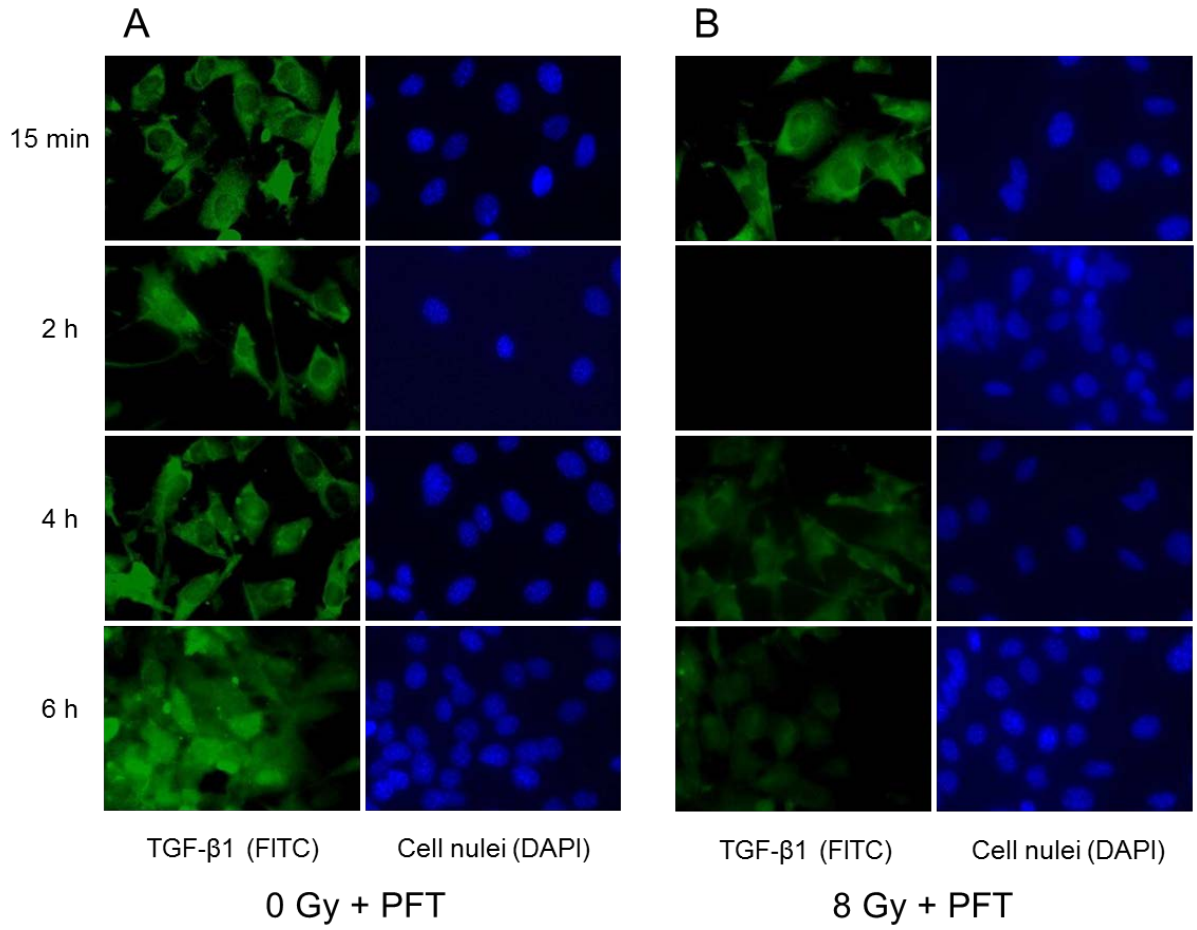

Figure 3-26 TGF-β1 expression in OCT-1 cells after X-ray exposure in presence of cyclic pifithrin-α

The staining was performed with fixed cells using polyclonal rabbit anti-TGF-β1 antibody 0.25, 2, 4 and 6 h after exposure to 8 Gy X-rays with 2 h cyclic pifithrin-α pre-incubation (B). The unirradiated samples with 2 h cyclic pifithrin-α pre-incubation are shown as controls (A). TGF-β1 was visualized by FITC in the fluorescence microscope. On the right side of the figures show the DAPI stained cell nuclei (object lens magnification: 63 ×).

3.3.5.2 Effects of radiation exposure on Runx2

OCT-1 cells were fixed and stained for Runx2 expression. The result shows that 8 Gy X-rays and cyclic pifithrin-α can alone or together suppress Runx2 expression early after treatment (**Figure 3-27, 3-28**). The expression does not recover within 6 h.

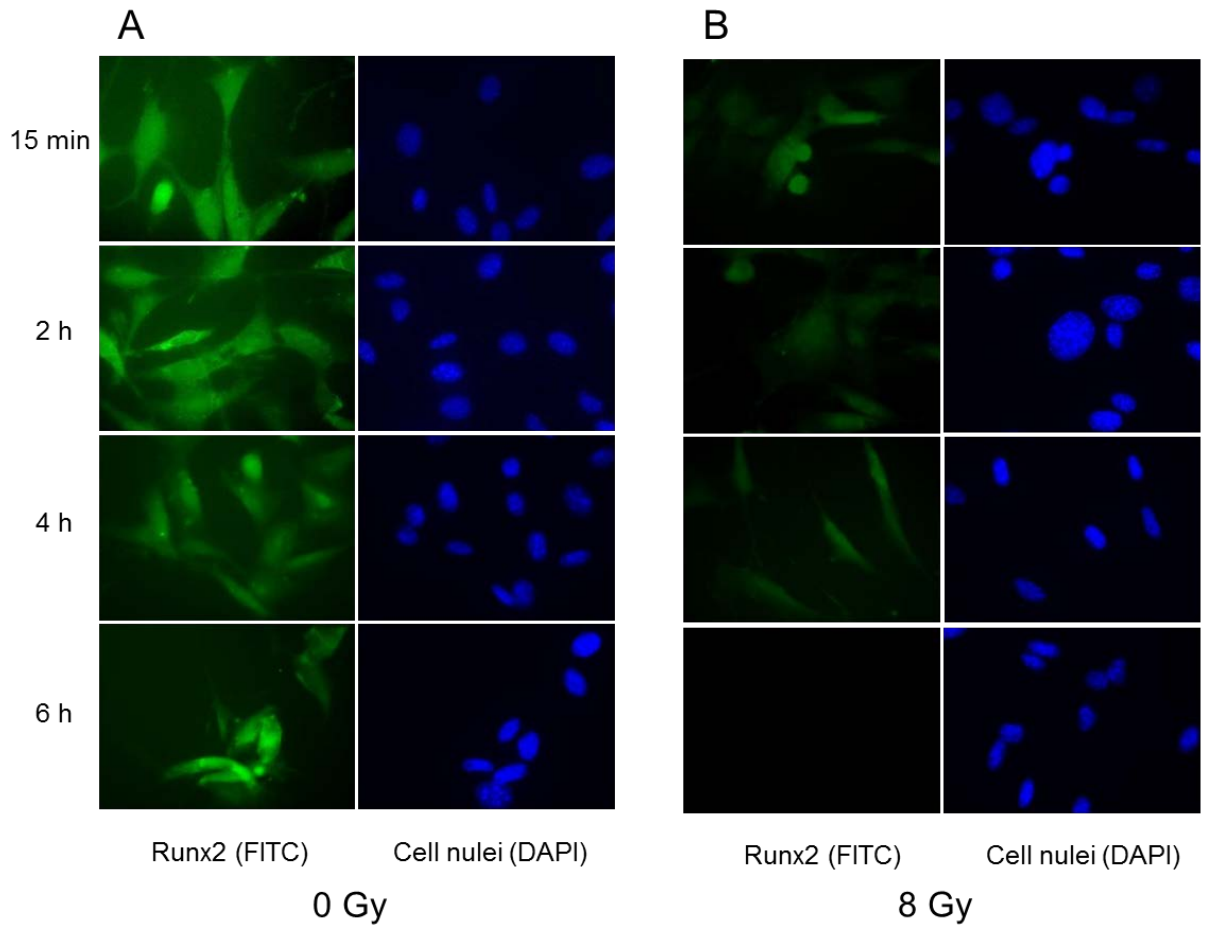

Figure 3-27 Runx2 expression in OCT-1 cells after X-irradiation

The staining was performed with fixed cells using polyclonal rabbit anti-Runx2 antibody 0.25, 2, 4 and 6 h after irradiation with 8 Gy X-rays (B). The unirradiated samples are shown as controls (A). Runx2 was visualized by FITC in the fluorescence microscope. On the right side of the figures the DAPI stained cell nuclei are shown (object lens magnification: 63 ×).

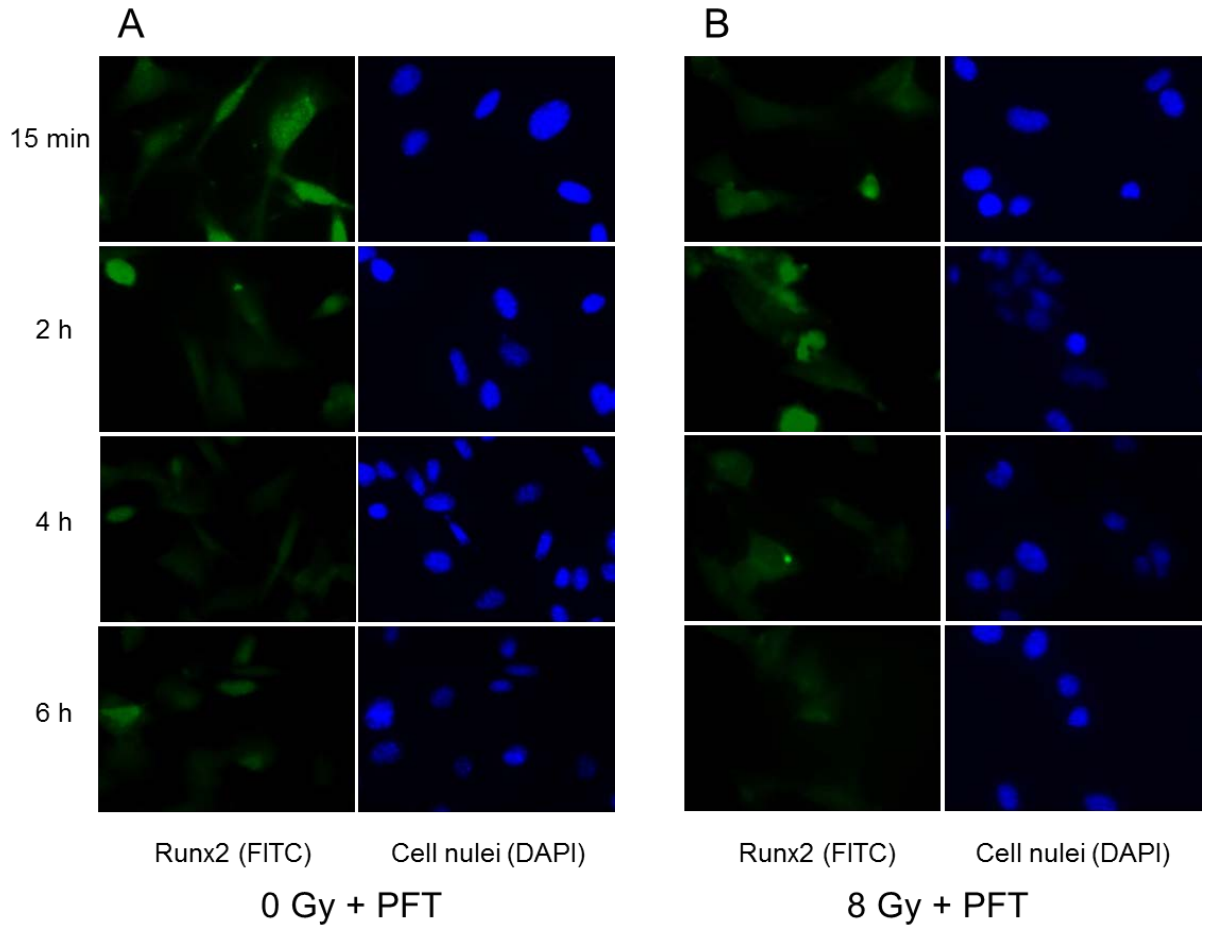

Figure 3-28 Runx2 expression in OCT-1 cells after X-ray exposure in presence of cyclic pifithrin-α

The staining was performed with fixed cells using polyclonal rabbit anti-Runx2 antibody 0.25, 2, 4 and 6 h after irradiation with 8 Gy X-rays in presence of cyclic pifithrin-α (pretreatment 2 h before radiation exposure) (B). The unirradiated samples are shown as controls (A). Runx2 was visualized by FITC in the fluorescence microscope. On the right side of the figures the DAPI stained cell nuclei are shown (object lens magnification: 63 ×).

4. Discussion

The aim of this study was to analyse how pre-osteoblasts respond to space relevant radiation. Depending on dose, dose rate, radiation quality, cell type and other factors, different outcomes can predominate (**Figure 4-1**). As pre-osteoblasts have the capability to differentiate to bone matrix secreting osteoblasts, this osteogenic differentiation process might be accelerated, induced, decelerated or stopped after radiation exposure. Therefore, besides the "classical" outcomes cell cycle arrest (**Figure 4-1 B**) and cell death (**Figure 4-1 A**), differentiation and senescence (**Figure 4-1 C**) were highlighted as potential endpoint of the cellular radiation response.

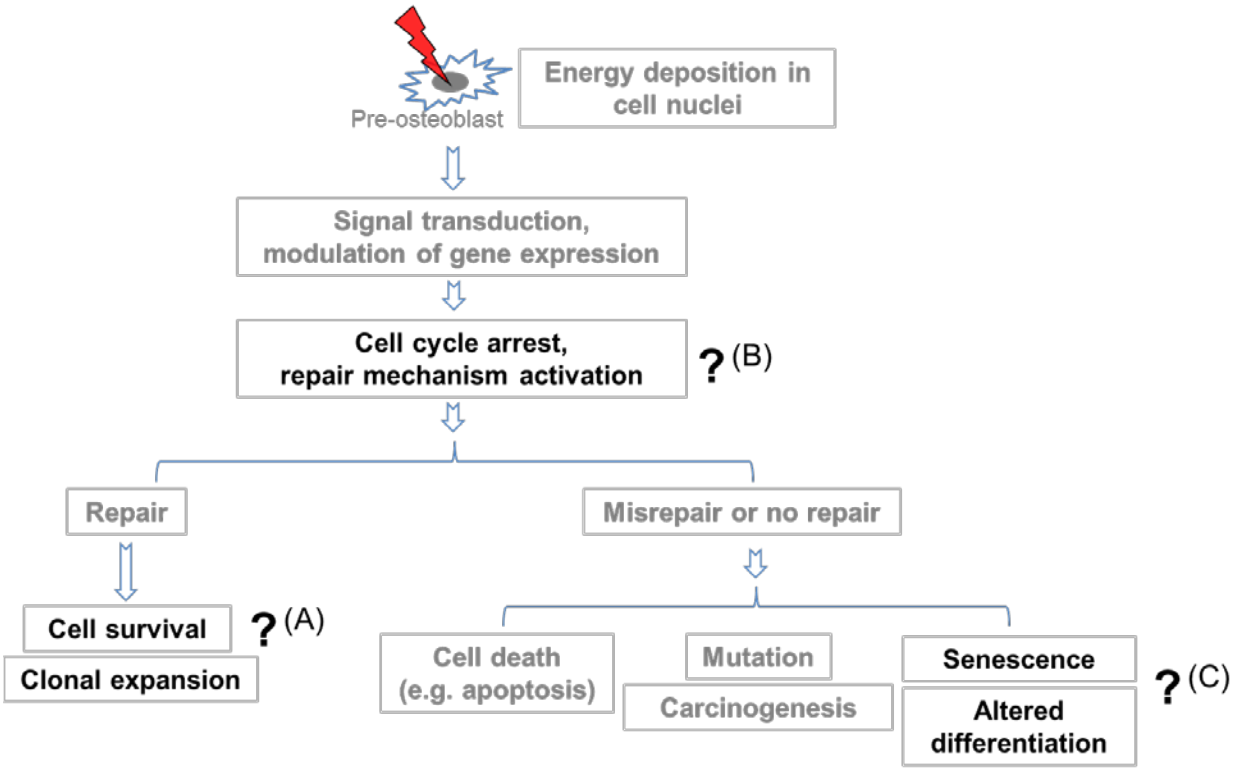

Figure 4-1 Cellular radiation effects in pre-osteoblasts

Deposited energy induces DNA damages in the cell nuclei. The immediate response to DNA damages is the activation of cell cycle checkpoints (B) and stimulation of the repair machinery in order to survive (A) and maintain the genomic integrity and stability. Misrepaired or not repaired DNA damage results in cellular responses such as cell death (e.g. apoptosis), mutation generation, altered differentiation or senescence induction (C).

The findings of this study indicate that radiation with a linear energy transfer (LET) of 150 keV/µm was most effective in inducing reproductive cell killing (**Figure 4-1 A**).

High LET radiation causes more pronounced cell cycle arrest (**Figure 4-1 B**). Cell cycle delay is more pronounced after exposure to high-LET compared to low-LET radiation. Expression analyses indicated that cells exposed to ionizing radiation exhibited significantly up-regulated CDKN1A gene expression (**Figure 4-1 B**).

Further study on cellular differentiation revealed its dose-dependent elevation after X-irradiation (**Figure 4-1 C**). p53 is mainly considered as a tumor suppressor for its ability to induce apoptosis and suppress proliferation after exposure to cell stress, including ionizing radiation exposure. Apart from that, some recent studies present evidence that p53 also affects bone cell differentiation (Liu and Li, 2010; Wang *et al.*, 2006a). Reversible inhibition of p53 by cyclic pifithrin-α enhanced radiation-induced cell cycle arrest (**Figure 4-1 B**) and inhibited X-ray-induced TGF-β1 expression taking charge in differentiation (**Figure 4-1 C**).

4.1 Cellular survival after exposure to ionizing radiation

In order to investigate the killing effect of exposure to different radiation qualities (LET 0.5 – 9674 keV/µm), clonogenic survival of the pre-osteoblast cell line OCT-1 and the mesenchymal stem cell line C3H10T1/2 was determined by applying the colony forming assay. Both cell lines possess the ability to be induced to differentiate to mature osteoblasts.

Up to now, series of studies have been carried out to determine cellular survival after X-ray exposure (D_0: dose reducing the survival to 37% of the original value) (**Table 4-1**). Survival of rat thyroid cells showed that the D_0 had a value of 1.90 Gy (irradiated *in vitro* and assayed *in vivo*) (DeMott *et al.*, 1979) and of 1.95 Gy (irradiated *in vivo* and removed immediately for assay) (Mulcahy *et al.*, 1980). Other *in vitro* studies on V79, human salivary gland tumor and T1 cells showed D_0 values of 1.85, 0.81 and 1.04 Gy (Furusawa *et al.*, 2000). An investigation of human diploid fibroblasts indicated D_0 values of 1.28 – 1.64 Gy (Weichselbaum *et al.*, 1980). *In vitro* studies with the murine osteocyte like cell line MLO-Y4 and two subclones of MC3T3-E1 cells, MC3T3-E1-S4

and MC3T3-E1-S24, which were isolated from the calvaria of a C57BL/6 mouse indicated D_0 values of 2.16, 1.50 and 1.94 Gy, respectively (Lau et al. 2005). In this study, the analysis on OCT-1 and C3H10T1/2 cells revealed that D_0 values of 1.44 Gy and 1.66 Gy (**Table 3-1, Table 3-2**). The D_0 of OCT-1 and MC3T3-E1-S4 are comparable. Both cell lines are capable to differentiate to mature mature osteoblasts. The less radiosensitive MC3T3-E1-S24 cell line produces only very few mineralized extracellular matrix (Wang *et al.*, 1999). The also less radiosensitive osteocyte like cell line MLO-Y4 does not produce mineralized extracellular matrix at all (Bonewald, 1999; Kato *et al.*, 1997).

These results indicate a clear difference of radiation sensitivity between different cell types. The main cause for the different radiosensitivity of diverse cell lines is regarded to be the DNA repair ability, including the efficiency to recognize DNA damage and to activate repair (Chavaudra *et al.*, 2004; Szumiel, 1998). Specifically for tumor cells, increased radiation sensitivity is due to deficiencies in specific kinases needed for repair activation and checkpoint control (Szumiel, 2005; Szumiel, 2008). Another important influencing factor is the cell division activity. Cells are most radiosensitive in the mitotic and the G2 phase of the cell cycle (Pawlik and Keyomarsi, 2004; Sinclair and Morton, 1966). Therefore, a high mitotic activity correlates with a higher percentage of cells in the radiosensitive phases of the cell cycle.

Table 4-1 Cell survival parameters after X-ray exposure (single fraction survival curve)

Cell line	Cell type	Origin	Voltage (kV)	D_0	n	D_q	Reference
Primary cells	Thyroid cells[a]	Rat	250	1.90	4	2.63	DeMott *et al.*, 1979
Primary cells	Thyroid cells[b]	Rat	250	1.95	-	-	Mulcahy *et al.*, 1980
Diploid cell strains from patients	Diploid fibroblasts	Human	220	1.28 – 1.64	-	-	Weichselbaum *et al.*, 1980
V79	Fibroblasts	Chinese hamster	200	1.85	4.4	2.74	Furusawa *et al.*, 2000
HSG	Submandibular salivary gland cell line	Human	200	0.81	27	2.65	Furusawa *et al.*, 2000
T1	Cholangiocellular carcinoma cell line	Human	200	1.04	35	3.70	Furusawa *et al.*, 2000
S24	Pre-osteoblasts	Mouse	200	1.94	2.00	2.63	Lau *et al.*, 2005
S4	Pre-osteoblasts	Mouse	200	1.50	2.23	2.30	Lau *et al.*, 2005
MLO-Y4	Osteocyte	Mouse	200	2.16	4.94	4.94	Lau *et al.*, 2005
OCT-1	Pre-osteoblasts	Mouse	200	1.44 ± 0.09	6.37 ± 2.61	2.66 ± 0.69	This study
C3H10T1/2	Pluripotent stem cells	Mouse	200	1.66 ± 0.10	1.88 ± 0.39	1.05 ± 0.39	This study

Note. D_0, reciprocal value of the slope of the regression curves calculated within their exponential part; n, extrapolation number, obtained by extrapolating the exponential section of the curve to the abscissa; D_q, the quasi-threshold dose for a given population that measures the width of the shoulder.

[a] Irradiated *in vitro* and assayed *in vivo*

[b] Irradiated *in vivo* and removed immediately for assay

The survival curves show that the degree of killing depends on radiation dose and radiation quality. The slope of survival curves increases with augmenting LET up to ca. 150 keV/µm (Fe ions). For radiation qualities with an LET > 150 keV/µm, the slope decreases with increasing LET (**Figure 3-1**). These results clearly reflect that radiation qualities with an LET of ~150 keV/µm are most effective in killing murine pre-osteoblastic cells.

The relative biological effectiveness (RBE) of different radiation qualities is determined by comparing the doses of a test radiation and a reference radiation required to induce a defined biological endpoint. In this study, the RBE values for induction of reproductive cell death of OCT-1 cells were determined from the colony forming ability tests. X-rays were used as reference radiation. In the LET-RBE curve, RBE values, determined for cellular survival of pre-osteoblastic cells present a very distinct peak of 3.0 at an LET of ~150 keV/µm (**Figure 3-2**). Notably, for the tested radiation qualities, the two cell lines OCT-1 and C3H10T1/2 have comparable RBE values regarding the end point reproductive cell survival (**Figure 3-4**).

Previous studies on human lens epithelial cells (Chang *et al.*, 2005) or human skin fibroblasts (Tsuruoka *et al.*, 2008; Tsuruoka *et al.*, 2005) showed that high-LET radiation has a more pronounced effect on the survival ability than low-LET radiation. Some other studies on LET dependent mutagenic effects or tumor induction potential showed that high LET charged particles have stronger effects and indicate an LET-RBE dependency with a peak at an LET of 100-200 keV/µm (Alpen *et al.*, 1993; Chen *et al.*, 1994; Sorensen *et al.*, 2011; Tsuboi *et al.*, 1992).

When the LET values increase, the radiation energy deposition during its transversal through matter increases as well. The deposited energy can ionize water and biomolecules in the cell, resulting in damage. The more energy is deposited in the radiation track, the more DNA damage will be triggered and the more complex will it be. High LET radiation was shown to induce a greater number of DNA damages and more complex clustered DNA lesions than low LET radiation (Asaithamby *et al.*, 2008; Hada and Georgakilas, 2008). In addition, high-LET HZE particles induce more frequently

mis-rejoined and unrejoined DSBs in comparison to breaks induced by low-LET radiation (Rydberg *et al.*, 2005; Tsuruoka *et al.*, 2008). Thus, the time needed for repair of those high-LET radiation induced DSBs is longer compared to low-LET radiation induced DSBs (Anderson *et al.*, 2010; Autsavapromporn *et al.*, 2013; Ugenskiene *et al.*, 2009). The choice of DNA DSB repair pathway (NHEJ or HR) after exposure to high-LET and low-LET radiation might be influenced by the complexity of damage and in the following by the extent of DNA end resection (Yajima, 2013).

RBE values decrease when LET increases above 150 keV/µm, showing that radiation with an LET higher than 150 keV/µm is not as effective in cell killing, the so-called overkill effect. According to **Equation 2-1**, it can be expected that for the same absorbed dose, higher LET values lead to lower particle fluence. According to that assumption, high LET particle exposure results in increased energy deposition in more confined regions. When particles have a higher LET, the biological materials receiving the same absorbed dose receive fewer particles per area. An absorbed dose of 1 Gy is reached by irradiation with 4.0×10^6 P/cm^2 ^{56}Fe ions (LET 150 keV/µm) or with 6.4×10^5 P/cm^2 ^{58}Ni ions (LET 905 keV/µm), showing that 6.3 times more iron ions are required to reach the same dose compared to nickel ions. The energy deposition is locally extremely high for high-LET energetic particles, resulting in deadly DNA damage, but surrounding cells will not be hit and not damaged (in this example, 60 % of the cells are hit by at least one nickel ion, and 100 % by at least one iron ion). In the case of nickel ions, much of the deposited radiation energy is “wasted” and does not result in additional relevant biological damage. Therefore, the RBE decreases below 1 for heavy ions with very high LET values.

Energetic particles with an LET between 50 and 300 keV/µm have high RBE values. The maximal energy deposition occurs in the Bragg peak when traveling through matter. The depth at which the Bragg peak is achieved depends on energy and charge of the particle and on the material that is traversed. Heavy charged particle radiotherapy like carbon ion radiotherapy is one famous example in which these two principles (RBE, Bragg peak) are applied. Only those ions with small Z can be used for therapeutic purposes, because when the Z increases, the LET of the heavy charged particle will

also increase. The energy loss is very high when it reaches the surface of the tissue. This will increase normal tissue damage, radiation burning of the skin for example. Another problem with the particles heavier than carbon is that they produce a lot of secondary particles and therefore, their Bragg curves are not very “clean”.

To summarize this chapter, the LET dependency of cell killing that was previously described e.g. for fibroblasts and epithelial cells also applies for pre-osteoblasts. The high killing efficiency in the LET range of 50-300 keV/µm can lead to stronger deleterious effects on bone than low-LET radiation. This has to be considered in carbon ion radiotherapy if bone is in the radiation field and also for human spaceflight.

4.2 Radiation and p53 in cell cycle progression of OCT-1 cells

Ionizing radiation causes a variety of DNA damages including DSBs which pose great threat to cell survival. Cell cycle delays represent an active mechanism that responds to DNA damage (Budworth *et al.*, 2012; Wilson, 2004). Cell cycle checkpoints can function to halt cells temporarily or permanently and provide time for repair of damaged DNA before further cell cycle progression. The G2/M cell cycle checkpoint represents the last possibility to block the entry of cells with damaged DNA into mitosis to ensure that lesions are repaired and that each daughter cell receives an intact copy of the genome.

In this study, cell cycle analysis indicates that both, the extent and the length of G2/M delay are correlated to radiation dose and LET value (**Figure 3-5**). After X-irradiation, cell cycle arrest in G2/M (**Figure 3-8 A, Figure 3-10**) can be one of the reasons for the finding that the cell growth of irradiated cells is suppressed (**Figure 3-24 A B**). After exposure to high-LET ^{48}Ti-ions, cellular proliferation was diminished at higher doses (**Figure 3-24 C and D**).

In this study, cellular survival data indicate that ionizing radiation is most effective in killing pre-osteoblast cells around an LET of 150 keV/µm. In order to compare the effectiveness of different radiation qualities in inducing cell death and cell cycle arrest, cell cycle progression was determined after exposure of OCT-1 cells with X-rays, ^{13}C-ions, ^{22}Ne-ions and ^{64}Ni-ions (**Figure 3-8**) with $RBE_{cell\ killing}$ values of 1.0, 1.1, 2.3 and 2.7, respectively (**Table 3-1**). The effects of equitoxic doses on cell cycle were

compared, based on the 1% cellular survival level: 10, 5.6, 3.8 and 1.9 Gy (**Figure 3-6, 3-7 A, B, 3-8 B**). For comparison, cell cycle progression was studied after exposure to the same absorbed dose of 4 Gy (**Figure 3-8 C**).

Results from this work showed that, after irradiation with different qualities leading to 1% cellular survival, the cell cycle arrest is more pronounced after 1.9 Gy ^{64}Ni ion and 3.8 Gy ^{22}Ne ion exposure compared to 5.5 Gy ^{13}C ion and 10 Gy X-ray exposure. It is therefore suggested that radiation with a higher LET (above 90 keV/µm) possesses higher effects on cell cycle progression compared to low LET irradiation at the same survival dose. Therefore, it is concluded that compared to cellular survival ability, cell cycle progression delay is more sensitive after high-LET radiation exposure.

At the same absorbed dose of 4 Gy, ^{22}Ne and ^{64}Ni ions are much more efficient in inducing G2/M arrest than ^{13}C ions (LET 35 keV/µm) and X-rays. After exposure to the same absorbed dose, the G2/M arrest is LET dependent up to 90 keV/µm. This effect of LET on cell cycle arrest was shown also in normal human fibroblasts (with a delay in G1 phase) (Fournier and Taucher-Scholz, 2004; Tenhumberg *et al.*, 2007) and in Chinese hamster ovary cells (Nasonova *et al.*, 1998). In human mesenchymal stem cells, a stronger G2/M arrest was observed after exposure to ^{56}Fe ions than to X-rays (Kurpinski, 2009). In this work, the percentage of cells in G2/M reached saturation at around 80% after ^{64}Ni ion and ^{22}Ne ion exposure for both dose comparisons, based on 1% survival dose or on the same absorbed dose.

The increase of p21 after DNA damage induction was linked to the initiation of G2 arrest (Ando et al. 2001). In this context, p21 might act directly on CDK1 (Schneider et al. 1998). CDK1 associates with cyclin B at the G2/M transition and p21 plays a regulatory role in the maintenance of cell cycle arrest at G2 by blocking the interaction of Cdc25C with proliferating cell nuclear antigen (PCNA) which interacts with various CDK-cyclin complexes (Ando et al. 2001).

Therefore, CDKN1A gene expression was studied after exposure to the indicated radiation qualities with the 1% cellular survival dose (**Figure 3-9 A**), as well as 4 Gy absorbed dose (**Figure 3-9 B**). The result clearly indicates that the upregulation of

CDKN1A expression increases with the physical dose, independent from radiation quality (**Figure 3-9 A**). This upregulation of CDKN1A expression decreased with LET when cells were exposed to heavy ions at the same absorbed dose (4 Gy) (**Figure 3-9 B**), while increased dose dependently after X-irradiation (**Figure 3-13 A**). The observation that CDKN1A expression is dose dependently elevated cannot explain why cell cycle progression is more sensitive to high-LET radiation at an equal cellular survival level. One hypothesis to explain this observation might be that the cell cycle G2/M arrest is not merely mediated through an elevated CDKN1A expression but possibly also by ATR/Chk1 checkpoint activation (Liu *et al.*, 2000; Lobrich and Jeggo, 2007; Lossaint *et al.*, 2011). Another possibility is that it is sufficient if a certain threshold of CDKN1A expression is reached to induce G2/M arrest and that a further increase does not enhance the arrest.

It has been reported that over-expression of CDKN1A is capable of inducing both G1 and G2/M arrest, and CDKN1A induced G2/M arrest appears to be more prominent in retinoblastoma (pRb)-null cells (Roninson, 2002). There are no reports that pRb is not intact in OCT-1 cells.

The tumor suppressor protein p53 is known as upstream regulator of CDKN1A (**Figure 1-5**). P53 is involved in cell cycle regulation following exposure to DNA damaging agents like ionizing radiation in several cell lines including human osteosarcoma cells (U2OS), and human fibrosarcoma cell lines (Pellegata *et al.*, 1996; Petersen *et al.*, 2010; Stavridi *et al.*, 2001). The question was whether radiation-induced cell cycle arrest is under the regulation of p53.

In order to study the mechanism of the interplay between p53-p21 in ionizing radiation induced cell cycle arrest in the G2/M phase, cyclic pifithrin-α was used to temporarily inhibit p53 activity. The results show that G2/M blockage of the cell cycle is more pronounced after radiation exposure in combination with cyclic pifithrin-α treatment when compared to samples that were only irradiated (**Figure 3-10, Figure 3-11**). This indicates that functional p53 is not required for induction of cell cycle arrest after X-irradiation, and that this arrest is even enhanced. A slightly enhanced G2 arrest after

treatment with cyclic pifithrin-α was also observed in the human ovarian cancer cell line A2780 (Walton *et al.*, 2005). Cyclic pifithrin-α induced cell cycle arrest in G1 phase has been reported for murine embryonic stem cells and was related to decreased cyclin D1 expression (Abdelalim and Tooyama, 2012). Incubation of OCT-1 cells with cyclic pifithrin-α without irradiation slightly increased the percentage of cells in G2/M phase (Figure 3-11) and resulted in a transient increase of CDKN1A expression (Figure 3-12). This accumulation in G2/M phase already before radiation exposure might sensitize the cells for a stronger G2/M arrest by irradiation.

Gene expression analysis of the transcriptional level of TP53 revealed no significant difference early (up to 24 h) after irradiation. However, there is a slight down-regulation 48 h after exposure to 6 and 10 Gy in the presence of cyclic pifithrin-α (**Figure 3-12 C D**). Mdm2, the well-known negative feedback regulator of p53, was analyzed. Here, an up-regulation of Mdm2 4 h after exposure was observed, which peaked at 8 h after 6 and 10 Gy exposure both in presence or absence of cyclic pifithrin-α (**Figure 3-12 E F**). The rise and fall of CDKN1A levels (**Figure 3-12 A B**) was similar to the Mdm2 expression kinetics which can be explained by the fact that both Mdm2 and CDKN1A genes are strongly regulated by p53 at the transcriptional level. An increase of radiation-induced Mdm2 expression even in presence of cyclic pifithrin was also observed in human colon adenocarcinoma cells HCT116 and in A2780 cells (both wild-type p53 expressing cell lines) (Walton *et al.*, 2005).

Notably, 6 h after X-irradiation, p53 expression at protein level was slightly reduced and it totally vanished after supplementation with cyclic pifithrin-α (**Figure 3-14, 3-15**). The immunofluorescence staining of Mdm2 shows reduced expression both after X-ray exposure and cyclic pifithrin-α supplementation (**Figure 3-16, 3-17**), which is not consistent with the mRNA expression studies showing up-regulation 4 h after 10 Gy irradiation and 8 h after 6 or 10 Gy irradiation in the presence or absence of cyclic pifithrin-α. This discrepancy between mRNA and protein expression of Mdm2 was also found in non-small lung cancer specimens from patients (Ko *et al.*, 2000) and in clinicopathological studies in normal and tumorigenic breast epithelial cells (Gudas *et al.*,

1995). Further studies are needed to quantify Mdm2 protein levels in irradiated OCT-1 cells.

Cyclic pifithrin-α was found in the 1990's and is a small molecule isolated for its ability to reversibly block p53-dependent transcriptional activation and apoptosis (Pietrancosta *et al.*, 2005; Proietti De *et al.*, 2003). The cyclic pifithrin-α concentration which was used in this study (30 µM) was optimized and shown to be sufficient by several studies (Pietrancosta et al. 2005; Proietti De et al. 2003).

Inhibition of p53 activity by cyclic pifithrin-α has been reported to suppress cell proliferation by down regulating cyclin D1 and thus blocking cell cycle progression in G1 phase of the cell cycle (Abdelalim and Tooyama, 2012) and affecting the repair kinetics of X-ray induced DNA lesions leading to mis-repair events (Meschini *et al.*, 2010).

The findings on cell cycle progression after irradiation suggest that cell cycle regulation of pre-osteoblasts is much more sensitive to high-LET radiation than to low LET radiation. Up-regulation of p21 is influenced by radiation quality. The CDKN1A upregulation seems to be at least partly independent of p53 at the tested radiation doses and qualities.

The G2/M cell cycle regulation is complex and involves multiple molecular processes under different conditions. Overlapping p53-dependent and p53-independent pathways regulate the G2/M transition in response to genotoxic stress. Induction of p21 is implicated in a G2/M arrest in both p53-proficient (Chan *et al.*, 2000) and p53-deficient cancer cells (Ando *et al.*, 2001; De *et al.*, 2004). Since DNA damage and inhibition of replication also trigger p53-independent pathways, up-regulation of p21 expression independent of p53 might have caused G2/M cell cycle block (Eccles *et al.*, 2010; Taylor and Stark, 2001). Chk1 and Chk2 phosphorylation, independent of p53-p21, and subsequent phosphorylation of Cdc25C on serine 216 inhibits the cyclin B-CDK1 complex in order to block damaged cells in G2/M.

Further studies should be carried out concerning the role of p53-p21 pathway signaling, Chk1, Chk2 activation in cell cycle G2/M arrest and osteogenic differentiation in pre-osteoblasts after ionizing radiation exposure.

4.3 Radiation and p53 in the osteoblast differentiation and mineralization

One of the main engines that drives cellular senescence, differentiation or cellular transformation, is the loss of proper control of the cell cycle. Concerning radiation effects on OCT-1 cells, it was found that radiation can dose and LET dependently kill OCT-1 cells; and dose and LET dependently trigger G2/M cell cycle arrest with a concurrent elevation in CDKN1A expression.

To further address radiation effects, OCT-1 osteoblastic differentiation including the production of mineralized matrix was analyzed.

The OCT-1 cells have been reported to possess the capability of differentiating along the osteoblastic lineage (Chen *et al.*, 1995; Lau *et al.*, 2010). Mature functional osteoblasts are capable of depositing extracellular matrix that mineralizes (Aubin, 1998a). ARS staining was used to verify the calcium incorporation in extracellular matrix deposited by differentiated cells. ARS staining is one of the commonly used techniques for the detection of calcium deposition in bone nodules. Under standard culture conditions and incubation for up to 21 days, no positive red staining could be visualized (data not shown). Apparently, OCT-1 cells were not able to start the osteoblastic differentiation process solely after radiation exposure and without osteogenic induction.

Therefore, osteogenic supplementation was used to induce of OCT-1 cells to differentiate into bone-matrix secreting mature osteoblasts. Since it was established (Bellows *et al.*, 1986), this method has been widely applied for osteogenic differentiation (Jaiswal *et al.*, 1997; Jeon *et al.*, 2013; Yokota *et al.*, 2013). Studies on differentiation induced by adding osteogenic supplements (50 µg/ml ascorbic acid and 10 mmol/l β-glycerophosphate) showed accelerated transcriptional expression in Runx2 (Wang *et al.*, 2013) and increased expression of osteogenic marker genes including ALP, osteocalcin and osteopontin, and stimulated ALP activity in MC3T3-E1 cells (Suh *et al.*, 2008). Other studies showed accelerated differentiation of primary human osteoblasts through enhanced Runx2 expression after osteogenic induction (Perinpanayagam *et al.*, 2006). This was found also in C3H10T1/2 and mouse pluripotent mesenchymal precursor cells C2C12 (Pregizer *et al.*, 2007).

Up to now, the effect of osteogenic supplementation on DNA repair after radiation exposure has not yet been analyzed. In this study, cells cultured in both media showed the same pattern in senescence formation (**Figure 3-18, 3-19**), surviving ability (**Figure 3-22**), repair ability (**Figure 3-23**), and cellular proliferation (**Figure 3-24**) in a dose and LET dependent manner. This indicates that culturing in OI medium did not change the radiation response of OCT-1 cells compared to growth in SC medium. Therefore, the osteogenic differentiation pathway seems not to be connected with DNA repair pathways and survival pathways.

Surprisingly, the results on osteogenic induction after exposure to higher radiation doses suggest that X-iradiation accelerates the mineralization process. Thus, calcium phosphate deposition could be detected 10 d after exposure to 6, 8 and 10 Gy X-rays, but not after 0, 2 and 4 Gy (**Figure 3-20; Figure 4-2**). Quantification of the hydroxyapatite content of the extracellular matrix secreted by mature osteoblasts revealed a significant, dose-dependent elevation of mineralized material (**Figure 3-21**).

Other studies of the effects of ionizing radiation on osteoblast differentiation revealed a reduced ALP activity and decreased expression of mRNA encoding ALP and collagen type I. These studies were performed with C2C12 cells originating from myoblasts which have multipotentiality to differentiate into osteoblasts. The cells were supplementated with BMP-2 after X-irradiation at doses of 2 and 4 Gy (Sakurai *et al.* 2007). The mechanism for the radiation induced down-regulation of differentiation seems to be down-regulation of the BMP-2/receptor complex and blockage of cellular responsiveness to BMP-2-induced osteoblastic differentiation (Pohl *et al.*, 2003). In the mesenchymal stem cell line C3H10T1/2 derived from a mouse embryo it was shown that ionizing radiation inhibited the growth and decreased ALP activity which indicated decreased differentiation (Sakurai *et al.*, 2011). Other studies on MC3T3-E1 cells indicated that ionizing radiation caused dose-dependent decreases in cellular proliferation and promoted differentiation (increased ALP production) (Dudziak *et al.*, 2000). This radiation-induced (4 Gy) promotion of osteoblastic differentiation in MC3T3-E1 cells determined by measurement of ALP activity was confirmed by other studies (Dare *et al.*, 1997; DeMott *et al.*, 1979; Sakurai *et al.*, 2007).

The results on TGF-β1 expression showed enhanced expression after 8 Gy X-ray exposure (**Figure 3-25)**; while decreased expression was found in samples supplemented with cyclic pifithrin-α 2 h before radiation exposure (**Figure 3-26; Figure 4-2**). The Runx2 expression results presented evidence that both radiation exposure and cyclic pifithrin-α can suppress Runx2 expression (**Figure 3-27, 3-28; Figure 4-2**).

TGF-β1 signaling interferes with the stress response through coordinated transcriptional and translational repression of p53 levels, which reduces p53-activated transcription, and apoptosis in precancerous cells (Lopez-Diaz *et al.*, 2013). P53 was also found to negatively regulate osteoblast differentiation and bone development and to reduce the level of Runx2 (Lengner *et al.*, 2006; Zambetti *et al.*, 2006).

It has been reported that TGF-β1 regulates a broad range of biological processes, including decreases in ALP activity, suppression of BMP mediated Smads signaling in osteoblasts (Liu *et al.*, 2013), and increased bone formation *in vitro* mainly by recruiting osteoblast progenitors, stimulating their proliferation and promoting the early stages of differentiation (Zhao *et al.*, 2010). TGF-β1 blocks late stages of osteoblast differentiation (Alliston *et al.*, 2001; Maeda *et al.*, 2004).

This enhanced expression of TGF-β1 after radiation exposure is controversial to the findings of radiation-reduced cellular proliferation (**Figure 3-24**) and induced cell cycle arrest (**Figure 3-5**) but coincides with the enhanced mineralization observed 10 days after exposure to high radiation doses (6, 8, 10 Gy) (**Figure 3-20**). The mechanism behind decreased expression of TGF-β1 when p53 was suppressed and the role of TGF-β1 during late osteoblastic differentiation should be further addressed.

Runx2 is a common target of TGF-β1. It has been reported that TGF-β1 stimulated osteoblast differentiation and the synthesis of matrix proteins and their receptors (for example, fibronectin, fibronectin receptor, collagen, osteonectin, osteopontin, and integrins) (Kasagi and Chen, 2013; Lee *et al.*, 2000). TGF-β1 can be induced by the course of osteogenic supplementation during MC3T3-E1 cell differentiation (Seth *et al.*, 2000).

Radiation induced suppression of Runx2 expression is coincident with radiation induced cell cycle progression arrest (**Figure 3-5**) and reduced cellular proliferation (**Figure 3-24**). It has also been reported earlier that Runx2 promotes osteoblast cell growth (Pratap *et al.*, 2003). Therefore, the early Runx2 downregulation after irradiation might be involved in cell growth reduction.

Some studies present evidence that p53 has an anti-differentiation function through a reduced level of the bone specific master transcription factor Runx2 (Franceschi and Xiao, 2003; Lengner *et al.*, 2006). This might indicate that p53-Runx2 plays an inhibitory role in the early stage of osteoblast differentiation after radiation exposure in order to ensure genome maintenance.

Accelerated differentiation was found not until 10 days after X-ray exposure. Further experiments are needed to explore the role of Runx2 in the late accelerated and enhanced osteoblast differentiation after radiation exposure.

Several studies showing that, depending on the specific cell type and the specific differentiation program, p53 may have a positive or a negative effect on cell differentiation, and thus can be referred as a “guardian of the genome” at large (Lane, 1992; Molchadsky *et al.*, 2008). The exact regulation of p53, Runx2 and TGF-β1 in osteoblast differentiation has not yet been fully elucidated. Further studies should be carried out to define p53-Runx2 and p53-TGF-β1 regulation during late differentiation after ionizing radiation exposure (**Figure 4-2**).

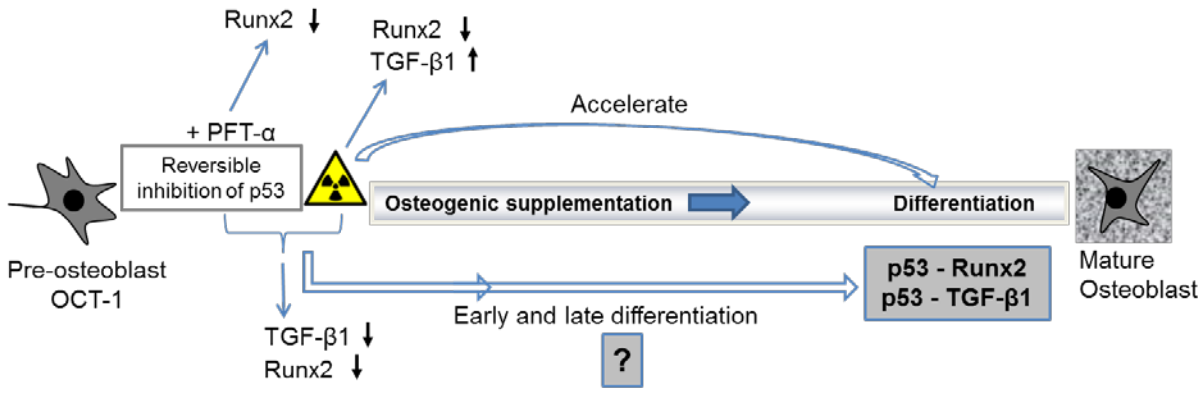

Figure 4-2 The effect of radiation and cyclic pifithrin-α on Runx2 and TGF-β1 during OCT-1 osteogenic differentiation

Radiation and cyclic pifithrin-α can modulate early expression of Runx2 and TGF-β1. Further experiments are needed to address the regulation of p53-Runx2 and p53-TGF-β1 in accelerated osteogenic differentiation.

4.4 Outlook

Radiation dose- and LET-dependently kills pre-osteoblasts and delays cell cycle progression. The cell cycle regulation is more sensitive to high-LET radiation than cell survival. Radiation-induced cell cycle arrest is not solely regulated through elevated CDKN1A expression. The cellular differentiation study revealed dose-dependent acceleration after X-irradiation. X-ray exposure and/or p53 can modulate Runx2 and TGF-β1 expression during osteoblast differentiation.

To better understand the mechanism behind accelerated osteoblast differentiation after X-irradiation, further experiments should be designed to analyze p53-Runx2, p53-TGF-β1 regulation during the early and late differentiation after radiation exposure.

Osteoblasts regulate osteoclast differentiation and resorption activity by the secretion of cytokines or by direct cell contact. Skeletal development and its maintenance in post-natal life in response to local and systemic stimuli are constantly remodeled by coordinated activity among osteoblasts, osteocytes and osteoclasts. Thus, studies of the ability of osteoblastic, osteoclastic and osteocytic cells to communicate in a co-culture system or *in vivo* investigations after radiation exposure are necessary.

Humans travelling in space are exposed to both microgravity (µ×g) and radiation and studies already confirmed that unloading leads to bone loss. There is a good chance that radiation might have the synergistic effects on the µ×g induced bone loss. This needs to be further addressed either by combined radiation and simulated µ×g exposure or by the space flight experiments.

5. Summary

Until now limited research has been conducted to address the mechanisms leading ionizing radiation exposure induced bone loss. This is relevant for cancer radiotherapy and human spaceflight. Exposure to radiation can result in elevated bone fracture risk in patients receiving cancer radiotherapy. In human spaceflight, astronauts are exposed to space radiation which is a very complex mixture consisting primarily of high-energy charged particles.

Osteoblasts are of mesenchymal origin and responsible for creating and maintaining skeletal architecture; these cells produce extracellular matrix proteins and regulators of matrix mineralization during initial bone formation and later bone remodeling.

The aim of this work was to investigate the effects of ionizing radiation on pre-osteoblasts including cellular survival, cell cycle regulation and differentiation modification.

Experiments with the pre-osteoblast cell line OCT-1 and the mesenchymal stem cell line C3H10T1/2 showed that radiation cell killing depends on dose and linear energy transfer (LET) and is most effective at an LET of ~150 keV/µm.

High-LET radiation has a much more pronounced ability to induce cell cycle arrest in the G2/M phase. After both X-rays and heavy ions exposure, expression of the cell cycle regulator CDKN1A was significantly up-regulated in a dose-dependent manner. The findings suggest that cell cycle regulation is more sensitive to high-LET radiation than cell survival, which is not solely regulated through elevated CDKN1A expression.

Radiation exposure enhances osteoblastic differentiation and maturation, and mediates Runx2 and TGF-β1 expression during early differentiation of pre-osteoblasts. Osteogenic differentiation did not alter cellular radiosensitivity, DNA repair of radiation-induced damages and the effects of radiation on proliferation.

Further experiments are needed to elucidate possible synergistic effects of microgravity and radiation on osteoblast differentiation. This may provide the necessary foundation for the development for space travel countermeasures.

6. Reference list

Abdelalim, E.M. and Tooyama, I. 2012. The p53 inhibitor, pifithrin-alpha, suppresses self-renewal of embryonic stem cells. *Biochem.Biophys.Res.Commun.*, 420, (3) 605-610 available from: PM:22445757

Alliston, T., Choy, L., Ducy, P., Karsenty, G., and Derynck, R. 2001. TGF-beta-induced repression of CBFA1 by Smad3 decreases cbfa1 and osteocalcin expression and inhibits osteoblast differentiation. *EMBO J.*, 20, (9) 2254-2272 available from: PM:11331591

Alpen, E.L., Powers-Risius, P., Curtis, S.B., and DeGuzman, R. 1993. Tumorigenic potential of high-Z, high-LET charged-particle radiations. *Radiat.Res.*, 136, (3) 382-391 available from: PM:8278580

Anderson, J.A., Harper, J.V., Cucinotta, F.A., and O'Neill, P. 2010. Participation of DNA-PKcs in DSB repair after exposure to high- and low-LET radiation. *Radiat.Res.*, 174, (2) 195-205 available from: PM:20681786

Ando, T., Kawabe, T., Ohara, H., Ducommun, B., Itoh, M., and Okamoto, T. 2001. Involvement of the interaction between p21 and proliferating cell nuclear antigen for the maintenance of G2/M arrest after DNA damage. *J.Biol.Chem.*, 276, (46) 42971-42977 available from: PM:11559705

Asaithamby, A., Uematsu, N., Chatterjee, A., Story, M.D., Burma, S., and Chen, D.J. 2008. Repair of HZE-particle-induced DNA double-strand breaks in normal human fibroblasts. *Radiat.Res.*, 169, (4) 437-446 available from: PM:18363429

Aubin, J.E. 1998a. Advances in the osteoblast lineage. *Biochemistry and Cell Biology-Biochimie et Biologie Cellulaire*, 76, (6) 899-910 available from: WOS:000080844900002

Aubin, J.E. 1998b. Bone stem cells. *J.Cell Biochem.Suppl*, 30-31, 73-82 available from: PM:9893258

Autsavapromporn, N., Suzuki, M., Plante, I., Liu, C., Uchihori, Y., Hei, T.K., Azzam, E.I., and Murakami, T. 2013. Participation of gap junction communication in potentially lethal damage repair and DNA damage in human fibroblasts exposed to low- or high-LET radiation. *Mutat.Res.*, 756, (1-2) 78-85 available from: PM:23867854

Avkin, S., Sevilya, Z., Toube, L., Geacintov, N., Chaney, S.G., Oren, M., and Livneh, Z. 2006. p53 and p21 regulate error-prone DNA repair to yield a lower mutation load. *Mol.Cell*, 22, (3) 407-413 available from: PM:16678112

Bates, S., Ryan, K.M., Phillips, A.C., and Vousden, K.H. 1998. Cell cycle arrest and DNA endoreduplication following p21Waf1/Cip1 expression. *Oncogene*, 17, (13) 1691-1703 available from: PM:9796698

Baverstock, K. 2000. Radiation-induced genomic instability: a paradigm-breaking phenomenon and its relevance to environmentally induced cancer. *Mutat.Res.*, 454, (1-2) 89-109 available from: PM:11035163

Bellows, C.G., Aubin, J.E., Heersche, J.N., and Antosz, M.E. 1986. Mineralized bone nodules formed in vitro from enzymatically released rat calvaria cell populations. *Calcif.Tissue Int.*, 38, (3) 143-154 available from: PM:3085892

Bishay, K., Ory, K., Olivier, M.F., Lebeau, J., Levalois, C., and Chevillard, S. 2001. DNA damage-related RNA expression to assess individual sensitivity to ionizing radiation. *Carcinogenesis*, 22, (8) 1179-1183 available from: PM:11470746

Bogart, J.A., Alpert, T.E., Kilpatrick, M.C., Keshler, B.L., Pohar, S.S., Shah, H., Dexter, E., and Aronowitz, J.N. 2005. Dose-intensive thoracic radiation therapy for patients at high risk with early-stage non-small-cell lung cancer. *Clin.Lung Cancer*, 6, (6) 350-354 available from: PM:15943895

Bonewald, L.F. 1999. Establishment and characterization of an osteocyte-like cell line, MLO-Y4. *J.Bone Miner.Metab*, 17, (1) 61-65 available from: PM:10084404

Bucker, H. and Facius, R. 1986. Radiation protection problems for the space station and approaches to their mitigation. *Adv.Space Res.*, 6, (11) 305-314 available from: PM:11537238

Budworth, H., Snijders, A.M., Marchetti, F., Mannion, B., Bhatnagar, S., Kwoh, E., Tan, Y., Wang, S.X., Blakely, W.F., Coleman, M., Peterson, L., and Wyrobek, A.J. 2012. DNA repair and cell cycle biomarkers of radiation exposure and inflammation stress in human blood. *PLoS.One.*, 7, (11) e48619 available from: PM:23144912

Canney, P.A. and Dean, S. 1990. Transforming growth factor beta: a promotor of late connective tissue injury following radiotherapy? *Br.J.Radiol.*, 63, (752) 620-623 available from: PM:2400878

Chan, T.A., Hwang, P.M., Hermeking, H., Kinzler, K.W., and Vogelstein, B. 2000. Cooperative effects of genes controlling the G(2)/M checkpoint. *Genes Dev.*, 14, (13) 1584-1588 available from: PM:10887152

Chang, P.Y., Bjornstad, K.A., Rosen, C.J., McNamara, M.P., Mancini, R., Goldstein, L.E., Chylack, L.T., and Blakely, E.A. 2005. Effects of iron ions, protons and X rays on human lens cell differentiation. *Radiat.Res.*, 164, (4 Pt 2) 531-539 available from: PM:16187763

Chavaudra, N., Bourhis, J., and Foray, N. 2004. Quantified relationship between cellular radiosensitivity, DNA repair defects and chromatin relaxation: a study of 19 human tumour cell lines from different origin. *Radiother.Oncol.*, 73, (3) 373-382 available from: PM:15588885

Chen, D., Ceng, J.Q., Windle, J.J., Koop, B.A., Harris, M.A., Bonewald, L.F., Boyce, B.F., Wozney, J.M., Mundy, G.R., and Harris, S.E. 1995. Osteoblastic cell lines derived from a transgenic mouse containing the osteocalcin promoter driving SV40 T-antigen. *Mol Cell Differentiation*, 3, (3) 193-212

Chen, D.J., Tsuboi, K., Nguyen, T., and Yang, T.C. 1994. Charged-particle mutagenesis II. Mutagenic effects of high energy charged particles in normal human fibroblasts. *Adv.Space Res.*, 14, (10) 347-354 available from: PM:11539970

Chen, G., Deng, C., and Li, Y.P. 2012a. TGF-beta and BMP Signaling in Osteoblast Differentiation and Bone Formation. *Int.J.Biol.Sci.*, 8, (2) 272-288 available from: PM:22298955

Chen, H., Kolman, K., Lanciloti, N., Nerney, M., Hays, E., Robson, C., and Chandar, N. 2012b. p53 and MDM2 are involved in the regulation of osteocalcin gene expression. *Exp.Cell Res.*, 318, (8) 867-876 available from: PM:22405968

Cimprich, K.A. and Cortez, D. 2008. ATR: an essential regulator of genome integrity. *Nat.Rev.Mol.Cell Biol.*, 9, (8) 616-627 available from: PM:18594563

Coderre, J.A., Morris, G.M., Micca, P.L., Hopewell, J.W., Verhagen, I., Kleiboer, B.J., and van der Kogel, A.J. 2006. Late effects of radiation on the central nervous system: role of vascular endothelial damage and glial stem cell survival. *Radiat.Res.*, 166, (3) 495-503 available from: PM:16953668

Cucinotta, F.A. and Durante, M. 2006. Cancer risk from exposure to galactic cosmic rays: implications for space exploration by human beings. *Lancet Oncol.*, 7, (5) 431-435 available from: PM:16648048

Cucinotta, F.A., Manuel, F.K., Jones, J., Iszard, G., Murrey, J., Djojonegro, B., and Wear, M. 2001. Space radiation and cataracts in astronauts. *Radiat.Res.*, 156, (5 Pt 1) 460-466 available from: PM:11604058

Dare, A., Hachisu, R., Yamaguchi, A., Yokose, S., Yoshiki, S., and Okano, T. 1997. Effects of ionizing radiation on proliferation and differentiation of osteoblast-like cells. *J.Dent.Res.*, 76, (2) 658-664 available from: PM:9062559

De, S.A., Marinissen, M., Diggs, J., Wang, X.F., Pages, G., and Senderowicz, A. 2004. Transcriptional activation of p21(waf1/cip1) by alkylphospholipids: role of the mitogen-activated protein kinase pathway in the transactivation of the human p21(waf1/cip1) promoter by Sp1. *Cancer Res.*, 64, (2) 743-750 available from: PM:14744793

Deb, S.P. 2002. Function and dysfunction of the human oncoprotein MDM2. *Front Biosci.*, 7, d235-d243 available from: PM:11779693

DeMott, R.K., Mulcahy, R.T., and Clifton, K.H. 1979. The survival of thyroid cells following irradiation: a directly generated single-dose survival curve. *Radiat.Res.*, 77, (2) 395-403 available from: PM:441251

Denker, A.E., Haas, A.R., Nicoll, S.B., and Tuan, R.S. 1999. Chondrogenic differentiation of murine C3H10T1/2 multipotential mesenchymal cells: I. Stimulation by bone morphogenetic protein-2 in high-density micromass cultures. *Differentiation*, 64, (2) 67-76 available from: PM:10234804

DiBiase, S.J., Zeng, Z.C., Chen, R., Hyslop, T., Curran, W.J., Jr., and Iliakis, G. 2000. DNA-dependent protein kinase stimulates an independently active, nonhomologous, end-joining apparatus. *Cancer Res.*, 60, (5) 1245-1253 available from: PM:10728683

Dudziak, M.E., Saadeh, P.B., Mehrara, B.J., Steinbrech, D.S., Greenwald, J.A., Gittes, G.K., and Longaker, M.T. 2000. The effects of ionizing radiation on osteoblast-like cells in vitro. *Plast.Reconstr.Surg.*, 106, (5) 1049-1061 available from: PM:11039376

Durante, M. and Cucinotta, F.A. 2008. Heavy ion carcinogenesis and human space exploration. *Nat.Rev.Cancer*, 8, (6) 465-472 available from: PM:18451812

Eccles, L.J., Lomax, M.E., and O'Neill, P. 2010. Hierarchy of lesion processing governs the repair, double-strand break formation and mutability of three-lesion clustered DNA damage. *Nucleic Acids Res.*, 38, (4) 1123-1134 available from: PM:19965771

Edwards, B.J., Raisch, D.W., Shankaran, V., McKoy, J.M., Gradishar, W., Bunta, A.D., Samaras, A.T., Boyle, S.N., Bennett, C.L., West, D.P., and Guise, T.A. 2011. Cancer therapy associated bone loss: implications for hip fractures in mid-life women with breast cancer. *Clin.Cancer Res.*, 17, (3) 560-568 available from: PM:21288927

Eidemuller, M., Holmberg, E., Jacob, P., Lundell, M., and Karlsson, P. 2011. Breast cancer risk after radiation treatment at infancy: potential consequences of radiation-induced genomic instability. *Radiat.Prot.Dosimetry.*, 143, (2-4) 375-379 available from: PM:21296770

Eidemuller, M., Jacob, P., Lane, R.S., Frost, S.E., and Zablotska, L.B. 2012. Lung cancer mortality (1950-1999) among Eldorado uranium workers: a comparison of models of carcinogenesis and empirical excess risk models. *PLoS.One.*, 7, (8) e41431 available from: PM:22936975

Fakir, H., Sachs, R.K., Stenerlow, B., and Hofmann, W. 2006. Clusters of DNA double-strand breaks induced by different doses of nitrogen ions for various LETs: experimental measurements and theoretical analyses. *Radiat.Res.*, 166, (6) 917-927 available from: PM:17149976

Fernet, M., Megnin-Chanet, F., Hall, J., and Favaudon, V. 2010. Control of the G2/M checkpoints after exposure to low doses of ionising radiation: implications for hyper-radiosensitivity. *DNA Repair (Amst)*, 9, (1) 48-57 available from: PM:19926348

Fokas, E., Kraft, G., An, H., and Engenhart-Cabillic, R. 2009. Ion beam radiobiology and cancer: time to update ourselves. *Biochim.Biophys.Acta*, 1796, (2) 216-229 available from: PM:19682551

Fournier, C. and Taucher-Scholz, G. 2004. Radiation induced cell cycle arrest: an overview of specific effects following high-LET exposure. *Radiother.Oncol.*, 73 Suppl 2, S119-S122 available from: PM:15971325

Fournier, C., Zahnreich, S., Kraft, D., Friedrich, T., Voss, K.O., Durante, M., and Ritter, S. 2012. The fate of a normal human cell traversed by a single charged particle. *Sci.Rep.*, 2, 643 available from: PM:22966418

Franceschi, R.T. and Xiao, G. 2003. Regulation of the osteoblast-specific transcription factor, Runx2: responsiveness to multiple signal transduction pathways. *J.Cell Biochem.*, 88, (3) 446-454 available from: PM:12532321

Freedman, D.A. and Levine, A.J. 1999. Regulation of the p53 protein by the MDM2 oncoprotein--thirty-eighth G.H.A. Clowes Memorial Award Lecture. *Cancer Res.*, 59, (1) 1-7 available from: PM:9892174

Freedman, D.A., Wu, L., and Levine, A.J. 1999. Functions of the MDM2 oncoprotein. *Cell Mol.Life Sci.*, 55, (1) 96-107 available from: PM:10065155

Fry, D.C., Graves, B., and Vassilev, L.T. 2005. Development of E3-substrate (MDM2-p53)-binding inhibitors: structural aspects. *Methods Enzymol.*, 399, 622-633 available from: PM:16338385

Fu, W., Ma, Q., Chen, L., Li, P., Zhang, M., Ramamoorthy, S., Nawaz, Z., Shimojima, T., Wang, H., Yang, Y., Shen, Z., Zhang, Y., Zhang, X., Nicosia, S.V., Zhang, Y., Pledger, J.W., Chen, J., and Bai, W. 2009. MDM2 acts downstream of p53 as an E3 ligase to promote FOXO ubiquitination and degradation. *J.Biol.Chem.*, 284, (21) 13987-14000 available from: PM:19321440

Furusawa, Y., Fukutsu, K., Aoki, M., Itsukaichi, H., Eguchi-Kasai, K., Ohara, H., Yatagai, F., Kanai, T., and Ando, K. 2000. Inactivation of aerobic and hypoxic cells from three different cell lines by accelerated (3)He-, (12)C- and (20)Ne-ion beams. *Radiat.Res.*, 154, (5) 485-496 available from: PM:11025645

Gaziev, A.I. 1999. [DNA damage in cells exposed to ionizing radiation]. *Radiats.Biol.Radioecol.*, 39, (6) 630-638 available from: PM:10689430

George, K., Durante, M., Willingham, V., Wu, H., Yang, T.C., and Cucinotta, F.A. 2003. Biological effectiveness of accelerated particles for the induction of chromosome damage measured in metaphase and interphase human lymphocytes. *Radiat.Res.*, 160, (4) 425-435 available from: PM:12968931

Gogineni, V.R., Nalla, A.K., Gupta, R., Dinh, D.H., Klopfenstein, J.D., and Rao, J.S. 2011. Chk2-mediated G2/M cell cycle arrest maintains radiation resistance in malignant meningioma cells. *Cancer Lett.*, 313, (1) 64-75 available from: PM:21945852

Gudas, J.M., Nguyen, H., Klein, R.C., Katayose, D., Seth, P., and Cowan, K.H. 1995. Differential expression of multiple MDM2 messenger RNAs and proteins in normal and tumorigenic breast epithelial cells. *Clin.Cancer Res.*, 1, (1) 71-80 available from: PM:9815889

Guise, T.A. 2006. Bone loss and fracture risk associated with cancer therapy. *Oncologist.*, 11, (10) 1121-1131 available from: PM:17110632

Guo, X. and Wang, X.F. 2009. Signaling cross-talk between TGF-beta/BMP and other pathways. *Cell Res.*, 19, (1) 71-88 available from: PM:19002158

Hada, M. and Georgakilas, A.G. 2008. Formation of clustered DNA damage after high-LET irradiation: a review. *J.Radiat.Res.*, 49, (3) 203-210 available from: PM:18413977

Hadjidakis, D.J. and Androulakis, I.I. 2006. Bone remodeling. *Ann.N.Y.Acad.Sci.*, 1092, 385-396 available from: PM:17308163

Hall, E.J., Worgul, B.V., Smilenov, L., Elliston, C.D., and Brenner, D.J. 2006. The relative biological effectiveness of densely ionizing heavy-ion radiation for inducing ocular cataracts in wild type versus mice heterozygous for the ATM gene. *Radiat.Environ.Biophys.*, 45, (2) 99-104 available from: PM:16799786

Hamilton, S.A., Pecaut, M.J., Gridley, D.S., Travis, N.D., Bandstra, E.R., Willey, J.S., Nelson, G.A., and Bateman, T.A. 2006. A murine model for bone loss from therapeutic and space-relevant sources of radiation. *J.Appl.Physiol*, 101, (3) 789-793 available from: PM:16741258

Harper, J.W., Adami, G.R., Wei, N., Keyomarsi, K., and Elledge, S.J. 1993. The p21 Cdk-interacting protein Cip1 is a potent inhibitor of G1 cyclin-dependent kinases. *Cell*, 75, (4) 805-816 available from: PM:8242751

Hellweg, C.E. and Baumstark-Khan, C. 2007. Getting ready for the manned mission to Mars: the astronauts' risk from space radiation. *Naturwissenschaften*, 94, (7) 517-526 available from: PM:17235598

Hellweg, C.E., Baumstark-Khan, C., Schmitz, C., Lau, P., Meier, M.M., Testard, I., Berger, T., and Reitz, G. 2011. Activation of the nuclear factor kappaB pathway by heavy ion beams of different linear energy transfer. *Int.J.Radiat.Biol.*, 87, (9) 954-963 available from: PM:21732726

Iliakis, G., Wang, Y., Guan, J., and Wang, H. 2003. DNA damage checkpoint control in cells exposed to ionizing radiation. *Oncogene*, 22, (37) 5834-5847 available from: PM:12947390

Itahana, K., Mao, H., Jin, A., Itahana, Y., Clegg, H.V., Lindstrom, M.S., Bhat, K.P., Godfrey, V.L., Evan, G.I., and Zhang, Y. 2007. Targeted inactivation of Mdm2 RING finger E3 ubiquitin ligase activity in the mouse reveals mechanistic insights into p53 regulation. *Cancer Cell*, 12, (4) 355-366 available from: PM:17936560

Jaiswal, N., Haynesworth, S.E., Caplan, A.I., and Bruder, S.P. 1997. Osteogenic differentiation of purified, culture-expanded human mesenchymal stem cells in vitro. *J.Cell Biochem.*, 64, (2) 295-312 available from: PM:9027589

Janssens, K., ten, D.P., Janssens, S., and Van, H.W. 2005. Transforming growth factor-beta1 to the bone. *Endocr.Rev.*, 26, (6) 743-774 available from: PM:15901668

Jeon, Y.M., Kook, S.H., Rho, S.J., Lim, S.S., Choi, K.C., Kim, H.S., Kim, J.G., and Lee, J.C. 2013. Fibroblast growth factor-7 facilitates osteogenic differentiation of embryonic stem cells through the activation of ERK/Runx2 signaling. *Mol.Cell Biochem.*, 382, (1-2) 37-45 available from: PM:24026476

Kasagi, S. and Chen, W. 2013. TGF-beta1 on osteoimmunology and the bone component cells. *Cell Biosci.*, 3, (1) 4 available from: PM:23321200

Katagiri, T. and Takahashi, N. 2002. Regulatory mechanisms of osteoblast and osteoclast differentiation. *Oral Dis.*, 8, (3) 147-159 available from: PM:12108759

Kato, Y., Windle, J.J., Koop, B.A., Mundy, G.R., and Bonewald, L.F. 1997. Establishment of an osteocyte-like cell line, MLO-Y4. *J.Bone Miner.Res.*, 12, (12) 2014-2023 available from: PM:9421234

Ko, J.L., Cheng, Y.W., Chang, S.L., Su, J.M., Chen, C.Y., and Lee, H. 2000. MDM2 mRNA expression is a favorable prognostic factor in non-small-cell lung cancer. *Int.J.Cancer*, 89, (3) 265-270 available from: PM:10861503

Komori, T. 2010. Regulation of bone development and extracellular matrix protein genes by RUNX2. *Cell Tissue Res.*, 339, (1) 189-195 available from: PM:19649655

Kozubek, S. and Krasavin, E.A. 1984. Cell sensitivity to irradiation and DNA repair processes. II. The cell sensitivity to ionizing radiation of different LETs. *Neoplasma*, 31, (6) 685-695 available from: PM:6395028

Kurpinski, K. 2009. Differential effects of x-rays and high-energy 56Fe ions on human mesenchymal stem cells.

Kvam, E. and Tyrrell, R.M. 1997. Induction of oxidative DNA base damage in human skin cells by UV and near visible radiation. *Carcinogenesis*, 18, (12) 2379-2384 available from: PM:9450485

Laird, N.M. 1987. Thyroid cancer risk from exposure to ionizing radiation: a case study in the comparative potency model. *Risk Anal.*, 7, (3) 299-309 available from: PM:3685539

Land, C.E., Hayakawa, N., Machado, S.G., Yamada, Y., Pike, M.C., Akiba, S., and Tokunaga, M. 1994. A case-control interview study of breast cancer among Japanese A-bomb survivors. II. Interactions with radiation dose. *Cancer Causes Control*, 5, (2) 167-176 available from: PM:8167264

Lane, D.P. 1992. Cancer. p53, guardian of the genome. *Nature*, 358, (6381) 15-16 available from: PM:1614522

Lang, T., LeBlanc, A., Evans, H., Lu, Y., Genant, H., and Yu, A. 2004. Cortical and trabecular bone mineral loss from the spine and hip in long-duration spaceflight. *J.Bone Miner.Res.*, 19, (6) 1006-1012 available from: PM:15125798

Lau, P., Baumstark-Khan, C., Hellweg, C.E., and Reitz, G. 2010. X-irradiation-induced cell cycle delay and DNA double-strand breaks in the murine osteoblastic cell line OCT-1. *Radiat.Environ.Biophys.*, 49, (2) 271-280 available from: PM:20232074

Lee, K.S., Kim, H.J., Li, Q.L., Chi, X.Z., Ueta, C., Komori, T., Wozney, J.M., Kim, E.G., Choi, J.Y., Ryoo, H.M., and Bae, S.C. 2000. Runx2 is a common target of transforming growth factor beta1 and bone morphogenetic protein 2, and cooperation between Runx2 and Smad5 induces osteoblast-specific gene expression in the pluripotent mesenchymal precursor cell line C2C12. *Mol.Cell Biol.*, 20, (23) 8783-8792 available from: PM:11073979

Lengner, C.J., Steinman, H.A., Gagnon, J., Smith, T.W., Henderson, J.E., Kream, B.E., Stein, G.S., Lian, J.B., and Jones, S.N. 2006. Osteoblast differentiation and skeletal development are regulated by Mdm2-p53 signaling. *J.Cell Biol.*, 172, (6) 909-921 available from: PM:16533949

Li, Y., Jenkins, C.W., Nichols, M.A., and Xiong, Y. 1994. Cell cycle expression and p53 regulation of the cyclin-dependent kinase inhibitor p21. *Oncogene*, 9, (8) 2261-2268 available from: PM:7913544

Little, M.P. 2009. Cancer and non-cancer effects in Japanese atomic bomb survivors. *J.Radiol.Prot.*, 29, (2A) A43-A59 available from: PM:19454804

Little, M.P. and Charles, M.W. 1997. The risk of non-melanoma skin cancer incidence in the Japanese atomic bomb survivors. *Int.J.Radiat.Biol.*, 71, (5) 589-602 available from: PM:9191904

Liu, D.D., Zhang, J.C., Zhang, Q., Wang, S.X., and Yang, M.S. 2013. TGF-beta/BMP signaling pathway is involved in cerium-promoted osteogenic differentiation of mesenchymal stem cells. *J.Cell Biochem.*, 114, (5) 1105-1114 available from: PM:23150386

Liu, H. and Li, B. 2010. p53 control of bone remodeling. *J.Cell Biochem.*, 111, (3) 529-534 available from: PM:20589754

Liu, Q., Guntuku, S., Cui, X.S., Matsuoka, S., Cortez, D., Tamai, K., Luo, G., Carattini-Rivera, S., DeMayo, F., Bradley, A., Donehower, L.A., and Elledge, S.J. 2000. Chk1 is an essential kinase that is regulated by Atr and required for the G(2)/M DNA damage checkpoint. *Genes Dev.*, 14, (12) 1448-1459 available from: PM:10859164

Lloyd, S.A., Bandstra, E.R., Travis, N.D., Nelson, G.A., Bourland, J.D., Pecaut, M.J., Gridley, D.S., Willey, J.S., and Bateman, T.A. 2008. Spaceflight-relevant types of ionizing radiation and cortical bone: Potential LET effect? *Adv.Space Res.*, 42, (12) 1889-1897 available from: PM:19122806

Lobrich, M. and Jeggo, P.A. 2007. The impact of a negligent G2/M checkpoint on genomic instability and cancer induction. *Nat.Rev.Cancer*, 7, (11) 861-869 available from: PM:17943134

Lopez-Diaz, F.J., Gascard, P., Balakrishnan, S.K., Zhao, J., Del Rincon, S.V., Spruck, C., Tlsty, T.D., and Emerson, B.M. 2013. Coordinate transcriptional and translational repression of p53 by TGF-beta1 impairs the stress response. *Mol.Cell*, 50, (4) 552-564 available from: PM:23706820

Lossaint, G., Besnard, E., Fisher, D., Piette, J., and Dulic, V. 2011. Chk1 is dispensable for G2 arrest in response to sustained DNA damage when the ATM/p53/p21 pathway is functional. *Oncogene*, 30, (41) 4261-4274 available from: PM:21532626

Lovejoy, C.A. and Cortez, D. 2009. Common mechanisms of PIKK regulation. *DNA Repair (Amst)*, 8, (9) 1004-1008 available from: PM:19464237

Maeda, S., Hayashi, M., Komiya, S., Imamura, T., and Miyazono, K. 2004. Endogenous TGF-beta signaling suppresses maturation of osteoblastic mesenchymal cells. *EMBO J.*, 23, (3) 552-563 available from: PM:14749725

Manfredi, J.J. 2010. The Mdm2-p53 relationship evolves: Mdm2 swings both ways as an oncogene and a tumor suppressor. *Genes Dev.*, 24, (15) 1580-1589 available from: PM:20679392

Marine, J.C. and Lozano, G. 2010. Mdm2-mediated ubiquitylation: p53 and beyond. *Cell Death.Differ.*, 17, (1) 93-102 available from: PM:19498444

Meschini, R., Berni, A., Ortenzi, V., Mancinelli, P., and Palitti, F. 2010. Relation between DNA repair, apoptosis and chromosomal aberrations in presence of pifithrin-alpha, an inhibitor of p53. *Mutat.Res.*, 701, (1) 92-97 available from: PM:20348016

Metting, N.F. and Little, J.B. 1995. Transient failure to dephosphorylate the cdc2-cyclin B1 complex accompanies radiation-induced G2-phase arrest in HeLa cells. *Radiat.Res.*, 143, (3) 286-292 available from: PM:7652166

Mishra, K.P. 2004. Cell membrane oxidative damage induced by gamma-radiation and apoptotic sensitivity. *J.Environ.Pathol.Toxicol.Oncol.*, 23, (1) 61-66 available from: PM:14994996

Molchadsky, A., Shats, I., Goldfinger, N., Pevsner-Fischer, M., Olson, M., Rinon, A., Tzahor, E., Lozano, G., Zipori, D., Sarig, R., and Rotter, V. 2008. p53 plays a role in mesenchymal differentiation programs, in a cell fate dependent manner. *PLoS.One.*, 3, (11) e3707 available from: PM:19002260

Mukherjee, P., Winter, S.L., and Alexandrow, M.G. 2010. Cell cycle arrest by transforming growth factor beta1 near G1/S is mediated by acute abrogation of prereplication complex activation involving an Rb-MCM interaction. *Mol.Cell Biol.*, 30, (3) 845-856 available from: PM:19948884

Mulcahy, R.T., Gould, M.N., and Clifton, K.H. 1980. The survival of thyroid cells: in vivo irradiation and in situ repair. *Radiat.Res.*, 84, (3) 523-528 available from: PM:7005928

Multhoff, G. and Radons, J. 2012. Radiation, inflammation, and immune responses in cancer. *Front Oncol.*, 2, 58 available from: PM:22675673

Muranov, K.O., Polianskii, N.B., Kurova, V.S., Riabokon', A.M., Sheremet, N.L., Fedorov, A.A., Bannik, K.I., Abrosimova, A.N., and Ostrovskii, M.A. 2010. [Comparative study of aging, UV treatment, and radiation on cataract formation]. *Radiats.Biol.Radioecol.*, 50, (3) 276-285 available from: PM:20734799

Nagaraja, M.P. and Risin, D. 2013. The current state of bone loss research: data from spaceflight and microgravity simulators. *J.Cell Biochem.*, 114, (5) 1001-1008 available from: PM:23150462

Nakashima, K., Zhou, X., Kunkel, G., Zhang, Z., Deng, J.M., Behringer, R.R., and de, C.B. 2002. The novel zinc finger-containing transcription factor osterix is required for osteoblast differentiation and bone formation. *Cell*, 108, (1) 17-29 available from: PM:11792318

Nasonova, E., Ritter, S., Fomenkova, T., and Kraft, G. 1998. Induction of chromosomal damage in CHO-K1 cells and their repair-deficient mutant XRS5 by X-ray and particle irradiation. *Adv.Space Res.*, 22, (4) 569-578 available from: PM:11542787

Niculescu, A.B., III, Chen, X., Smeets, M., Hengst, L., Prives, C., and Reed, S.I. 1998. Effects of p21(Cip1/Waf1) at both the G1/S and the G2/M cell cycle transitions: pRb is a critical

determinant in blocking DNA replication and in preventing endoreduplication. *Mol.Cell Biol.*, 18, (1) 629-643 available from: PM:9418909

Noda, A., Ning, Y., Venable, S.F., Pereira-Smith, O.M., and Smith, J.R. 1994. Cloning of senescent cell-derived inhibitors of DNA synthesis using an expression screen. *Exp.Cell Res.*, 211, (1) 90-98 available from: PM:8125163

Owen, T.A., Aronow, M., Shalhoub, V., Barone, L.M., Wilming, L., Tassinari, M.S., Kennedy, M.B., Pockwinse, S., Lian, J.B., and Stein, G.S. 1990. Progressive development of the rat osteoblast phenotype in vitro: reciprocal relationships in expression of genes associated with osteoblast proliferation and differentiation during formation of the bone extracellular matrix. *J.Cell Physiol*, 143, (3) 420-430 available from: PM:1694181

Pan, M.H., Chen, W.J., Lin-Shiau, S.Y., Ho, C.T., and Lin, J.K. 2002. Tangeretin induces cell-cycle G1 arrest through inhibiting cyclin-dependent kinases 2 and 4 activities as well as elevating Cdk inhibitors p21 and p27 in human colorectal carcinoma cells. *Carcinogenesis*, 23, (10) 1677-1684 available from: PM:12376477

Park, C.C., Henshall-Powell, R.L., Erickson, A.C., Talhouk, R., Parvin, B., Bissell, M.J., and Barcellos-Hoff, M.H. 2003. Ionizing radiation induces heritable disruption of epithelial cell interactions. *Proc.Natl.Acad.Sci.U.S.A*, 100, (19) 10728-10733 available from: PM:12960393

Park, S.S., Kim, K.A., Lee, S.Y., Lim, S.S., Jeon, Y.M., and Lee, J.C. 2012. X-ray radiation at low doses stimulates differentiation and mineralization of mouse calvarial osteoblasts. *BMB.Rep.*, 45, (10) 571-576 available from: PM:23101511

Pawlik, T.M. and Keyomarsi, K. 2004. Role of cell cycle in mediating sensitivity to radiotherapy. *Int.J.Radiat.Oncol.Biol.Phys.*, 59, (4) 928-942 available from: PM:15234026

Pellegata, N.S., Antoniono, R.J., Redpath, J.L., and Stanbridge, E.J. 1996. DNA damage and p53-mediated cell cycle arrest: a reevaluation. *Proc.Natl.Acad.Sci.U.S.A*, 93, (26) 15209-15214 available from: PM:8986789

Perinpanayagam, H., Martin, T., Mithal, V., Dahman, M., Marzec, N., Lampasso, J., and Dziak, R. 2006. Alveolar bone osteoblast differentiation and Runx2/Cbfa1 expression. *Arch.Oral Biol.*, 51, (5) 406-415 available from: PM:16253204

Petersen, L., Hasvold, G., Lukas, J., Bartek, J., and Syljuasen, R.G. 2010. p53-dependent G(1) arrest in 1st or 2nd cell cycle may protect human cancer cells from cell death after treatment with ionizing radiation and Chk1 inhibitors. *Cell Prolif.*, 43, (4) 365-371 available from: PM:20590661

Pfaffl, M.W., Horgan, G.W., and Dempfle, L. 2002. Relative expression software tool (REST) for group-wise comparison and statistical analysis of relative expression results in real-time PCR. *Nucleic Acids Res.*, 30, (9) e36 available from: PM:11972351

Pfaffl, M.W., Tichopad, A., Prgomet, C., and Neuvians, T.P. 2004. Determination of stable housekeeping genes, differentially regulated target genes and sample integrity: BestKeeper--Excel-based tool using pair-wise correlations. *Biotechnol.Lett.*, 26, (6) 509-515 available from: PM:15127793

Pietrancosta, N., Maina, F., Dono, R., Moumen, A., Garino, C., Laras, Y., Burlet, S., Quelever, G., and Kraus, J.L. 2005. Novel cyclized Pifithrin-alpha p53 inactivators: synthesis and biological studies. *Bioorg.Med.Chem.Lett.*, 15, (6) 1561-1564 available from: PM:15745797

Pohl, F., Hassel, S., Nohe, A., Flentje, M., Knaus, P., Sebald, W., and Koelbl, O. 2003. Radiation-induced suppression of the Bmp2 signal transduction pathway in the pluripotent mesenchymal cell line C2C12: an in vitro model for prevention of heterotopic ossification by radiotherapy. *Radiat.Res.*, 159, (3) 345-350 available from: PM:12600237

Pratap, J., Galindo, M., Zaidi, S.K., Vradii, D., Bhat, B.M., Robinson, J.A., Choi, J.Y., Komori, T., Stein, J.L., Lian, J.B., Stein, G.S., and van Wijnen, A.J. 2003. Cell growth regulatory role of Runx2 during proliferative expansion of preosteoblasts. *Cancer Res.*, 63, (17) 5357-5362 available from: PM:14500368

Pregizer, S., Barski, A., Gersbach, C.A., Garcia, A.J., and Frenkel, B. 2007. Identification of novel Runx2 targets in osteoblasts: cell type-specific BMP-dependent regulation of Tram2. *J.Cell Biochem.*, 102, (6) 1458-1471 available from: PM:17486635

Preston, D.L., Shimizu, Y., Pierce, D.A., Suyama, A., and Mabuchi, K. 2012. Studies of mortality of atomic bomb survivors. Report 13: solid cancer and noncancer disease mortality: 1950-1997. 2003. *Radiat.Res.*, 178, (2) AV146-AV172 available from: PM:22870966

Proietti De, S.L., Balajee, A.S., Lorenti, G.C., Pepe, G., Worboys, A.M., and Palitti, F. 2003. Inhibition of p53, p21 and Bax by pifithrin-alpha does not affect UV induced apoptotic response in CS-B cells. *DNA Repair (Amst)*, 2, (8) 891-900 available from: PM:12893085

Puck, T.T., Marcus, P.I., and Cieciura, S.J. 1956. Clonal growth of mammalian cells in vitro; growth characteristics of colonies from single HeLa cells with and without a feeder layer. *J.Exp.Med*, 103, (2) 273-283 available from: PM:13286432

Quaas, M., Muller, G.A., and Engeland, K. 2012. p53 can repress transcription of cell cycle genes through a p21(WAF1/CIP1)-dependent switch from MMB to DREAM protein complex binding at CHR promoter elements. *Cell Cycle*, 11, (24) 4661-4672 available from: PM:23187802

Reeves, G.I. and Ainsworth, E.J. 1995. Description of the chronic radiation syndrome in humans irradiated in the former Soviet Union. *Radiat.Res.*, 142, (2) 242-243 available from: PM:7724741

Reznikoff, C.A., Brankow, D.W., and Heidelberger, C. 1973. Establishment and characterization of a cloned line of C3H mouse embryo cells sensitive to postconfluence inhibition of division. *Cancer Res.*, 33, (12) 3231-3238 available from: PM:4357355

Romanov, V.S., Pospelov, V.A., and Pospelova, T.V. 2012. Cyclin-dependent kinase inhibitor p21(Waf1): contemporary view on its role in senescence and oncogenesis. *Biochemistry (Mosc.)*, 77, (6) 575-584 available from: PM:22817456

Roninson, I.B. 2002. Oncogenic functions of tumour suppressor p21(Waf1/Cip1/Sdi1): association with cell senescence and tumour-promoting activities of stromal fibroblasts. *Cancer Lett.*, 179, (1) 1-14 available from: PM:11880176

Ruegg, D.G., Kakebeeke, T.H., Gabriel, J.P., and Bennefeld, M. 2003. Conduction velocity of nerve and muscle fiber action potentials after a space mission or a bed rest. *Clin.Neurophysiol.*, 114, (1) 86-93 available from: PM:12495768

Rydberg, B., Cooper, B., Cooper, P.K., Holley, W.R., and Chatterjee, A. 2005. Dose-dependent misrejoining of radiation-induced DNA double-strand breaks in human fibroblasts: experimental and theoretical study for high- and low-LET radiation. *Radiat.Res.*, 163, (5) 526-534 available from: PM:15850414

Sakurai, T., Ito, M., Mikamoto, T., Ohshio, R., and Miyakoshi, J. 2011. Ionising irradiation-induced inhibition of differentiation of C3H10T1/2 cells to the osteoblastic lineage. *Int.J.Radiat.Biol.*, 87, (5) 447-452 available from: PM:21219113

Sakurai, T., Sawada, Y., Yoshimoto, M., Kawai, M., and Miyakoshi, J. 2007. Radiation-induced reduction of osteoblast differentiation in C2C12 cells. *J.Radiat.Res.*, 48, (6) 515-521 available from: PM:17928745

Sawajiri, M., Mizoe, J., and Tanimoto, K. 2003. Changes in osteoclasts after irradiation with carbon ion particles. *Radiat.Environ.Biophys.*, 42, (3) 219-223 available from: PM:13680258

Schneider, U. and Walsh, L. 2008. Cancer risk estimates from the combined Japanese A-bomb and Hodgkin cohorts for doses relevant to radiotherapy. *Radiat.Environ.Biophys.*, 47, (2) 253-263 available from: PM:18157543

Schroeder, A., Mueller, O., Stocker, S., Salowsky, R., Leiber, M., Gassmann, M., Lightfoot, S., Menzel, W., Granzow, M., and Ragg, T. 2006. The RIN: an RNA integrity number for assigning integrity values to RNA measurements. *BMC.Mol.Biol.*, 7, 3 available from: PM:16448564

Schwartz, K.A., Lanciloti, N.J., Moore, M.K., Campione, A.L., and Chandar, N. 1999. p53 transactivity during in vitro osteoblast differentiation in a rat osteosarcoma cell line. *Mol.Carcinog.*, 25, (2) 132-138 available from: PM:10365915

Seth, A., Lee, B.K., Qi, S., and Vary, C.P. 2000. Coordinate expression of novel genes during osteoblast differentiation. *J.Bone Miner.Res.*, 15, (9) 1683-1696 available from: PM:10976989

Shay, J.W., Cucinotta, F.A., Sulzman, F.M., Coleman, C.N., and Minna, J.D. 2011. From mice and men to earth and space: joint NASA-NCI workshop on lung cancer risk resulting from space and terrestrial radiation. *Cancer Res.*, 71, (22) 6926-6929 available from: PM:21900398

Shea, C.M., Edgar, C.M., Einhorn, T.A., and Gerstenfeld, L.C. 2003. BMP treatment of C3H10T1/2 mesenchymal stem cells induces both chondrogenesis and osteogenesis. *J.Cell Biochem.*, 90, (6) 1112-1127 available from: PM:14635186

Shioyama, Y., Tokuuye, K., Okumura, T., Kagei, K., Sugahara, S., Ohara, K., Akine, Y., Ishikawa, S., Satoh, H., and Sekizawa, K. 2003. Clinical evaluation of proton radiotherapy for non-small-cell lung cancer. *Int.J.Radiat.Oncol.Biol.Phys.*, 56, (1) 7-13 available from: PM:12694818

Shrivastav, M., De Haro, L.P., and Nickoloff, J.A. 2008. Regulation of DNA double-strand break repair pathway choice. *Cell Res.*, 18, (1) 134-147 available from: PM:18157161

Siegel, P.M. and Massague, J. 2003. Cytostatic and apoptotic actions of TGF-beta in homeostasis and cancer. *Nat.Rev.Cancer*, 3, (11) 807-821 available from: PM:14557817

Sinclair, W.K. and Morton, R.A. 1966. X-ray sensitivity during the cell generation cycle of cultured Chinese hamster cells. *Radiat.Res.*, 29, (3) 450-474 available from: PM:5924188

Sohn, D., Graupner, V., Neise, D., Essmann, F., Schulze-Osthoff, K., and Janicke, R.U. 2009. Pifithrin-alpha protects against DNA damage-induced apoptosis downstream of mitochondria independent of p53. *Cell Death.Differ.*, 16, (6) 869-878 available from: PM:19229248

Sonnenfeld, G. 2005. The immune system in space, including Earth-based benefits of space-based research. *Curr.Pharm.Biotechnol.*, 6, (4) 343-349 available from: PM:16101473

Sorensen, B.S., Overgaard, J., and Bassler, N. 2011. In vitro RBE-LET dependence for multiple particle types. *Acta Oncol.*, 50, (6) 757-762 available from: PM:21767171

Stavridi, E.S., Chehab, N.H., Malikzay, A., and Halazonetis, T.D. 2001. Substitutions that compromise the ionizing radiation-induced association of p53 with 14-3-3 proteins also compromise the ability of p53 to induce cell cycle arrest. *Cancer Res.*, 61, (19) 7030-7033 available from: PM:11585729

Suh, J.H., Lee, H.W., Lee, J.W., and Kim, J.B. 2008. Hes1 stimulates transcriptional activity of Runx2 by increasing protein stabilization during osteoblast differentiation. *Biochem.Biophys.Res.Commun.*, 367, (1) 97-102 available from: PM:18162173

Suzuki, A., Kariya, M., Matsumura, N., Baba, T., Yagi, H., Mandai, M., Konishi, I., and Fujii, S. 2012. Expression of p53 and p21(WAF-1), apoptosis, and proliferation of smooth muscle cells in normal myometrium during the menstrual cycle: implication of DNA damage and repair for leiomyoma development. *Med.Mol.Morphol.*, 45, (4) 214-221 available from: PM:23224600

Szumiel, I. 1998. Monitoring and signaling of radiation-induced damage in mammalian cells. *Radiat.Res.*, 150, (5 Suppl) S92-101 available from: PM:9806612

Szumiel, I. 2005. L5178Y sublines: a look back from 40 years. Part 2: response to ionizing radiation. *Int.J.Radiat.Biol.*, 81, (5) 353-365 available from: PM:16076750

Szumiel, I. 2008. Intrinsic radiation sensitivity: cellular signaling is the key. *Radiat.Res.*, 169, (3) 249-258 available from: PM:18302493

Szymczyk, K.H., Shapiro, I.M., and Adams, C.S. 2004. Ionizing radiation sensitizes bone cells to apoptosis. *Bone*, 34, (1) 148-156 available from: PM:14751572

Taylor, W.R. and Stark, G.R. 2001. Regulation of the G2/M transition by p53. *Oncogene*, 20, (15) 1803-1815 available from: PM:11313928

Tenhumberg, S., Gudowska-Nowak, E., Nasonova, E., and Ritter, S. 2007. Cell cycle arrest and aberration yield in normal human fibroblasts. II: Effects of 11 MeV u-1 C ions and 9.9 MeV u-1 Ni ions. *Int.J.Radiat.Biol.*, 83, (8) 501-513 available from: PM:17613123

Thirsk, R., Kuipers, A., Mukai, C., and Williams, D. 2009. The space-flight environment: the International Space Station and beyond. *CMAJ.*, 180, (12) 1216-1220 available from: PM:19487390

Tichy, A., Vavrova, J., Pejchal, J., and Rezacova, M. 2010. Ataxia-telangiectasia mutated kinase (ATM) as a central regulator of radiation-induced DNA damage response. *Acta Medica.(Hradec.Kralove)*, 53, (1) 13-17 available from: PM:20608227

Townsend, L.W. and Fry, R.J. 2002. Radiation protection guidance for activities in low-Earth orbit. *Adv.Space Res.*, 30, (4) 957-963 available from: PM:12539765

Trikalinos, T.A., Terasawa, T., Ip, S., Raman, G., and Lau, J. 2009. available from: PM:20704058

Tsuboi, K., Yang, T.C., and Chen, D.J. 1992. Charged-particle mutagenesis. 1. Cytotoxic and mutagenic effects of high-LET charged iron particles on human skin fibroblasts. *Radiat.Res.*, 129, (2) 171-176 available from: PM:1734447

Tsuji, K., Komori, T., and Noda, M. 2004. Aged mice require full transcription factor, Runx2/Cbfa1, gene dosage for cancellous bone regeneration after bone marrow ablation. *J.Bone Miner.Res.*, 19, (9) 1481-1489 available from: PM:15312248

Tsuruoka, C., Suzuki, M., Hande, M.P., Furusawa, Y., Anzai, K., and Okayasu, R. 2008. The difference in LET and ion species dependence for induction of initially measured and non-rejoined chromatin breaks in normal human fibroblasts. *Radiat.Res.*, 170, (2) 163-171 available from: PM:18666815

Tsuruoka, C., Suzuki, M., Kanai, T., and Fujitaka, K. 2005. LET and ion species dependence for cell killing in normal human skin fibroblasts. *Radiat.Res.*, 163, (5) 494-500 available from: PM:15850410

Ugenskiene, R., Prise, K., Folkard, M., Lekki, J., Stachura, Z., Zazula, M., and Stachura, J. 2009. Dose response and kinetics of foci disappearance following exposure to high- and low-LET ionizing radiation. *Int.J.Radiat.Biol.*, 85, (10) 872-882 available from: PM:19863201

Vassilev, L.T., Vu, B.T., Graves, B., Carvajal, D., Podlaski, F., Filipovic, Z., Kong, N., Kammlott, U., Lukacs, C., Klein, C., Fotouhi, N., and Liu, E.A. 2004. In vivo activation of the p53 pathway by small-molecule antagonists of MDM2. *Science*, 303, (5659) 844-848 available from: PM:14704432

Vousden, K.H. 2000. p53: death star. *Cell*, 103, (5) 691-694 available from: PM:11114324

Walton, M.I., Wilson, S.C., Hardcastle, I.R., Mirza, A.R., and Workman, P. 2005. An evaluation of the ability of pifithrin-alpha and -beta to inhibit p53 function in two wild-type p53 human tumor cell lines. *Mol.Cancer Ther.*, 4, (9) 1369-1377 available from: PM:16170029

Wan, M. and Cao, X. 2005. BMP signaling in skeletal development. *Biochem.Biophys.Res.Commun.*, 328, (3) 651-657 available from: PM:15694398

Wang, C.Y., Yang, S.F., Wang, Z., Tan, J.M., Xing, S.M., Chen, D.C., Xu, S.M., and Yuan, W. 2013. PCAF acetylates Runx2 and promotes osteoblast differentiation. *J.Bone Miner.Metab*, 31, (4) 381-389 available from: PM:23468178

Wang, D., Christensen, K., Chawla, K., Xiao, G., Krebsbach, P.H., and Franceschi, R.T. 1999. Isolation and characterization of MC3T3-E1 preosteoblast subclones with distinct in vitro and in vivo differentiation/mineralization potential. *J.Bone Miner.Res.*, 14, (6) 893-903 available from: PM:10352097

Wang, H., Zeng, Z.C., Bui, T.A., Sonoda, E., Takata, M., Takeda, S., and Iliakis, G. 2001. Efficient rejoining of radiation-induced DNA double-strand breaks in vertebrate cells deficient in genes of the RAD52 epistasis group. *Oncogene*, 20, (18) 2212-2224 available from: PM:11402316

Wang, X., Kua, H.Y., Hu, Y., Guo, K., Zeng, Q., Wu, Q., Ng, H.H., Karsenty, G., de, C.B., Yeh, J., and Li, B. 2006a. p53 functions as a negative regulator of osteoblastogenesis, osteoblast-dependent osteoclastogenesis, and bone remodeling. *J.Cell Biol.*, 172, (1) 115-125 available from: PM:16380437

Wang, Y.H., Liu, Y., Maye, P., and Rowe, D.W. 2006b. Examination of mineralized nodule formation in living osteoblastic cultures using fluorescent dyes. *Biotechnol.Prog.*, 22, (6) 1697-1701 available from: PM:17137320

Wani, M.A., Wani, G., Yao, J., Zhu, Q., and Wani, A.A. 2002. Human cells deficient in p53 regulated p21(waf1/cip1) expression exhibit normal nucleotide excision repair of UV-induced DNA damage. *Carcinogenesis*, 23, (3) 403-410 available from: PM:11895854

Warmerdam, D.O. and Kanaar, R. 2010. Dealing with DNA damage: relationships between checkpoint and repair pathways. *Mutat.Res.*, 704, (1-3) 2-11 available from: PM:20006736

Weichselbaum, R.R., Nove, J., and Little, J.B. 1980. X-ray sensitivity of fifty-three human diploid fibroblast cell strains from patients with characterized genetic disorders. *Cancer Res.*, 40, (3) 920-925 available from: PM:7471105

Weston, A.D., Rosen, V., Chandraratna, R.A., and Underhill, T.M. 2000. Regulation of skeletal progenitor differentiation by the BMP and retinoid signaling pathways. *J.Cell Biol.*, 148, (4) 679-690 available from: PM:10684250

Wilson, G.D. 2004. Radiation and the cell cycle, revisited. *Cancer Metastasis Rev.*, 23, (3-4) 209-225 available from: PM:15197324

Wilson, J.W., Cucinotta, F.A., Shinn, J.L., Simonsen, L.C., Dubey, R.R., Jordan, W.R., Jones, T.D., Chang, C.K., and Kim, M.Y. 1999. Shielding from solar particle event exposures in deep space. *Radiat.Meas.*, 30, (3) 361-382 available from: PM:11543148

Wilson, J.W., Kim, M., Schimmerling, W., Badavi, F.F., Thibeault, S.A., Cucinotta, F.A., Shinn, J.L., and Kiefer, R. 1995. Issues in space radiation protection: galactic cosmic rays. *Health Phys.*, 68, (1) 50-58 available from: PM:7989194

Windhofer, F., Wu, W., and Iliakis, G. 2007. Low levels of DNA ligases III and IV sufficient for effective NHEJ. *J.Cell Physiol*, 213, (2) 475-483 available from: PM:17492771

Wu, W., Wang, M., Wu, W., Singh, S.K., Mussfeldt, T., and Iliakis, G. 2008. Repair of radiation induced DNA double strand breaks by backup NHEJ is enhanced in G2. *DNA Repair (Amst)*, 7, (2) 329-338 available from: PM:18155970

Xu, B. and Kastan, M.B. 2004. Analyzing cell cycle checkpoints after ionizing radiation. *Methods Mol.Biol.*, 281, 283-292 available from: PM:15220537

Xu, B., Kim, S.T., Lim, D.S., and Kastan, M.B. 2002. Two molecularly distinct G(2)/M checkpoints are induced by ionizing irradiation. *Mol.Cell Biol.*, 22, (4) 1049-1059 available from: PM:11809797

Yadav, V., Sultana, S., Yadav, J., and Saini, N. 2012. Gatifloxacin induces S and G2-phase cell cycle arrest in pancreatic cancer cells via p21/p27/p53. *PLoS.One.*, 7, (10) e47796 available from: PM:23133524

Yajima, H. 2013. The complexity of DNA double strand breaks is a critical factor enhancing end-resection.

Yang, M., Ma, Q.J., Dang, G.T., Ma, K.T., Chen, P., and Zhou, C.Y. 2005. Adeno-associated virus-mediated bone morphogenetic protein-7 gene transfer induces C2C12 cell differentiation into osteoblast lineage cells. *Acta Pharmacol.Sin.*, 26, (8) 963-968 available from: PM:16038629

Yi, X., Hong, M., Gui, B., Chen, Z., Li, L., Xie, G., Liang, J., Wang, X., and Shang, Y. 2012. RNA processing and modification protein, carbon catabolite repression 4 (Ccr4), arrests the cell cycle through p21-dependent and p53-independent pathway. *J.Biol.Chem.*, 287, (25) 21045-21057 available from: PM:22547059

Yokota, H., Hamamura, K., Chen, A., Dodge, T.R., Tanjung, N., Abedinpoor, A., and Zhang, P. 2013. Effects of salubrinal on development of osteoclasts and osteoblasts from bone marrow-derived cells. *BMC.Musculoskelet.Disord.*, 14, 197 available from: PM:23816340

Yu, Z.K., Geyer, R.K., and Maki, C.G. 2000. MDM2-dependent ubiquitination of nuclear and cytoplasmic P53. *Oncogene*, 19, (51) 5892-5897 available from: PM:11127820

Zambetti, G.P., Horwitz, E.M., and Schipani, E. 2006. Skeletons in the p53 tumor suppressor closet: genetic evidence that p53 blocks bone differentiation and development. *J.Cell Biol.*, 172, (6) 795-797 available from: PM:16533941

Zeitlin, C., Hassler, D.M., Cucinotta, F.A., Ehresmann, B., Wimmer-Schweingruber, R.F., Brinza, D.E., Kang, S., Weigle, G., Bottcher, S., Bohm, E., Burmeister, S., Guo, J., Kohler, J., Martin, C., Posner, A., Rafkin, S., and Reitz, G. 2013. Measurements of energetic particle radiation in transit to Mars on the Mars Science Laboratory. *Science*, 340, (6136) 1080-1084 available from: PM:23723233

Zhao, L., Jiang, S., and Hantash, B.M. 2010. Transforming growth factor beta1 induces osteogenic differentiation of murine bone marrow stromal cells. *Tissue Eng Part A*, 16, (2) 725-733 available from: PM:19769530

7. Abbreviations

#	Number
°C	Degree centigrade
λ	Wavelength
1 × g	Earth gravity
γ-H2AX	Phosphorylated histone variant H2AX
α-MEM	α-minimum essential medium
µg	Microgram (1×10^{-6} g)
µl	Microliter (1×10^{-6} L)
µm	Micrometer (1×10^{-6} m)
µmol/l	Micromole per liter
ALP	Alkaline phosphatase
Aqua dest.	Aqua destillatum
Ar	Argon
ATM	Ataxia telangiectasia mutated protein
B2M	β_2 microglobulin
BME	Basal Medium Eagle
bp	Base pairs
BSA	Bovine Serum Albumin
C	Carbon
CAK	Cyclin dependent activating kinase
CDK	Cyclin-dependent kinase
CDKN1A	Cyclin-dependent kinase inhibitor 1
cDNA	Complementary DNA
CFA	Colony forming ability
cm	Centimeter
Col-Type I	Type I collagen
C_T	Threshold cycle

d	Day (s)
D	Dose
DAPI	4’,6-diamidino-2-phenylindole
Deq	Equivalent dose
DLR	Deutsches Zentrum für Luft- und Raumfahrt e.V. (German Aerospace Center)
DMSO	Dimethyl sulfoxide
DNA	Deoxyribonucleic acid
DNA-PK	DNA protein kinase
DSB	Double strand break
Eff	Efficiency
EDTA	Ethylene diamine tetraacetic acid
ESA	European Space Agency
eV	Electron volt
FA	Formaldehyde
FAR	Fraction of activity released
FACS	Fluorescence-activated cell sorting
FBS	Fetal Bovine Serum
Fe	Iron
FSC	Forward scatter
g	Gram
GANIL	Grand Accélérateur National d’Ions lourds
GAPDH	Glyceraldehyde 3-phosphate dehydrogenase
GCR	Galactic cosmic rays
GSI	Helmholtzzentrum für Schwerionenforschung, Helmholtz Center for Heavy Ion Research, Darmstadt, Germany
Gy	Gray (J kg^{-1}), unit of irradiation dose
h	Hour (s)
HR	Homologous recombination
HZE	Energetic heavy nuclei with high atomic number (Z) and energy €

IL	Interleukin
ISS	International Space Station
keV	Kilo electron volt
kg	Kilogram
kV	Kilovolt
LEO	Low Earth orbit
LET	Linear energy transfer
mA	Milli ampere
Mdm2	Mouse double minute 2 homolog
MeV	Mega electron volt
MeV/n	Mega electron volt per nucleon
min	Minute (s)
ml	Milliliter (1×10^{-3} l)
mm	Millimeter (1×10^{-3} m)
mmol/l	Millimole per liter
ms	Millisecond (s)
mSv	Milli sievert
NASA	National Aeronautics and Space Administration
Ne	Neon
ng	Nanogram (1×10^{-9} g)
NHEJ	Non-homologous end joining
Ni	Nickel
nmol/l	Nanomole per liter
nm	Nanometer (1×10^{-9} m)
O	Oxygen
OI	Osteogenic induction
Osx	Osterix
Pb	Lead
PBS	Phosphate buffered saline
PCR	Polymerase chain reaction

PE	Plating efficiency
pH	*Pondus Hydrogenii* (-log [H^+])
PI	Propidium iodide ($C_{27}H_{34}I_2N_4$)
pRb	Phosphorylated retinoblastoma protein
RT-qPCR	Reverse Transcriptase quantitative real time polymerase chain reaction
RBE	Relative biological effectiveness
REST	Relative Expression Software Tool
RNA	Ribonucleic acid
Runx2	Runt-related transcription factor 2
s	Second (s)
S	Relative survival
SC	Standard culture medium
SPEs	Solar particle events
SSB	Single-strand break
SSC	Side scatter
Sv	Sievert
T_A	Annealing temperature
TBE	Tris/Borate/EDTA
Thr	Threonine
TGF-β1	Transforming growth factor beta 1
Ti	Titanium ion
Tyr	Tyrosine
V	Volt

Acknowledgements

Firstly, I would like to thank Hon.-Prof. Dr. Christa Baumstark-Khan for giving me a chance to work in her group, for sharing her enlightening ideas during my research, and for making my stay in Germany very warm and homely. She is truly an ideal mentor. I would like to extend my gratitude to PD Dr. Christine Hellweg who organizes the SpaceLife Ph.D program for all her time and patience answering all my questions during everyday laboratory work and especially for her valuable feedbacks on my thesis. Many appreciation and thanks to Dr. Patrick Lau who supervised me in carrying out experiments, spent much time discussing the results with me together, and cared about the progress of my thesis. His guidance helped me all the time.

I would like to take this opportunity to express my sincere gratitude to my first supervisor Prof. Dr. Waldemar Kolanus for accepting me as one of his students. His guidance, encouragement and immense knowledge helped me during my research and completion the thesis. Many thanks to PD Dr. Ruth Remmersbach as the second supervisor who always gave me nice suggestions during my studies. Her enthusiasm, positive attitude and encouragement have always inspired me.

I am grateful to Dr. Ralf Moeller for being my mentor for my Ph.D study. From the beginning he has shared with me the experience of Ph.D studies, has always given me his time and nice suggestions. His optimistic values were always very encouraging and motivating.

In my daily research work, especially during beam times in GANIL and GSI, I've been blessed with a friendly and cheerful group together with the SpaceLife Ph.D students Tina and Arif. I would also thank Kashish and Bikash for helping me in laboratory work and writing, Bernd for giving me many 'nicknames' and all Biodiagnostics group members for their kind help during my Ph.D studies. I would like to thank Claudia and Sebastian for all the technical help from ordering consumables and chemicals to help in the laboratory. I really appreciate the help from all the members of Radiation Biology department in German Aerospace Center (DLR) led by Dr. Guenter Reitz.

I would like to thank Prof. Iliakis and Dr. Moscariello at the Institute of Medical Radiation Biology in the University of Duisburg-Essen for good cooperation. It was a pleasure working with them.

Most of all, I would like to express my heartfelt gratitude to my family who helped me in every possible way to support me in completing this thesis.